Stony Brook University

The Role of MESD in WNT Signaling and Lipoprotein Metabolism

A Dissertation Presented

by

Janet Kathleen Lighthouse

to

The Graduate School

in Partial Fulfillment of the

Requirements

for the Degree of

Doctor of Philosophy

in

Molecular and Cellular Biology

(Cellular and Developmental Biology)

Stony Brook University

December 2010

Stony Brook University

The Graduate School

Janet Kathleen Lighthouse

We, the dissertation committee for the above candidate for the

Doctor of Philosophy degree, hereby recommend

acceptance of this dissertation.

Dr. Bernadette C. Holdener –Dissertation Advisor
Associate Professor
Department of Biochemistry and Cell Biology

Dr. John Peter Gergen - Chairperson of Defense
Professor
Department of Biochemistry and Cell Biology

Dr. Deborah A. Brown
Professor
Department of Biochemistry and Cell Biology

Dr. Michael A. Frohman
Professor
Department of Pharmacology

Dr. Howard Crawford
Associate Professor, Department of Pharmacology
State University of New York, Stony Brook

This dissertation is accepted by the Graduate School

Lawrence Martin
Dean of the Graduate School

Abstract of the Dissertation

Role of MESD in WNT Signaling and Lipoprotein Metabolism

By

Janet Kathleen Lighthouse

Doctor of Philosophy

In

Molecular and Cellular Biology

(Cellular and Developmental Biology)

Stony Brook University

2010

Deletion of the mesoderm development (Mesd) gene region blocks gastrulation and mesoderm differentiation in mice. In cell culture, MESD is required for the localization of WNT co-receptors LRP5/6 to the cell membrane. For this reason, loss of LRP5/6 from the cell surface in *Mesd* mutants likely prevents WNT signaling and is responsible for the polarity defects observed in *Mesd*-deficient embryos. In this study, we generated a targeted *Mesd* knockout and verified that loss of *Mesd* blocks WNT signaling *in vivo* and mesoderm differentiation. We also identified essential domains in the MESD protein, and demonstrated that MESD function in vitro was essential for maturation of the LRP5/6 β-propeller/EGFs. Based on these results, we hypothesized that MESD function may extend more broadly to the LRP family of receptors.

The majority of LRPs contain at least one extracellular β-propeller and C-terminal EGF, but several, including LRP1 and LRP2, contain multiple β-propeller/EGF domains in tandem and therefore likely require MESD for function. LRP1 and LRP2 are classified as scavenger receptors, but also play important signaling roles in preventing atherosclerosis and holoprosencephaly, respectively. We observed that LRP1 and LRP2 transcripts are present in mid-gastrulation embryos, and demonstrated that LRP2 is strongly expressed in the apical membrane of the visceral endoderm (VE). Consistent with our prediction, we show that MESD function in vivo extends to MEGALIN (LRP2) and is essential for the apical localization of LRP2 in the VE and the normal function of this absorptive epithelia.

The phenotype of *Mesd* mutants is more severe than either *Lrp5/6*, *Lrp1*, or *Lrp2* mutants. Although development of both *Mesd* and *Lrp5/6* mutants arrests before gastrulation (E6.5), the size of the *Mesd* embryo is considerably smaller than *Lrp5/6* mutants by E7.5. In contrast, *Lrp1* mutants can be recovered through E13.5, and *Lrp2* can be recovered at birth. Combined, phenotypic differences as well as the biochemical results described above provides evidence that MESD likely functions as a general LRP chaperone, and that the *Mesd* phenotype results from a combination of endocytic and signaling defects resulting from mis-folding of multiple LRP receptors.

TABLE OF CONTENTS

LIST OF FIGURES

LIST OF TABLES

LIST OF ABBREVIATIONS

Alb	Albumin
AMN	Amnionless
AVE	Anterior visceral endoderm
CLR, LDL-A	Complement-like repeat, Low density lipoprotein A motif
CUBN	Cubilin
EGF	Epidermal growth factor-like domain
EGFP	Enhanced green fluorescent protein
EP	Epiblast, embryonic ectoderm
ER	Endoplasmic reticulum
FEVR	Familial exudative vitreoretinopathy
ICM	Inner cell mass
IgG	Immunoglobulin G
LRP	Low density lipoprotein receptor-related protein
M	Mesoderm
MEG/LRP2	Megalin
MESD, *Mesd*	Mesoderm development (PROTEIN, *Gene*)
Nes	Nestin
OPPG	Osteoporosis-pseudoglioma syndrome
PCR	Polymerase chain reaction
PE	Parietal endoderm
PGK	Phosphoglycerate kinase
RAP	Receptor associated protein
VE	Visceral endoderm
VSR	Vertebrate specific region
Wg	Wingless (*Drosophila*)
WNT	Wingless/Integration signaling pathway

ACKNOWLEDGEMENTS

I am eternally grateful to my advisor, Dr. Bernadette Holdener, who always believed in me. She showed me the beauty of a gastrulating mouse embryo, and that adaptability and communication are cornerstones of good science. She has been an exceptional role model and mentor, who encouraged my growth as a developmental biologist, instructor, and community scientist. Her guidance and friendship over the last four years deepened my appreciation for other aspects of science including resolve, perspective, and digging. I genuinely appreciate the honor of being her student.

I also thank my committee, Dr. Peter Gergen, Dr. Debbie Brown, Dr. Michael Frohman, and Dr. Howard Crawford for always providing helpful suggestions, encouraging comments, and fresh insight, as well as reagents and guidance for new techniques.

I am deeply indebted to Jerry Thomsen and Bob Haltiwanger for their generous support and encouragement. In addition, I thank the Thomsen lab, Ballas lab, Sirotkin lab, and Takemaru lab for their helpful comments during lab meetings. I thank Dr. Rolf Sternglanz and Carol Juliano from the MCB program, Dianna Berger from the Biochemistry office, and Jonathan Wood from the CDG. I also thank the animal facility at Stony Brook for taking exceptional care of my mice.

I am especially grateful to have wonderful friends and family who supported me mentally and emotionally for the last five years. I thank Dr. Joseph Gall for fostering a love of science and showing me that curiosity is the best tool a scientist can have. Lastly, I thank my husband, who accompanied me through the entirety of graduate school from Baltimore to Stony Brook, and loved me through all the challenges and celebrated in all the successes.

CHAPTER 1:

Introduction

Early mouse development

Four and a half days after fertilization, three distinct cell types can be identified at the blastocyst stage. One cell type encases the entire embryo as an epithelium of trophectoderm, which is immediately responsible for blastocyst implantation. Later, this trophectoderm layer will contribute to several extraembryonic tissues. Within this epithelial layer, there is an asymmetric clumping of cells known as the inner cell mass (ICM), epiblast, or primitive ectoderm, which will develop into the embryo proper. A third cell type, the primitive endoderm, differentiates from the ICM to separate it from the blastocoel cavity. The primitive endoderm becomes parietal endoderm (PE), which secretes a basement membrane (also known as Reichert's membrane), and visceral endoderm (VE), which will later regulate early embryonic nutrition and polarity (Hogan, 1994; Beddington and Robertson, 1999; Ralston and Rossant, 2005).

Between embryonic day (E) 4.5 and E 6.5, anterior-posterior polarity is established. It was previously believed that formation of the primitive streak at E 6.5 in the posterior embryo initiated anterior-posterior polarity. However, *in situ* data indicates that molecular asymmetry of anterior visceral endoderm (AVE) markers such as *Hex*, *Lefty1*, and *Cerberus-1* precedes morphological asymmetry by approximately 1 day (Rivera-Perez, 2007; Shen, 2007). *Wnt3*, *Bmp4*, and *Nodal* signals are essential for polarity establishment. Nodal belongs to the TGFβ family of signaling proteins and is

expressed ubiquitously at E 3.5 in the ICM (Takaoka et al., 2006). Expression of Nodal activates expression of *Lefty1* and *Cer1* in the future AVE. As the AVE migrates from the distal tip of the embryo to the future anterior pole, *Lefty1*, *Cer1*, and *Dkk* inhibit *Nodal* and *Wnt* expression and regionalize *Nodal* and *Wnt* to the future posterior by E 5.75 (Tam et al., 2006; Shen, 2007).

Establishment of the posterior is regulated by complex feedback signaling loops between *Nodal*, *Bmp4*, and *Wnt*. In addition to inducing AVE expression of *Lefty1* and *Cerberus-1*, which will regionalize *Nodal* to the future posterior, early *Nodal* can also stimulate expression of *Bmp4* in the extraembryonic ectoderm. As *Nodal* expression becomes restricted to the posterior of the embryo, both *Nodal* and BMP4 signals induce *Wnt3* expression in the epiblast, which is required for primitive streak formation (Takaoka et al., 2006; Shen, 2007) (Figure 1). Thus, the AVE, marked by expression of *Hex*, *Dkk*, *Lefty1*, and *Cer1*, represses posterior primitive streak markers in the anterior epiblast, restricting primitive streak markers to the posterior where formation of the primitive streak will occur (Beddington and Robertson, 1999; Tam et al., 2006) (Figure 1).

Gastrulation and WNT Signaling

At 6.5 days of gestation, the embryo begins gastrulation, which will produce the three germ layers: ectoderm, definitive endoderm, and mesoderm. During gastrulation, E-cadherin expression is down regulated in the posterior primitive streak. This facilitates differentiation of the mesoderm and endoderm of the embryo (Beddington and Robertson, 1999; Tam and Loebel, 2007). The primitive streak elongates distally and

anteriorly, ending in a structure at the very distal tip of the embryo called the node. Cells migrating through the node migrate anteriorly to form the axial mesoderm of the embryo, cells migrating through the mid-streak form the lateral plate mesoderm, and cells emerging from the most posterior primitive streak form extra-embryonic mesoderm and germ cells (Beddington and Robertson, 1999). During this period, *Wnt3* is expressed in a gradient in the epiblast and associated VE, highest in the posterior and lowest in the anterior of the embryo (Liu et al., 1999). Nascent mesoderm emerging from the primitive streak also expresses *Brachyury* (*T),* visible by *in situ* hybridization as a thin line extending proximally to distally along the posterior embryo.

Canonical WNT signaling occurs through binding of nuclear β-catenin to WNT target genes (Figure 2, left). Binding of canonical WNTs such as WNT3 to the membrane receptors Frizzled (Fz) and LRP5/6 triggers phosphorylation of the cytoplasmic tail of LRP5/6, disabling a destruction complex and allowing cytoplasmic levels of β-catenin to increase (Clevers, 2006). As the cytoplasmic concentration of β-catenin increases, β-catenin can translocate into the nucleus where it forms a complex with TCF/Lef to activate target genes (Bejsovec, 2005; Daniels and Weis, 2005; Cadigan and Liu, 2006; Lai et al., 2009). Maturation of LRP5/6 occurs in the endoplasmic reticulum (ER) where a putative chaperone protein, mesoderm development (MESD), promotes proper folding of the receptor (Figure 2, left). In the absence of MESD, unfolded LRP5/6 is likely retained within the ER and not membrane-localized. As a result, WNT ligands cannot bind, and cytoplasmic β-catenin is constantly degraded by a destruction complex (Clevers, 2006) where CK1 and GSK3 phosphorylate β-catenin and flag it for proteosomal degradation. Cytoplasmic β-catenin concentrations remain low and β-

catenin cannot translocate into the nucleus. This ultimately prevents transcription of WNT target genes (Figure 2, right).

Mesd-deficient embryos have gastrulation defects

In mice, deletion of the *Mesd* (*mesoderm development*) functional interval blocks gastrulation and mesoderm differentiation (Holdener et al., 1994) (Figure 3A). Detailed analysis of the *Mesd* deletion phenotype revealed that the mutant embryos lacked posterior polarity and failed to form a primitive streak or differentiated mesoderm (Hsieh et al., 2003). The phenotype of the *Mesd* mutant embryos is remarkably similar to the phenotype of embryos mutant for *Wnt3*, or the WNT co-receptors, *Lrp5/6*, suggesting MESD is involved in WNT signaling (Liu et al., 1999; Hsieh et al., 2003; Kelly et al., 2004).

The *Mesd* deletion interval was originally identified by complementation studies using overlapping albino deletions Ai-1 (*Del(7)Tyr*$^{c\text{-}1DThWb}$), Ai-2 (*Del(7)Tyr*$^{c\text{-}23DVT}$), or Ai-3 (*Del(7)Tyr*$^{c\text{-}3YPSD}$) which caused embryonic lethality after implantation (Russell, 1949; Wines et al., 2000) (Figure 3A). All three albino deletions remove the mesoderm development functional gene region, defined by the proximal breakpoints of *Del(7)Tyr*$^{c\text{-}3YPSD}$, also known as 3YPSD, and *Del(7)Tyr*^{c112k} (Holdener et al., 1994; Wines et al., 1998; Wines et al., 2000). Physical mapping with BAC clones and DNA markers refined the location of the interval, and successful rescue of the deletion phenotype with one of the BAC clones, 171M12, identified two potential genes responsible for the *Mesd* deletion primitive streak defect (Wines et al., 2000)(Figure 3B). Subsequent transgene rescue demonstrated that the primitive streak and mesoderm differentiation defects could

be attributed to loss of single gene *Mesd* (previously named *Mesdc2*) rather than any of the other 26 protein coding genes located within the 3YPSD deletion (Figure 3C) (Wines et al., 2000). *Mesd* encodes for a putative chaperone protein for the WNT co-receptors LRP5/6 (Hsieh et al., 2003). The *Mesd* phenotype is characterized by an unusually small embryo not observed in *Wnt3* or *Lrp5/6* mutant embryos. The small size of the embryo is emphasized by the expanded parietal endoderm which is normally in close proximity to the embryonic endoderm. These phenotypic differences raise the possibility that MESD has multiple roles in embryonic development such as trafficking multiple LRP receptors.

This hypothesis is supported by observations in *Drosophila* investigating the homologue for MESD, *boca*. Disruption of *boca* phenocopies defective Wg signaling in the wing imaginal disc (Culi and Mann, 2003). However, while *Mesd*-deficient embryos die early during embryogenesis, flies homozygous for the boca mutation survive to pupation suggesting that either maternal boca can partially rescue the embryonic phenotype or the boca mutation retains residual function (Culi and Mann, 2003). Boca is responsible for trafficking Arrow (similar to LRP5/6) and Yolkless *in vivo*, and promotes trafficking of LpR2 and human LDLR in cell culture (Culi and Mann, 2003).

The Low-density lipoprotein Receptor-related Protein (LRP) family

LRP5/6 are transmembrane receptors that belong to a structurally similar, but functionally diverse family of proteins called the low-density lipoprotein Receptor-related protein (LRP) family. These receptors can be divided into three major domains: a cytoplasmic domain, a transmembrane domain, and an extracellular domain. The extracellular domain can be further subdivided into a complement-like repeat (CLR, also

known as LDL-A motif), an EGF domain, and a β-propeller. All LRP family members contain at least one CLR domain, and the majority of LRP family members contain at least one β-propeller domain followed by a C-terminal EGF (Strickland et al., 2002). In this dissertation, I propose that the *Mesd* mutant phenotype results from the mislocalization of multiple LRP receptors. This hypothesis introduces an interesting new role for MESD in mediating general LRP maturation and regulating the myriad of LRP-associated diseases.

LDLR and atherosclerosis

The founding member of the LRP family is the Low-Density Lipoprotein Receptor (LDLR). Unlike other family members, the primary role of LDLR is to internalize cholesterol by binding Apo-B100 in circulating LDL particles. This cholesterol can be used in one of two ways: to provide the cholesterol needed for membrane maintenance, and to serve as a component in steroid hormone synthesis (Goldstein and Brown, 1974). In the absence of LDLR, mice on a normal chow diet (0.04% cholesterol) developed a two-fold increase in plasma cholesterol levels. When this diet was increased to 1.25% cholesterol, this resulted in an additional ten-fold increase in plasma cholesterol and development of atherosclerosis by 7 months of age (Ishibashi et al., 1994). In humans, mutations in LDLR frequently lead to development of hypercholesteremia, due to impaired uptake of plasma lipoproteins. This can then lead to obesity, cholesterol plaque formation, and atherosclerosis (Goldstein and Brown, 2001). Atherosclerosis is a disease that is responsible for over 30% of deaths in the United States (Goldstein and Brown, 2001). Characterization of this disease began with the observation

of a patient with “black urine” (Brown and Goldstein, 1986). Over the last few decades, there have been significant advances to explain the molecular mechanisms of this disease. In humans, four monogenic disorders in the cholesterol uptake pathway can result in atherosclerosis. The disorder that is most applicable to our studies of receptor maturation is the mutation and regulation of LDLR trafficking (Goldstein and Brown, 2001). Many of the LDLR mutations that cause hypercholesterolemia are predicted to result in intracellular receptor aggregation (Li et al., 2002), suggesting that mutations in proteins required for receptor maturation could contribute to development of vascular disease. MESD is a chaperone that interacts with basic structural features shared within the LRP family, and is therefore a candidate to investigate.

VLDLR, obesity, ApoER2, and Reeler and Scrambler

VLDLR is structurally the most similar to LDLR, differing by only one N-terminal CLR domain. Unlike LDLR, mutation of VLDLR in mouse alone does not increase lipoprotein concentration in the blood (Frykman et al., 1995). This may be due in part to the expression pattern of the two different receptors: LDLR is expressed ubiquitously where VLDLR is mostly expressed in hepatic, neural, endothelial, and adipose tissues (May et al., 2005). In mouse, loss of VLDLR offers protection from obesity and a decrease in adipose tissue and overall body mass (Frykman et al., 1995; Goudriaan et al., 2001). However, when loss of VLDLR is combined with loss of LDLR, mice exhibit a phenotype similar to LDLR-deficiency with plasma triglyceride levels slightly elevated over LDLR-deficient mice, consistent with impaired clearance of VLDL from the blood (Tacken et al., 2000). Together, this suggests that VLDLR is required for

transport of triglycerides to adipose tissue and that in the absence of the receptor prevents triglyceride storage ultimately resulting in leaning body mass.

VLDLR may have a relatively mild role in regulating cholesterol levels, but it has an additional, more significant role in organizing neuronal layers in the brain. However, as the VLDLR-deficient mouse has no overt phenotype, VLDLR's role in the brain is not obvious until combined with ApoER2 deficiency. Mice deficient for ApoER2 alone also appear largely normal (Trommsdorff et al., 1999). However, when both receptors are non-functional, animals display characteristic ataxia similar to the reeler or scrambler mice. ApoER2 and VLDLR bind to the Reelin ligand triggering phosphorylation of the associated adaptor protein Dab1 by Src family kinases (Bock and Herz, 2003). Disruption of this binding results in impaired migration of Purkinje cells and inversion of cortical layers (Trommsdorff et al., 1999; Bock and Herz, 2003). Regulation of ApoER2 expression and localization also has a potential role in preventing Alzheimer's disease, as several studies have demonstrated that increased expression of ApoER2 results in increased processing of APP to produce amyloidogenic Aβ (Marzolo and Bu, 2009).

LRP1, LRP1B, vascular endothelia, neurons, macrophages and embryo survival

The second largest LRP family member is LRP1. LRP1 binds at least 38 different ligands (Strickland and Ranganathan, 2003) and is highly expressed in hepatocytes, neurons, and vascular SMC in the adult mouse (May et al., 2007). Due to its many ligands and broad expression pattern, LRP1 has roles in many different adult tissues. One of the most extensively studied tissues that express LRP1 is the vascular endothelia, where LRP1 can bind to tissue plasminogen activator (tPA) to regulate permeability in

the blood brain barrier (Yepes et al., 2003). LRP1 can also promote arterial vascular health by forming a complex with PDGFβ-receptor to bind PDGF cytokines and help prevent migration of smooth muscle cells, one of the initial steps in atherosclerosis (Swertfeger and Hui, 2001; Boucher et al., 2003; Doran et al., 2008). PDGF normally binds to the PDGF-receptor to induce cytoskeletal changes that promote cell migration (Gerthoffer, 2007). PDGF can also bind to LRP1 to trigger tyrosine phosphorylation of the cytoplasmic tail of LRP1 and association with the Shc adaptor protein (Loukinova et al., 2002). However, ApoE can compete with PDGF for binding of LRP1, which prevents activation of the PDGFRβ receptor and smooth muscle cell migration by negatively modulating PDGF signaling (Boucher et al., 2003).

LRP1 also has a number of other roles in adult tissues. In the neuron, LRP1 interacts with post-synaptic density protein PSD-95 and regulates calcium release, promoting neurotransmission (Qiu et al., 2002; May et al., 2004). LRP1 also has been linked to Alzheimer's disease, where LRP1 is thought to help clear both plaque-forming Aβ peptides and the Aβ precursor, APP (Kang et al., 2000; Waldron et al., 2008). Similarly, the relatively unknown LRP1B, which only differs from LRP1 by one extra complement-like repeat and placement of the intracellular NPxY motifs, can also mediate clearance of Aβ and APP (Marzolo and Bu, 2009). In macrophages derived from the lung or tumor cells, LRP1 promotes phagocytosis of red blood cells, or antigens recognized by lung collectins (Gardai et al., 2003; Patel et al., 2003). Finally, LRP1 is expressed in the embryonic trophoblast giant cells and visceral endoderm. Disruption of LRP1 results in lethality between E 10.5 and E 13.5 with visible developmental delay beginning at E 9.5 (Herz et al., 1992; Herz et al., 1993).

LRP2 (Megalin, gp330), kidney function and holoprosencephaly

LRP2 is the largest member of the LRP family and is another scavenger receptor in the LRP family. LRP2 ligands include high- and low-density lipoprotein, calcium, vitamin B12 complexes, and retinol-binding protein. LRP2 is involved in neural development and nutrient uptake in the kidney proximal tubule and embryonic VE (May et al., 2007). In neural development, LRP2 is hypothesized to bind to BMP4 ligands to regulate SHH signaling. In the absence of LRP2, mutant embryos display neural closure defects that resemble the holoprosencephalic phenotype characteristic of *Shh*-deficient animals (Spoelgen et al., 2005).

In the kidney and other absorptive epithelia, LRP2 usually forms a complex with cubilin and amnionless (Kozyraki and Gofflot, 2007). In the absence of LRP2, cubilin remains localized to the plasma membrane of kidney proximal tubule cells and retains the ability to bind transferrin, but fails to endocytose the ligand, indicating that cubilin ligands depend on LRP2 for endocytosis (Moestrup et al., 1998; Hammad et al., 2000; Kozyraki et al., 2001; Strope et al., 2004). Loss of LRP2 in the kidney results in proteinuria, or a failure to reabsorb crucial nutrients from the urine before excretion. This failure in tissue function is accompanied by a morphological defect in formation of apical endocytic organelles (Christensen and Willnow, 1999; Leheste et al., 1999). In Chapter 3, I similarly demonstrated that surface localization of LRP2 in the visceral endoderm depends on MESD. Disruption of MESD and subsequently LRP2 function impairs the endocytic ability of the VE by reducing the size and number of lysosomes.

LRP5 and LRP6, Wnt signaling and bone metabolism

Second to LDLR, LRP5 and LRP6 are arguably two of most well-studied LRPs. These two receptors traditionally function as co-receptors with Frizzled (Fz) for the Wnt ligand. The Wnt ligand binds to the Fz receptor, which complexes with LRP5/6 and ultimately results in the translocation of cytoplasmic β-catenin into the nucleus where binds to TCF/Lef to activate target genes (Bejsovec, 2005; Daniels and Weis, 2005; Cadigan and Liu, 2006; Lai et al., 2009). Knockout of the genes encoding either the WNT3 ligand or both LRP5 and LRP6 co-receptors in mouse results in the failure to establish a posterior primitive streak or differentiate mesoderm (Liu et al., 1999; Kelly et al., 2004).

LRP5 can also serve as the receptor for the Norrin ligand. Diseases such as Norrie and familial exudative vitreoretinopathy (FEVR) are characterized by incomplete vascularization of the retina, vitreous hemorrhage, and retinal detachment defects which have been linked to mutations in LRP5, FZD4, or Norrin disease protein (NDP) (Toomes et al., 2004; Xu et al., 2004). It has also been proposed that LRP6 may offer functional redundancy in *Lrp5-/-* animals since the vascularization defects in *Lrp5-/-* animals is not as severe as in *Fzd4-/-* or *Ndp-/-* animals (Ye et al., 2009). A similar human disease called osteoporosis-pseudoglioma disorder (OPPG) also has defects in eye vascularization, but is additionally characterized by defects in bone metabolism resulting in low bone density. The positional candidate approach was used to identify LRP5 as the gene responsible for OPPG, and targeted knockout of *Lrp5* in mice confirmed that LRP5 was responsible for the OPPG phenotype (Gong et al., 2001; Kato et al., 2002). At least one mutation that results in the OPPG phenotype falls within the first β-propeller of

LRP5. However, other mutations in this same domain, including the G171V, can result in high bone mass (Little et al., 2002; Zhang et al., 2004; Ferrari et al., 2005). The G171V mutation was decreases cell surface expression of LRP5, due to impaired interaction with MESD (Zhang et al., 2004). These data strongly suggest that the β-propeller domain is important for LRP5 function, and our *in vitro* data confirms that LRP5βP1 is highly dependent on MESD for maturation.

Targeted disruption of LRP6 results in perinatal lethality due to truncation in the axial skeleton, spina bifida, and limb defects (Pinson et al., 2000). A naturally occurring mutation, *ringelschwanz* (*rs*), is caused by the R886W mutation and results in somitogenesis defects and osteoporosis. Similar to the LRP5 mutations that affected bone metabolism, the R886W mutation occurs in the third β-propeller/EGF domain of LRP6 (Kokubu et al., 2004). This mutation also disrupts interaction of LRP6 with MESD (Kubota et al., 2008). Furthermore, mice heterozygous for null mutations in both LRP5 and LRP6 also exhibit bone mass defects (Holmen et al., 2004). This serves as further evidence that the MESD-dependent β-propeller domain found in LRPs is crucial for proper receptor function.

LRP4 and limb patterning

LRP4 (Megf7) is the only other LRP that is structurally similar to LRP5 and LRP6 (Strickland et al., 2002). Surprisingly, LRP4 does not promote Wnt signaling, bone or eye development. Instead, loss of LRP4 results in polysyndactyly, due to improper patterning of the apical ectodermal ridge (AER) (Johnson et al., 2005). Mutations in LRP4 are similar to that observed in the *doubleridge* and *Dkk1*-deficient animals

(Adamska et al., 2003; Adamska et al., 2004; Simon-Chazottes et al., 2006). For this reason, it was proposed that mutation of *Lrp4* antagonizes canonical Wnt signaling (Simon-Chazottes et al., 2006). An ENU-induced screen also identified the role of LRP4 in the formation of the early neuromuscular junction. One of the ENU induced *Lrp4* mutations, *mte*, generates a D1436G mutation in the fourth β-propeller/EGF domain of LRP4 (Weatherbee et al., 2006).

MESD-mediated trafficking of LRP family members in development and disease

My studies investigate the possibility that MESD functions as a general LRP chaperone. Understanding MESD-dependent LRP maturation will provide insight into how this functionally diverse family of receptors impacts embryonic development and adult tissue function. Currently, only one other chaperone, receptor associated protein (RAP), has been shown to promote maturation of LRP family members by interacting with the LDL-A (complement-like repeat) motif. Given the diverse roles and complex structure of the LRP family, there are likely other chaperones that contribute to proper receptor maturation and function. *In vitro* data indicates that MESD can help traffic a specific domain from LRP5/6 (Lighthouse et al., submitted). However, it is unclear how MESD interacts with LRPs, and whether MESD can function *in vivo* to promote maturation of other LRP family members. I will address these questions in three chapters of this dissertation.

In Chapter 2, I describe a mutagenesis screen that identifies key domains in MESD that are essential for LRP maturation. I discuss the relationship of these mutations to NMR-generated MESD structure models, and propose a possible mechanism for

MESD assisted -trafficking of the β-propeller/EGF domain found almost exclusively in LRPs. Chapter 3 describes the *in vivo* trafficking of LRP2 by MESD. This chapter establishes that MESD function extends beyond WNT signaling and LRP5/6 maturation, further supporting the hypothesis that MESD functions as a general LRP chaperone. This chapter also provides evidence that MESD is essential for visceral endoderm function and proposes that defects in endocytosis may contribute to the small embryo phenotype. In Chapter 4, I will discuss the generation of a conditional allele of *Mesd* to explore the various roles of the LRP family of receptors in both embryonic and adult tissue. Finally, I will conclude with a discussion of potential future directions for my studies and how MESD contributes to our understanding of human health and physiology.

FIGURES

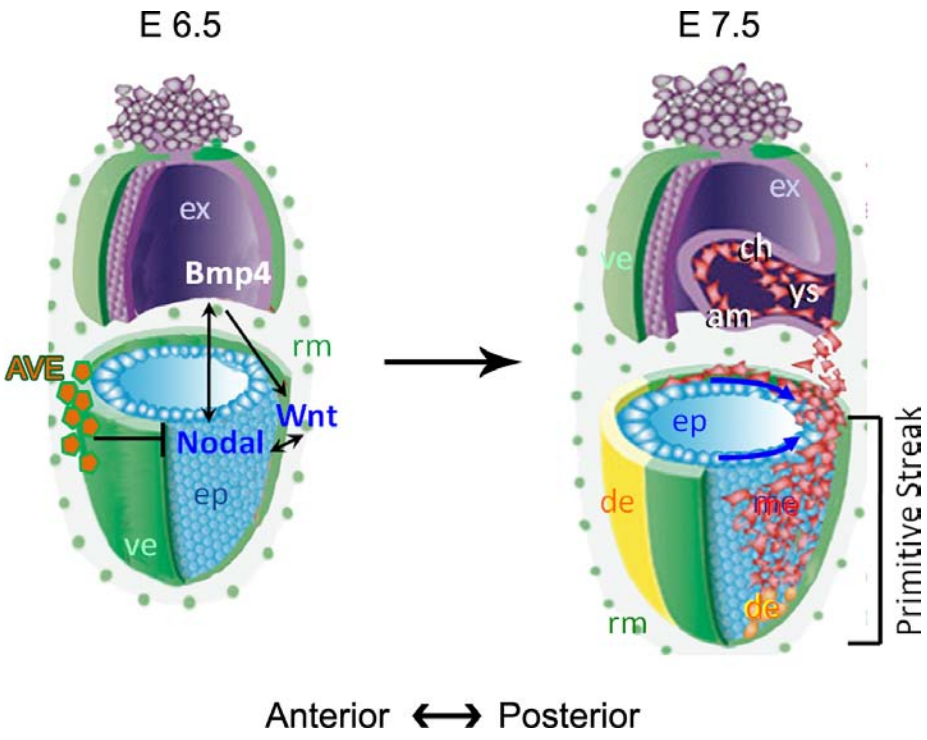

Figure 1. Inhibitors regionalize Nodal and Wnt signaling to the posterior epiblast, inducing primitive streak formation.

Modified from the Constam lab website (Constam). **(Left)** The pre-gastrulation E 6.5 mouse embryo is a two-cell layer cylinder consisting of an inner layer of extraembryonic ectoderm (ex) and embryonic ectoderm (epiblast, ep), and an outer layer of visceral endoderm (ve). The visceral endoderm is important for nutrient absorption and secretion, and helps pattern the underlying epiblast. Anterior visceral endoderm cells (AVE, orange pentagons) produce inhibitory signals that repress expression of WNT/Nodal in the anterior epiblast and regionalize their expression to the future posterior pole. **(Right)** Restriction of WNT/BMP4/Nodal signaling to the posterior induces formation of a visible structure called the primitive streak. Epiblast cells ingress (blue arrows) through the primitive streak to form mesoderm (me) and definitive endoderm (de). Nascent mesoderm migrates proximally to contribute to extraembryonic structures such as the chorion (ch) and amnion (am), and distally to contribute to the embryonic mesodermal layer.

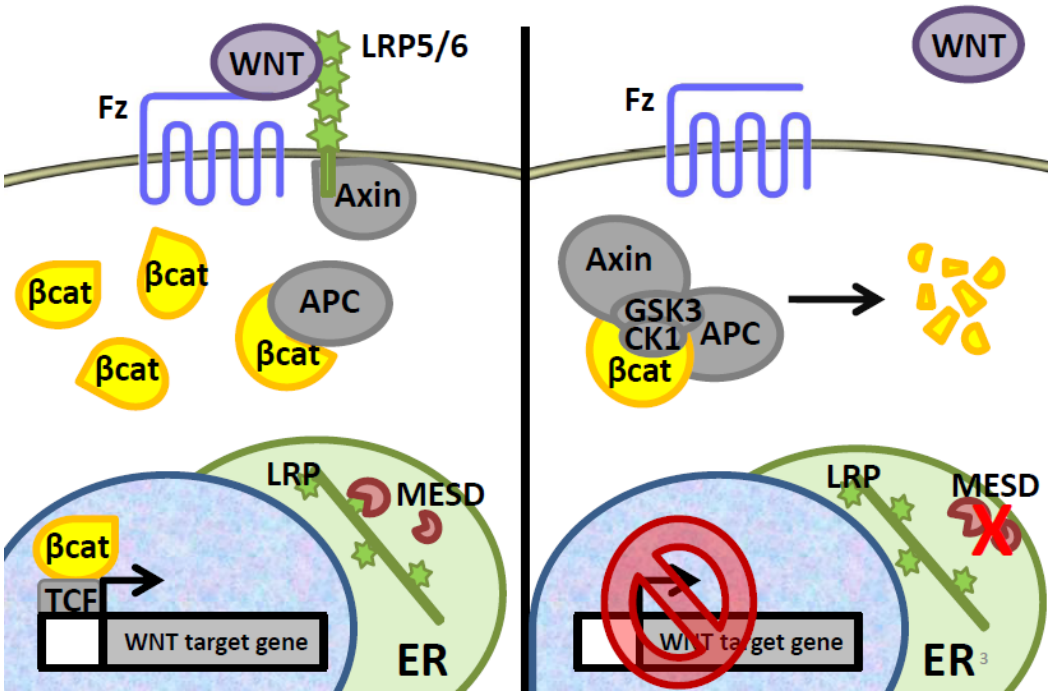

Figure 2. Canonical WNT signaling.

(Left) Canonical WNT signaling occurs through binding of the WNT ligand to LRP5/6 and Frizzled (Fzd) co-receptors. Binding triggers the dissociation of a destruction complex that contains Axin and APC, which allows intracellular levels of β-catenin to increase. When cytoplasmic levels of β-catenin are high enough, β-catenin can translocate into the nucleus to bind to TCF and turn on transcription of WNT target genes. LRP5/6 originates as an unfolded receptor in the endoplasmic reticulum (ER) and MESD promotes maturation of the β-propeller/EGF domains (green stars) to allow LRP5/6 to become membrane localized. **(Right)** Loss of MESD results in defects in LRP5/6 maturation, which prevent LRP5/6 membrane localization and blocks WNT signaling. Loss of membrane localized LRP5/6 prevents WNT ligands from activating the receptor. As a consequence, the destruction complex (composed of casein kinase 1 (CK1), axin, adenomatous polyposis coli (APC), and glycogen-synthase kinase 3 (GSK3)) remains active, and continually phosphorylates and targets β-catenin for ubiquitination and proteasomal degradation. This results in low intracellular levels of β-catenin, and prevents β-catenin from translocating into the nucleus. Consequently, transcription of WNT target genes is blocked.

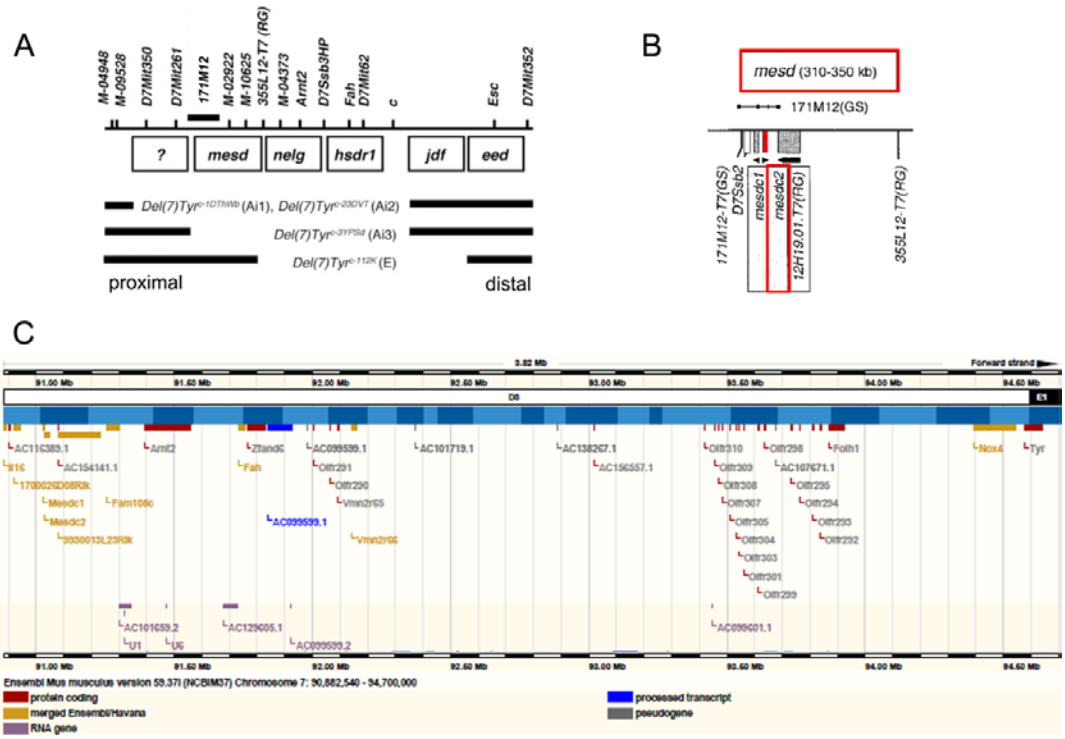

Figure 3. The *Mesd* functional region on mouse chromosome 7 is delinated by the proximal breakpoints of *Del(7)Tyr$^{c\text{-}3YPSD}$* and *Del(7)Tyr$^{c\text{-}112K}$*.

Modified from Wines, M. E., et al., 2000, Wines, M. E., et al., 2001 (Wines et al., 2000; Wines et al., 2001). **(A)** Albino deletions *c1DThWb*, *c23DVT*, and *c3YPSD* all remove the *Mesd* functional region. Mapping of this region revealed that the breakpoints for *c3YPSD* and *c112K* mark the boundaries for the mesd functional region. The 171M12 BAC clone used for rescue experiments is labeled and shown as a black bar above the mesd functional region. **(B)** The *Mesd* phenotype observed in c3YPSD homozygotes can be rescued with BAC clone 171M12 which contains two candidate genes, *Mesdc1* and *Mesdc2*. Further rescue experiments demonstrate that only *Mesdc2* is responsible for the mutant phenotype (Hsieh et al., 2003). The *Mesd* functional region and rescuing transgene are highlighted in red. **(C)** A detailed map of genes removed in the *c3YPSD* deletion. The *c3YPSD* deletion encompasses a 3.82 Mbp region that includes 26 protein coding genes and 8 Ensembl/Havana predicted genes. Only loss of *Mesdc2* (fourth yellow gene from the left) is responsible for the mutant phenotype. *c3YPSD* endpoints are roughly marked by D7Mit261 (7:90882540) and Tyr (7:94641899). Reproduced from EnsEMBL, mouse chromosome 7:90882540-94700000. Red – protein coding gene, yellow – merged Ensembl/Havana, purple – RNA gene, blue – processed transcript, grey – pseudogene.

CHAPTER 2:

Identification of the MESD domains required to interact with low-density lipoprotein receptor-related proteins (LRPs).

Co-contributors: Anne Marter, Michael Bellone, Xiping Zhang, Christian Köhler, Tobias Werther, Olav M. Andersen, Annette Diehl, Peter Schmieder, Jianguang Du, Hartmut Oschkinat.

SUMMARY

MESD is a putative chaperone protein for WNT co-receptors LRP5/6. LRP5/6 are two members of a large family of structurally related receptors called the low-density lipoprotein receptor-related proteins (LRPs). A common feature shared between the LRP receptors is a β-propeller/EGF domain that depends on MESD for maturation (Chapter 3, (Culi and Mann, 2003; Lighthouse et al., submitted). As a first step toward understanding how MESD promotes trafficking of LRPs, we generated a series of MESD mutations and assayed their effects on MESD activity using an LRP6 maturation assay. These analyses identified that the N-terminal α-helix and acidic domain and hydrophobic patch on the MESD core are required for MESD function. Two structural predictions of full-length MESD have been proposed. Mapping of the mutations onto these models allow us to visualize the domains and propose a model for MESD-LRP interaction.

INTRODUCTION

MESD structure

MESD is a 25kDa, ER-resident protein that is 224 residues long. It has a signal peptide at the N-terminus that is cleaved after MESD is directed into the ER. NMR studies predicted that the MESD core is organized into an α-β-α-β-β-α-β structure (Koehler et al., 2006). The core is predicted to extend N-terminally to include an ER signal peptide (residues 1-30) an N-terminal α-helix connected by a flexible linker region (residues 43-103) (Chen et al., 2010; Koehler et al., submitted). C-terminal to the core is a vertebrate-specific region (residues 184-220, VSR) and a four-residue (REDL) ER retention signal (residues 221-224) which composes the ER-retention sequence (Koehler et al., 2006). MESD is hypothesized to function as a chaperone protein for the Low-density lipoprotein Receptor-related Protein (LRPs) family of receptors.

LRP structure

LRPs are a large family of structurally related, transmembrane receptor proteins. Most of these receptors contain at least one NPxY sequence in the intracellular domain, coupling the receptor to endocytic machinery and signaling cascades. The general LRP extracellular domain consists of three major motifs: a cysteine-rich complement-like repeat unit also known as LDL-A repeats, an EGF-like domain, and a six-bladed β-propeller domain. Each of the six blades contains a YWTD repeat, and is arranged as four β-sheets in a head-to-tail orientation (Jeon et al., 2001; Strickland et al., 2002; Willnow et al., 2007). The β-propeller domain is predicted to be closely associated with the

C-terminal EGF (Jeon et al., 2001). The interface between the β-propeller and C-terminal EGF domain largely consists of hydrophobic residues that extend from the EGF side chains and is positioned between the second and third propeller blades of the β-propeller domain. This encourages the EGF domain to pack tightly against N-terminal β-propeller, burying the β-propeller/EGF interface (Jeon et al., 2001).

Individual LRP family members differ in both the number and orientation of these three different extracellular domains. Nine out of eleven LRP family members found in mouse contain at least one β-propeller/EGF domain (Strickland et al., 2002). As might be predicted from the significant differences in extracellular domain organization between family members, the LRP receptors have diverse functions in various tissues that include, but are not limited to, fatty acid clearance from the blood, neuronal organization, protein reabsorption from the urine, signaling in a variety of tissues, and limb patterning (Willnow et al., 2007).

Biological Significance of MESD/Boca

Loss of MESD in the mouse results in posterior polarity defects and mutant embryos that do not form mesoderm (Hsieh et al., 2003). As a consequence, *Mesd*-deficient embryos cannot be recovered after E 10.5 (Holdener et al., 1994). These defects are similar to those observed in *Wnt3* and *Lrp5/6* mutant embryos, suggesting that MESD is involved in WNT signaling (Liu et al., 1999; Kelly et al., 2004). Cell culture experiments demonstrated that MESD is a putative chaperone that interacts with and promotes trafficking of LRP5 and LRP6, two members of the low-density lipoprotein receptor-related (LRP) family (Hsieh et al., 2003). In *Drosophila*, the MESD homologue

Boca has a similar role in trafficking the *Drosophila* homolog of LRP5/6 (also known as Arrow) and Yolkless, and promotes trafficking of LpR2 and human LDLR in cell culture (Culi and Mann, 2003). The majority of LRP family members contain this MESD dependent β-propeller/EGF domain (Strickland et al.). In this chapter, I demonstrate that the dependence on MESD may be dictated by individual β-propeller/EGF sequence and increases as multiple β-propeller/EGF domains are linked in tandem (Culi et al., 2004) (Lighthouse et al., submitted). With the exception of the precursor for the mouse epidermal growth factor (pro-EGF), this particular β-propeller/EGF domain combination is not found in other proteins (Culi et al., 2004). Taken together, this suggests that MESD may function as a specific chaperone for members of the LRP family, and may also potentially extend to the epidermal growth factor (EGF).

Despite the discovery of a MESD-dependent domain in LRPs, the resolution of the core structure, and an understanding of the basic consequences of MESD deficiency in the embryo, little was known about the functional domains within MESD that are responsible for facilitating LRP folding. To begin to understand how MESD facilitates maturation of the β-propeller/EGF domains, we developed a functional screen to identify residues critical for MESD function. These studies formed the basis for interpretation of NMR structural models and MESD/LRP peptide interaction studies.

RESULTS

MESD promotes maturation of LRP6 in cell culture

To identify residues important for MESD function, I screened a collection of MESD mutations (including: truncations, PCR-generated random substitutions, and site-directed *Mesd* mutations) using a cell culture-based LRP6 maturation assay (Brown et al., 1998; Hsieh et al., 2003; Khan et al., 2007; Abrami et al., 2008). In this assay, I compared the efficiency of *wild-type* and mutant MESD to promote maturation of LRP6 from a low-molecular weight ER-retained form to a mature higher molecular weight glycosylated form. In the absence of exogenously added MESD, approximately 94% of LRP6 is retained in the ER. In contrast, *wild-type* MESD promotes maturation of over 60% of total LRP6 (Figure 4). Using the amount of mature LRP6 expressed as a way to measure MESD activity, we predicted that this assay could be used to rank mutations that affected MESD function.

Alignment of the MESD amino acid sequence from multiple species suggests that vertebrate MESD contains a C-terminal domain not found in *Drosophila*, *Anopheles*, or *Caenorhabditis* (Culi and Mann, 2003). In co-transfection assays, MESD lacking this vertebrate specific domain (VSR, residues 184-220) promoted maturation of LRP6 at levels comparable to *wild-type* MESD, despite a significant reduction in detectable MESD (Figure 4 B and C). These data suggest that the disordered (Koehler et al., 2006), C-terminal, non-conserved region of MESD was dispensable for function, but may be required for stability or detection of MESD. This is in direct contrast to previous data suggesting that VSR is required for MESD activity (Koduri and Blacklow, 2007). In

contrast, a slightly larger internal deletion (Δ154-216) eliminates MESD activity, suggesting that residues 154-184 were important for MESD function (Figure 4). This is also confirmed by NMR spectra from two groups demonstrating that this region significantly shifted from *wild-type* MESD spectra in a W61R mutation of MESD (Chen et al., 2010; Koehler et al., submitted). Since our results suggested that deletion of the VSR did not affect MESD function, we did not focus on individual mutations within this domain.

To begin to identify MESD residues important for LRP5/6 trafficking, a former undergraduate, Anne Marter, generated random PCR-induced MESD mutants by using a mixture of error-prone DNA polymerases. Using this stategy, Anne generated and sequenced 200 clones. Among these clones she identified 87 mutant clones of which 51 contained between 1 – 7 mutations and did not introduce a premature stop codon. In total, she generated 115 unique non-conservative amino acid substitutions throughout MESD (Appendix A). Prior to analyzing individual mutations, I determined how much MESD was required to traffic a fixed amount of LRP6. A dosage curve of increasing concentrations of transfected *Mesd* with a constant concentration of transfected *Lrp6* and human IgG indicated that up to 300ng of *Mesd* produced the optimal amount of mature LRP6 (Figure 5). Above this level, general protein production was reduced (Figure 5). Using this established ratio of *Mesd* to *Lrp6* transfected DNA, I screened (with the assistance of Xiping Zhang and Jianguang Du) individual clones that contained multiple MESD mutations to assess their efficiency in promoting LRP6 maturation; 19 clones had reduced activity compared to *wild-type* MESD (Appendix A). Since many of these clones contained several PCR-generated mutations, I generated 32 additional clones with

site-directed mutations to facilitate evaluation of the effects of individual substitutions. 16 of these mutant clones affected MESD function and 16 did not affect MESD function (Figure 4C, 4D).

By mapping the 16 mutations that affected MESD function onto the full-length MESD model, I identified MESD domains that are important for trafficking the LRP β-propeller/EGF (Figure 6, Appendix B and C). P40S was not mapped onto the model because it was not included in the full-length MESD sequence (residues 45-184). The mutations fall into three groups: those that disrupt the MESD core; those that disrupt the exposed hydrophobic patch on the MESD core, formed by residues in the second and third β-sheet; and those that map within the N-terminal α-helix of MESD. Together, these mutations helped identify residues important for MESD activity and determine whether these residues formed any functional domains that may interact with LRP β-propeller/EGF domains.

Tryptophan residues in MESD may disrupt packing of the MESD core

The MESD core consists of approximately 100 residues that form a compact structure of β-sheets and α-helices (Koehler et al., 2006). Structural integrity of protein core domains often depend greatly on interactions between certain amino acid side chains. Hydrophobic residues often form interactions that are important for maintaining the internal framework of a protein. Tryptophan residues are hydrophobic aromatic amino acids, and MESD contains three tryptophan residues, two of which (W127 and W159) are located in the core domain (Koehler et al., 2006). The third tryptophan (W61) is located

in the N-terminal α-helix (Chen et al., 2010; Koehler et al., submitted). Mutagenesis of MESD revealed that mutation of any one of the three tryptophan residues greatly reduced MESD activity without altering the level of MESD (Figure 4). Based on these observations, we predict that the tryptophan residue substitutions (W61R, W127R, and W159R) alter the structure of MESD by disrupting hydrophobic interactions, but do not destabilize MESD. Other mutations within the MESD core that significantly reduced MESD activity include N133Y, K103E, and A134T. In contrast to W127R which nearly abolished MESD activity, N133Y, K103E, A134T, and W159R only modestly reduced LRP maturation to 43-84% of *wild-type* MESD activity (Figure 4).

Partially exposed hydrophobic residues in MESD are required for protein function

Hydrophobic interactions also regulate protein-protein interaction. Using the full-length MESD model, we identified a domain of partially exposed hydrophobic residues. Mutation of these residues (I149R, F108R, F141R, M151R, V143R, and A134T) demonstrates that this hydrophobic patch is important for MESD function (Figure 4). A134T (hydrophobic to neutral-polar side chain) is a mutation isolated from a randomly generated *Mesd* clone, but all other mutations were targeted to replace the hydrophobic residue to a hydrophilic-basic residue, arginine. Strikingly, mutation of I149R reduces MESD activity to 17% of *wild-type*. Individually, F141R and F108R reduce LRP6 maturation to only 62-80% of *wild-type* MESD. However, the combined mutation of F141R/F108R reduces MESD function to 15% of *wild-type* activity. In contrast, V143R and M151R do not significantly alter MESD activity, and F141R/M151R is not significantly different from F141R, suggesting that V143 and M151 are functionally

distinct from F108, F141, and I149. Together, these data suggest that although a few residues such as I149 may be very important for MESD function, the majority of hydrophobic residues in this region likely work together to form a functional domain.

The MESD N-terminal α-helix is essential for MESD function

The full-length model (45-184) suggests that the hydrophobic domain is only partially exposed and that residues 45-89 correspond to an N-terminal α-helix that can be transiently positioned to cover the MESD hydrophobic domain (Figure 6) (Koehler et al., submitted). Several MESD substitutions (L57P, D(64-66)A (generated by undergraduate, Michael Bellone) , D53V, W61R, E62K) provided compelling evidence that the N-terminal α-helix (49-68) is important for function (Figure 4). MESD L57P and W61R each reduced LRP6 maturation to less than 25% of *wild-type* activity. These two randomly generated substitutions likely impair interaction between the N-terminal α-helix and core domain, or interfere with MESD interactions with the LRP β-propeller/EGF. Notably, W61R is analogous to the *Drosophila* boca mutation (Culi and Mann, 2003). The ability of MESD W61R to promote maturation of 16% of LRP6 receptor suggests that the *boca* mutant may retain residual function.

The N-terminal α-helix also contains a stretch of acidic residues that forms a protrusion just before the linker region. Mutation of D53V (randomly generated), D64-66A (targeted mutation), and E62K (targeted mutation) in this tip region reduces MESD activity to 34%, 55%, and 71% respectively of *wild-type*. These mutations illustrate the functional importance of negatively charged residues within the α-helical domain. Other

randomly generated N-terminal mutations that modestly affect MESD function include M54T (75% of WT) and P40S (80% of WT) (Figure 4).

The structural solution of full-length MESD also revealed a potential interaction between helix α1 and the core domain. Donor residues such as K103 on the MESD core and acceptor residue D64 on the first α-helix may form a salt bridge that would provide transient stabilization between the two domains (Kumar and Nussinov, 1999; Kumar and Nussinov, 2001; Bosshard et al., 2004). Combined with other non-covalent interactions that can be easily broken and reformed by changes in pH, this suggests that helix 1 may be tethered to the MESD core and cover the otherwise exposed hydrophobic patch. In support of this hypothesis, mutation of W61R not only disrupts the structure of the N-terminal α-helix, but it also disrupts residues in the MESD core that contact the N-terminal helix. Comparison of the amide signals of *wild-type* MESD to the W61R mutant indicates that the signals of a number of core residues in the β-sheets are slightly back-shifted in the W61R mutant (Koehler et al., submitted). Together, these mutations provide functional evidence for the importance of the N-terminal α-helix extension as well as its transient interaction with exposed hydrophobic residues of the core domains β-sheet.

DISCUSSION

The tertiary structure of MESD is flexible

MESD is a putative chaperone protein for the WNT co-receptors LRP5/6. Although MESD promotes maturation of β-propeller/EGF domains found in LRP family members, the physical mechanism of MESD-mediated LRP maturation remained unknown due to a lack of MESD structural predictions (Culi and Mann, 2003; Culi et al., 2004). We collaborated with Hartmut Oshkinat's structural biology group to propose a full-length model of MESD (residues 45-184) and identify MESD functional domains that may be responsible for promoting LRP maturation, (Koehler et al., submitted). MESD is composed of 4 α-helices and 4 β-sheets where helix 1 is a long N-terminal helix predicted to be loosely attached to the MESD core by a flexible linker region including helix 2 (Koehler et al., submitted). Helix 3 and helix 4 are held together behind a row of four β-sheets, separating the N-terminal helix from helix 3 and helix 4 with the β-sheets (Figures 6A, 8).

The structure of MESD has been difficult to crystallize or predict using NMR-spectroscopy, possibly due to the natively unstructured C-terminal domain (residues 184-220) (Koduri and Blacklow, 2007). Removing this domain allowed for the prediction that MESD may adopt at least three different conformations. Based on NMR relaxation parameters, Koehler et al propose that MESD is structurally dynamic and can adopt an open or a closed conformation (Figure 6)(Koehler et al., submitted). A third possible conformation was proposed by Chen et al. suggesting a different position for the third α-helix in the MESD core (Chen et al., 2010). To identify MESD functional domains, we

screened the effects of MESD mutations on LRP6 maturation. These mutations included deletions, random PCR-induced mutations, and targeted mutations dictated by structural predictions. We determined that the N-terminal α-helix and an exposed hydrophobic domain are crucial for MESD function, and that several residues may be required for MESD to adopt a closed conformation.

The N-terminal MESD helix contains charged and hydrophobic residues

Previous studies in *Drosophila* indicated that W49 in the homologous protein Boca was required for viability (Culi and Mann, 2003). Structural prediction of the homologous mutation, W61, in the N-terminal α-helix of mouse MESD revealed that the W61 mutant adopted only the open conformation, suggesting that the patterning defects and embryo lethality in *Drosophila* resulted from protein dysfunction (Koehler et al., submitted). In light of the predicted dynamic structure of MESD, we hypothesized that other mutations in the N-terminal helix would also be important for protein function. In addition to W61, mutation of acidic residues D64-66, D53 and E62 decreased MESD activity. When mapped onto the predicted Koehler model of MESD, these acidic residues corresponded to an acidic domain located at the end of the N-terminal helix in both the closed and open conformations (Figure 6B). The interior of the LRP β-propeller ring is composed of basic residues, and we predict that the acidic end of the N-terminal helix may interact with these positively charged residues to facilitate closure of the β-propeller (Figure 7A, 7B). D64-66 in helix 1 may also form a salt-bridge with K103 near the MESD core to strengthen a transient interaction between the N-terminal helix and MESD

core in the closed conformation. Acidic-basic interactions in LRP folding has been observed in cell culture with the LRP chaperone protein, receptor associated protein (RAP), which interacts with acidic patches located within the CLR domains of various LRPs (Andersen et al., 2000; Hsieh et al., 2003; Fisher et al., 2006; Lee et al., 2006). Taken together, these data suggest that disruption of these negatively charged solvent exposed residues would be consistent with disrupting a domain important for interacting with the positively charged residues in the LRP β-propeller ring. The N-terminal α-helix also contains other residues that, when mutated, disrupt MESD activity. These include hydrophobic residues M54T and L57P. In the closed conformation, these two residues face the MESD core and we predict that they promote close association of the N-terminal helix with the core by hydrophobic interactions. In the open conformation, they face away from the MESD core where they may act to stabilize the hydrophobic interfaces between each blade in the LRP β-propeller and facilitate the final folding of the β-propeller ring (Figure 6B, 7A, 7C).

The hydrophobic residues of MESD are important for MESD function

Nascent, unfolded proteins often require the assistance of molecular chaperones to promote proper folding and prevent mis-folding which would result in protein degradation. Many molecular chaperones have hydrophobic domains that recognize exposed hydrophobic residues in the unfolded protein (Gomez-Puertas et al., 2004; Kubota, 2009). Consistent with our prediction that MESD functions as a molecular chaperone, MESD contains a domain of hydrophobic residues that is covered by the N-terminal helix in the closed conformation and exposed in the open conformation. We

predicted that this region was crucial for MESD function and generated seven mutations targeting this hydrophobic patch. In the open conformation, these hydrophobic residues are clearly visible as a continuous patch on the face of the four β-sheets (Figure 6B). The position of these hydrophobic residues may help stabilize the unfolded β-propeller/EGF, similar to the hydrophobic residues on the N-terminal helix. In the closed conformation, this hydrophobic patch appears to contact the hydrophobic residues M54 and L57 in the N-terminal helix, potentially stabilizing MESD in the absence of unfolded LRP (Figure 6B). Our targeted disruption of this exposed hydrophobic domain may either preclude the ability of MESD to interact with unfolded LRP, or alternatively alter the conformation of MESD.

Core residues stabilize MESD

Although W61 is the only residue that has been currently shown to have an *in vivo* phenotype, several other residues in MESD may play a similar role. These include W127 and W159 which are located in helix 3 and 4 respectively. In addition to N133 and I123 which both fall within helix 3, we predict that mutation of these core residues may distort the helices and prevent MESD from adopting a functional conformation. W127 and I123 may especially be important in preserving interactions between secondary structures since they contact residues 154-184 which are required for MESD protein stability (Figure 6B). N133 may play a more important role in the overall integrity of helix 3, since it is located on the outer face of MESD and does not contact other regions of the protein.

Proposed model for MESD-LRP interaction

Unlike chaperonins which adopt an open conformation when bound to ADP and a closed conformation when bound to ATP, MESD does not contain an ATP binding site (Gomez-Puertas et al., 2004). Instead, in collaboration with Hartmut Oshkinat's group, we predict a dynamic model for MESD where the substrate (unfolded LRP β-propeller/EGF) competes with the interactions between the N-terminal α-helix and core (K103-D64, M54/L57-hydrophobic core) to generate the conformation change in the N-terminal α-helix.

In this model, binding of the basic residues from the first β-sheet of the fully unfolded β-propeller/EGF domain with the MESD acidic tip may disrupt the putative salt bridge formed between K103 and D64 and facilitate release of the loosely associated N-terminal helix from the core domain. This would expose the hydrophobic domain of MESD as well as several hydrophobic residues on the N-terminal helix, facilitating the stabilization of unfolded propeller blades as adjacent propeller blades are assembled. As a consequence, the positively charged β-propeller unit can then wrap around the negatively charged N-terminal helix of MESD, mediating the closure of the propeller ring (Figure 7B). Finally, hydrophobic contacts between the β-sheets of MESD and the adjacent EGF domain favor the critical positioning of the EGF with the third propeller blade (Figure 7C). Evidence supporting the interaction between these two domains comes from a binding assay that demonstrates the propensity of MESD to bind to the β-propeller/EGF interface (Koehler et al., submitted). Release of the β-propeller/EGF ring from the MESD N-terminal α-helix could potentially be mediated by a histidine switch in the LRP β-propeller, as the mature receptor encounters a pH change as it moves from the ER to

the Golgi. Alternatively, release may be facilitated by competitive substrate binding of another fully unfolded β-propeller/EGF domain.

An alternative structure for folding MESD

Recently, a third conformation for MESD was proposed by Chen et al (Chen et al., 2010). The Koehler model and the Chen model have very different structural predictions (Figure 8A, 8B). Chen predicts that the third α-helix occupies a different position in the MESD core on the opposite face of the four β-sheets, but similarly predicts that mutation of W61 disrupts interaction between MESD domains (Chen et al., 2010). Though no mechanism was hypothesized, Chen et al compared the NMR spectra between *wild-type* and W61R MESD, and determined that three independent regions exhibited large chemical shifts: the N-terminal helix, a lysine-rich linker region, and regions within the structural core residues 109-184. They predicted that these domains may be important for MESD function, but only their prediction of the importance of the N-terminal helix agrees with our data.

The lysine-rich domain was not included in the closed Koehler model, but the open Koehler model indicates a string of lysine residues in the flexible linker region between the helix 1 and the MESD core, ending with K103. I demonstrated in our mutagenesis screen that reversing the charge of K103E affects MESD activity (Figure 4). However, other lysine mutations did not affect MESD (Figure 4). Similar to individual mutations in the hydrophobic patch, it is possible that that these lysine residues cooperate to form a large positively charged domain. Although there are few acidic residues in the LRP β-propeller/EGF, each β-propeller blade contains a conserved aspartate residue in

the second β-sheet, which may interact with the positively charged MESD domain (Jeon et al., 2001). Additionally, there are a number of acidic residues in the complement-like repeats of LRPs, and the lysine-rich domain of MESD may help stabilize these domains while simultaneously promoting maturation of the β-propeller/EGF (Guo et al., 2004).

The structural core of the Koehler model can be further divided into two subdomains: one corresponds to residues 154-184, and another corresponds to the exposed hydrophobic patch. Consistent with our deletion analysis, Chen et al report chemical shifts for residues 159-184 in the W61R mutation. Residues 154-184 occupy an entire face of MESD in both the Koehler and Chen models which may account for the destabilization of MESD and subsequent inactivity when residues 154-216 are deleted. The second subdomain consists of a patch of hydrophobic residues that is transiently exposed in the Koehler model (Figure 8A). In conjunction with our mutagenesis results, the Koehler model proposes that a large number of hydrophobic residues are available to help mediate interaction with the unfolded LRP β-propeller/EGF (Figure 8A). In contrast, the Chen model proposes an alternate position for α-helix 3, masking these hydrophobic residues, rendering the hydrophobic patch unavailable to interact with LRP (Figure 8B, 8C). Although these hydrophobic residues fall within the structural core, Chen et al do not report significant chemical shifts for these residues, though they do predict that the regions around our targeted hydrophobic residues are affected in the W61R mutant (Chen et al., 2010).

Given the size and complexity of the LRP receptors we predict that regulation of receptor folding is an important task that may be the responsibility of LRP-dedicated chaperones. RAP has already been shown to promote maturation of the complement-like

repeats. I propose that the responsibility of folding the β-propeller/EGF domains falls to MESD, and will provide additional evidence to support this hypothesis in Chapter 3. Importantly, in this chapter we identified several functional domains of MESD and provided a foundation for future studies to address the previously uncharacterized physical interaction between MESD and LRP. Despite our successful mutagenesis screen, I believe that the structure of MESD directly interacting with LRP will be required to determine the absolute mechanism of MESD function given the discrepancies between the Chen and Koehler structural models for MESD.

FIGURES

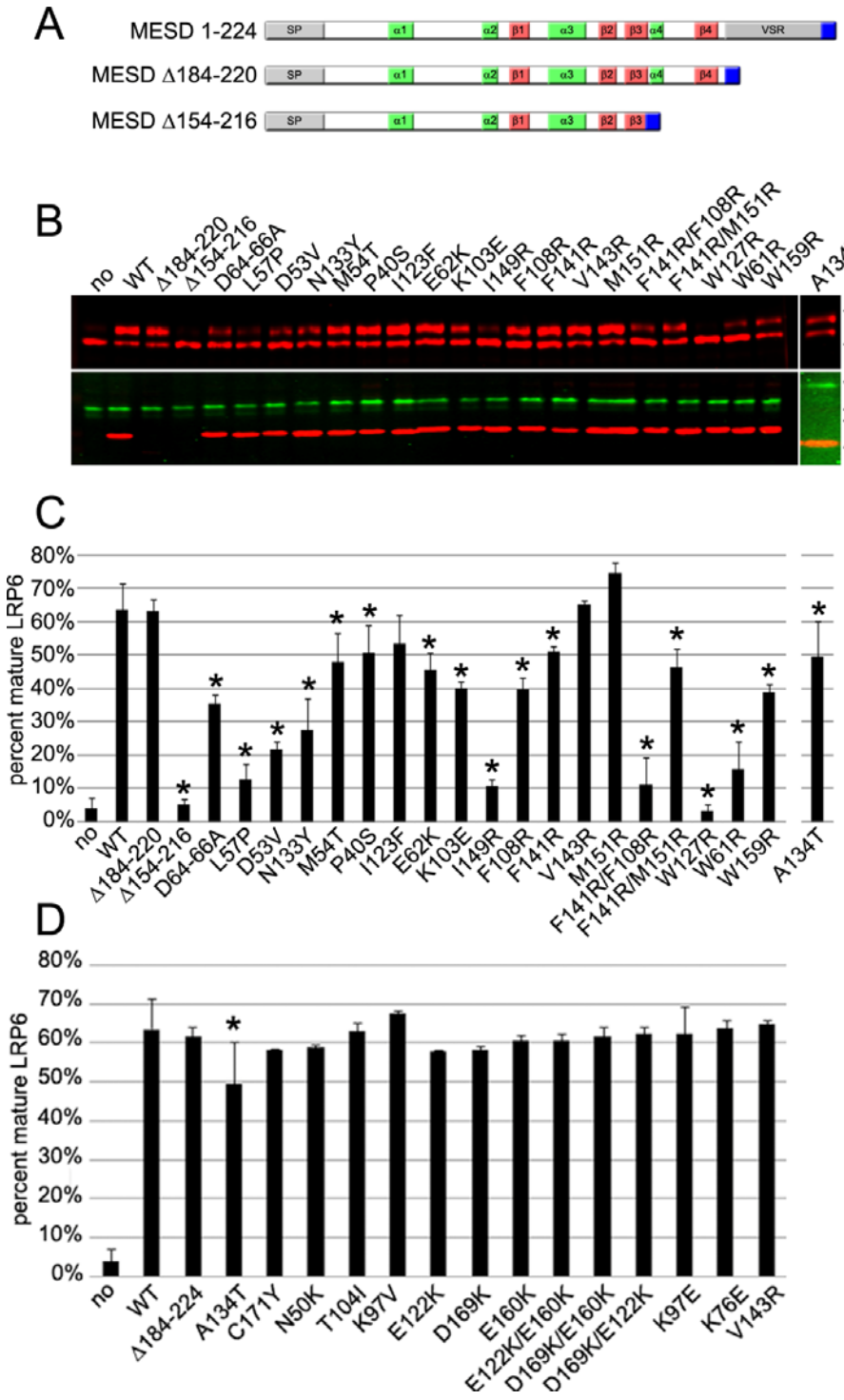
A
MESD 1-224
SP
α1
α2
β1
α3
β2
β3
α4
β4
VSR
MESD Δ184-220
MESD Δ154-216
B
no
WT
Δ184-220
Δ154-216
D64-66A
L57P
D53V
N133Y
M54T
P40S
I123F
E62K
K103E
I149R
F108R
F141R
V143R
M151R
F141R/F108R
F141R/M151R
W127R
W61R
W159R
A134T
LRP
IgG
MESD
C
percent mature LRP6
80%
70%
60%
50%
40%
30%
20%
10%
0%
D
percent mature LRP6
80%
70%
60%
50%
40%
30%
20%
10%
0%
no
WT
Δ184-224
A134T
C171Y
N50K
T104I
K97V
E122K
D169K
E160K
E122K/E160K
D169K/E160K
D169K/E122K
K97E
K76E
V143R

Figure 4. Mutations in MESD affect trafficking of full-length LRP6.

The ability of mutant MESD to traffic LRP6 was determined by assessing the maturation of LRP6 in co-transfection assays with MESD. **(A)** Diagram of MESD deletion mutants. Green boxes indicate α-helix, red boxes indicate β-sheet. Grey boxes labeled SP indicate the ER signal peptide cleaved off in the endoplasmic reticulum. Grey boxes labeled VSR indicate the vertebrate specific region. Blue boxes indicate the ER retention signal, REDL. (**B)** Western blot analysis of LRP6 maturation. COS cells at 75% confluency were co-transfected with a mixture of expression plasmids that contained full-length *Lrp6*, *Mesd*, or human IgG (*hIgG*). Cells were harvested 24 hours later, centrifuged into a pellet and lysed. 10µl of the cell lysates were run on a 6% acrylamide gel to separate the two forms of LRP6 (top gel), and another 10µl of the same lysates were simultaneously run on a 12% acrylamide gel to separate MESD and hIgG (bottom gel). (Top gel) Glycosylated mature LRP6-Rho (upper band) is separated from the lower molecular weight ER-retained LRP6-Rho (lower band) (200 kDa). (Lower gel) hIgG (transfection control, 36 kDa) and FLAG-tagged MESD are resolved (25 kDa). **(C)** The efficiency of LRP6 maturation was determined by calculating the percentage of the mature membrane form (upper band) out of total LRP6 (upper and lower bands). Mutation of acidic residues D64-66A, D53V, E62K; core residues W61R, W127R, W159R, N133Y; and hydrophobic residues F108R, F141R, I149R, F141/F108R, F141/M151R, all affected MESD activity suggesting these residues are crucial for function. **(D)** Graphical representation of the MESD mutations that do not affect MESD activity with the exception of A134T. Individual mutations of basic residues do not affect function, and combined mutation of acidic residues in the C-terminus of MESD also does not affect function. Asterisks (*) highlight mutations that result in a significant ($q < 0.05$, where q denotes the False Discovery Rate-adjusted p-value) change in the efficiency of LRP6 maturation with mutant MESD compared to *wild-type* MESD (as determined by 1-way ANOVA). Each mutation was analyzed in triplicate. Note: F141R/M151R is not significantly different compared to individual F141R or M151R mutations.

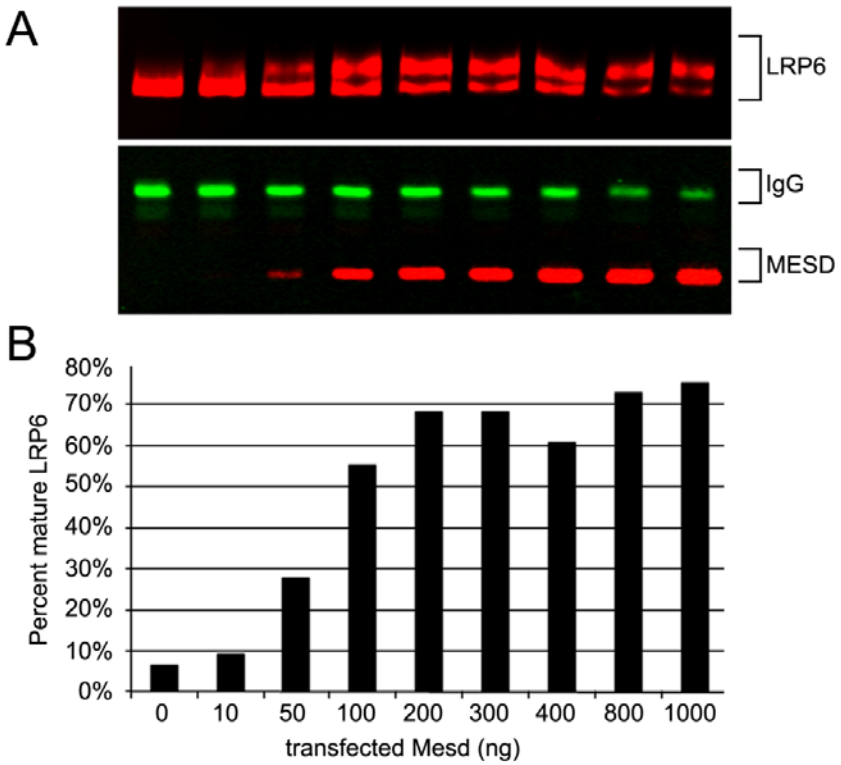

Figure 5. 300ng of *Mesd* promotes maximum LRP6 maturation.

The optimal amount of transfected *wild-type* MESD required to promote maximal amounts of mature LRP6 was determined by increasing the concentration of transfected *Mesd*, while maintaining a fixed concentration of transfected *human IgG* and *Lrp6* expression plasmids. **(A)** Western blot analysis of LRP6 maturation. (Top gel) Glycosylated mature LRP6-Rho (upper band) is separated from the lower molecular weight ER-retained LRP6-Rho (lower band) using a 6% SDS polyacrylamide gel (200 kDa). (Lower gel) hIgG (transfection control) and FLAG-tagged MESD are resolved on a 12% SDS polyacrylamide gel (25 kDa). Proteins were visualized and fluorescence quantified using the Odyssey infrared imaging system (LI-COR Biosciences). **(B)** Quantitative analysis of Western blot results. The efficiency of LRP6 maturation was determined by calculating the percentage of the mature membrane form (upper band) from the total LRP6 (upper and lower bands).

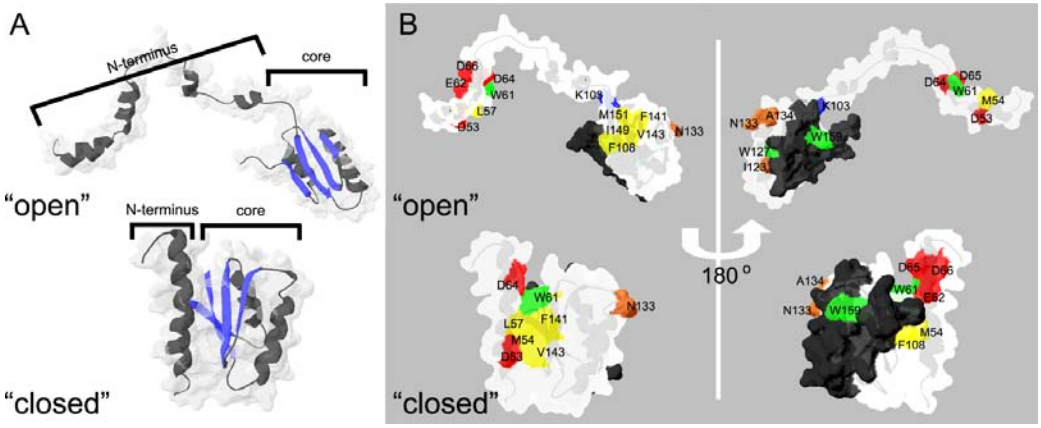

Figure 6. Mutations that affect MESD function are mapped onto the proposed protein structure of MESD 45-184 from Koehler et al.

Modified from Koehler et al 2010 (Koehler et al., submitted). MESD mutations that affect the efficiency of LRP6 maturation in Figure 5 are mapped onto the Koehler structural model for MESD. Mutations in the N-terminal helix (acidic – D64/65/66, D53, E62; hydrophobic – M54, L57; core – W61), exposed hydrophobic core (F108, F141, V143, I149, M151), or core MESD (W61, W127, W159, N133, I123, A134) residues decrease MESD function. **(A)** Ribbon diagram showing the predicted dynamic structure of MESD45-184 in the "open" and "closed" conformations. The N-terminal helix lies on one face of the β-sheets, and helix 3 and helix 4 are positioned together behind the β-sheets. Helix 2 and the linker region between the N-terminal helix and the MESD core were not shown in the Koehler model deposited in the Research Collaboratory for Structural Bioinformatics (RCSB) Protein Data Bank. β-sheets are highlighted in blue. **(B)** Space-fill diagram showing the location of mutations that affect MESD function. In the "open" conformation, the targeted hydrophobic domain is exposed (M151, I149, V143, F141, F108). In the closed conformation, only F108, F141, and V143 are visible, and the two hydrophobic residues in the N-terminal helix, L57 and M54, contact the hydrophobic patch. W61 also contacts this hydrophobic core, and I predict that the interactions between these hydrophobic residues help stabilize MESD in the closed conformation. Other stabilizing interactions include a potential salt bridge between K103 in the core and D64-66 in the N-terminus. β-sheets are highlighted in blue. Red – acidic residues, blue – lysine, yellow – hydrophobic core, green – tryptophan, brown – other core mutations, black – residues 154-184. I used Swiss PdbViewer v.4.0.1 to map the MESD mutations on the Koehler models (2RQM – open, 2RQK - closed).

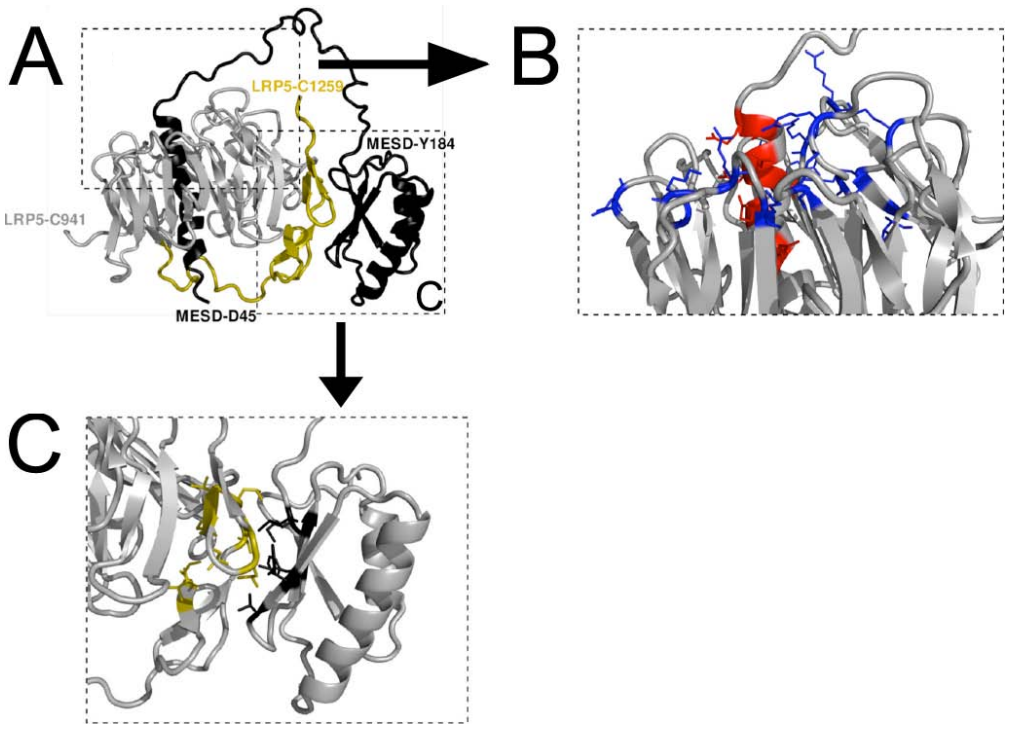

Figure 7. Proposed model for MESD-LRP β-propeller/EGF interaction.

Reproduced from Koehler, C. 2010 (Koehler et al., submitted) Folding of the LRP β-propeller/EGF is mediated by an exposed hydrophobic domain and acidic domain on MESD. **(A)** Ribbon diagram of the proposed interaction of a LRP5 β-propeller/EGF motif. MESD adopts an active, open conformation in the presence of a β-propeller/EGF where the N-terminal α-helix is extended away from the MESD core. This allows the acidic residues of the β-propeller/EGF to interact with the basic residues of the N-terminal helix and mediate the wrapping of the β-propeller around the N-terminal helix. The open conformation of MESD also exposes a hydrophobic patch normally masked by the N-terminal helix, which may stabilize the interaction of the EGF domain with the β-propeller. The N-terminus of the LRP5 β-propeller is labeled in grey (C941), and the C-terminus of the LRP5 EGF domain is labeled in yellow (C1259). MESD45-184 is in black. Box outlines indicate detailed views shown in (B) and (C). **(B)** Proposed interaction of the acidic residues at the end of the MESD N-terminal α-helix (red) and basic residues of a LRP5 β-propeller (blue). Mutation of the MESD N-terminal α-helix acidic residues may disrupt this contact, preventing the LRP β-propeller blades from wrapping around the MESD N-terminal helix. **(C)** Proposed interaction of the exposed MESD hydrophobic core (black) with the interface between the LRP5 β-propeller and EGF domains (yellow). Peptide binding assays identified an affinity for MESD to bind to the hydrophobic residues found in the packing region between LRP β-propellers and EGF domains (Koehler et al., submitted). Mutations in the MESD hydrophobic core may prevent proper alignment and packing of the EGF domain with the N-terminal β-propeller.

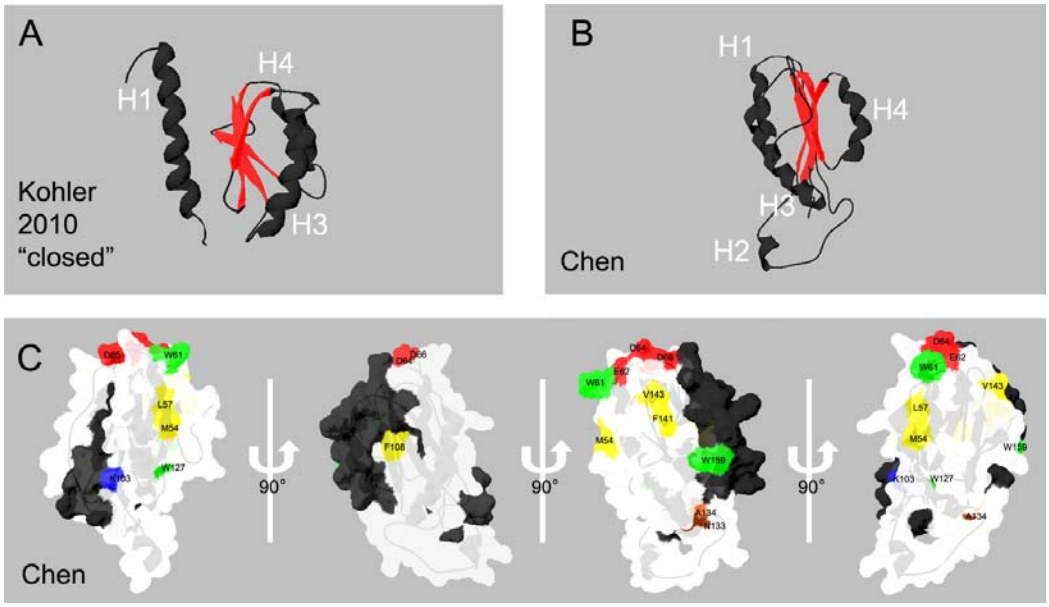

Figure 8. Comparison of Koehler and Chen structural models and mapping of mutations on the Chen model.

Modified from Chen et al 2010, and Koehler et al. (Chen et al., 2010; Koehler et al., submitted). **(A,B)** Comparison of the proposed structure of MESD from Koehler (45-184) (A) and Chen (41-184) (B). In the Koehler model, the third helix is located behind the β-sheets, separated from the N-terminal helix. In the Chen model, the third helix is instead located in front of the β-sheets and is closely associated with the N-terminal helix. **(C)** Rotations of the space-fill diagram of the proposed structure of MESD 41-184 by Chen et al. with the location of all the mutated residues that affect MESD activity from Figure 5. Mutation of exposed N-terminal acidic residues D64-66, E62 (red) affects MESD activity suggesting this domain is important for function, similar to Koehler et al. Mutation in the hydrophobic residues (yellow) also reduced activity, but may negatively affect folding of the MESD protein by altering the structure of the concealed hydrophobic core. Unlike Koehler et al, Chen et al proposes that these hydrophobic residues play a structural role in the integrity of the MESD core. Despite reducing function, these mutations do not affect MESD stability based on their expression in Figure 4B. Mutation in core residues such as W61, W127, W159, and N133 all significantly decrease MESD activity. Unlike the Koehler model, which proposes that the W61R mutant can only adopt an "open" conformation, the Chen model proposes only one conformation for MESD, and suggests that mutation of W61R shifts the position of MESD residues in the N-terminus, core, and C-terminus. Red – acidic residues, pink – other targeted N-terminal α-helix residues, blue – lysine, yellow – hydrophobic core, green – tryptophan, brown – other core residues, black – residues 154-184. RCSB Protein Data Bank accession numbers: 2RQK – Koehler closed, 2KMI – Chen.

MATERIALS AND METHODS

Expression Constructs – Construction of FLAG-Mesd and LRP6-Rho were previously described (Hsieh et al., 2003). Mesd-W61R, Mesd-Δ184-220 (Mesd-ΔVSR), and Mesd-Δ154-216 (Mesd-ΔDVSR) were generated from FLAG-Mesd by PCR amplification and subcloned into pcDNA3.1/V5-His-TOPO. EGFP-rho (EGFP/pRK5-SK) was a gift from Jen-Chih Hsieh. Human IgG heavy chain plasmid (hIgG-pRK5) was previously described (Hsieh et al., 1999; Hsieh et al., 2003). Random amino acid substitutions were generated by PCR using QuikChange Site-Directed Mutagenesis Kit (Invitrogen). Site directed mutations were generated by PCR using complementary primers encoding a single amino acid substitution. The entire pcDNA3.1/FLAG-Mesd plasmid was amplified and bacterial template was degraded with DpnI before transforming into DH5α competent cells.

Transfection of COS1 Cells – COS1 cells were seeded at 50% confluency in 12-well plates and transfected 24 hours later with a total of 1 µg plasmid DNA using Fugene 6 (Roche) following manufacturer's directions. Transfections contained 0.3 µg of *mesd,* 0.4 µg of LRP6, 0.1 µg of hIgG plasmid, 0.1µg of EGFP, and pCS2+ plasmid to bring total DNA to 1 µg. The cells were detached from the plate in 1ml of 5 mM EDTA/phosphate buffered saline (PBS), collected by centrifugation in a microfuge at 3000 rpm for 3 minutes, and lysed in 55 µl cold lysis buffer (1% Triton X-100/PBS containing final concentrations of 17mg/ml aprotinin, 10mg/ml benzamidine, 1mg/ml leupeptin, 3mg/ml antipain, 1M PMSF). 20µl of loading dye (Current Protocols in

Protein Science, vol 2) were added to each sample and boiled for 5 minutes. The lysates (10 µl each) were used for sodium dodecyl sulfate-polyacrylamide gel electrophoresis (SDS-PAGE) in the presence of β-mercaptoethanol followed by Western blot analysis. All transfections were repeated a minimum of three times. Representative Western blots are shown.

Western blotting, antibodies, image acquisition and quantitation – After transferring the proteins from SDS-polyacrylamide gels onto nitrocellulose membrane (.45µm PROTRAN, VWR) membranes were blocked overnight in 1% casein/Tris buffered saline (TBS) at 4°C, incubated with primary antibodies for 1 hour at room temperature, followed by fluorescently-labeled secondary antibody for 1 hour at room temperature. Membranes were washed with 1xTBST (0.05% Tween-20/TBS) 3x15 minutes before and after secondary antibody incubation. All antibodies were diluted in 1% casein/TBS. Rho-tagged LRP6 was detected using mouse monoclonal anti-rhodopsin (clone 1D4) at 1:1000. Flag-tagged MESD was detected using mouse monoclonal anti-FLAG (clone M2, Sigma) at 1:5000. Secondary antibody Alexa 680-labeled anti-mouse (Invitrogen) was used at 1:4000, and human IgG heavy chain was directly detected using IRDye800-labeled anti-human IgG (Rockland) at 1:10,000. Membranes were scanned using the Odyssey-Infrared Imaging System (LI-COR Biosciences), and the intensities of the bands of interest were determined from the captured images using the Odyssey imaging software.

CHAPTER 3:

MESD is Essential for the Localization of LRP2 in the Mouse Visceral Endoderm

Co-Contributors: Jen-Chih Hsieh, Liqun Zhang.

SUMMARY

MESD is a chaperone for the WNT co-receptors: Low-density lipoprotein receptor-Related Protein (LRP) 5 and 6. Loss of *Mesd* blocks gastrulation and mesoderm differentiation. Using a knockout allele, I demonstrated that *Mesd* was required for activation of WNT signaling in the epiblast and down regulation of pluripotency markers, *Oct4, Nanog, and Sox2*. Because the *Mesd* null embryo is considerably smaller than *Lrp5/6* or *Wnt3* mutants, and MESD was essential for maturation of the β-propeller/EGF domain common to LRPs in cell culture, I predicted that MESD function extends to the LRP family. Consistent with this prediction, I demonstrated that MESD was essential for apical localization of LRP2 (Megalin/MEG) and the endocytic function of the visceral endoderm. Combined, my results provide evidence that MESD functions as a general LRP chaperone, and suggest that the *Mesd* phenotype results from both signaling and endocytic defects that result from mis-folding of multiple LRP receptors.

INTRODUCTION

Functional significance of the visceral endoderm

Prior to the formation of the chorioallantoic placenta, the mouse embryo obtains maternal nutrients from the visceral endoderm (VE), which functions as a primitive placenta (Bielinska et al., 1999; Cox et al., 2009). The VE is characterized by a columnar appearance with a basally located nucleus and microvilli extending from the apical membrane (Jollie, 1990). It is morphologically and functionally similar to the gut endothelia as well as the absorptive epithelia in kidney proximal tubule cells (Bielinska et al., 1999). The VE is a tissue that is required to absorb proteins and fatty acids for early embryonic development. Receptors on the apical surface allow the VE to endocytose ligands and digest them to raw materials such as amino acids and fatty acids which can then be utilized by the developing embryo (Jollie, 1990).

Cholesterol and fatty acids play an integral role in early embryonic development. Both are found in lipoproteins, and constitute a large percentage of lipoprotein volume (Sibmooh et al., 2004). Cholesterol is not only required for membrane fluidity and lipid raft formation, but it is also required for steroid hormone synthesis (Woollett, 2005). Defects in fetal cholesterol synthesis often result in congenital birth defects, underscoring the importance of cholesterol in development (Herman, 2003). In the adult, lipoproteins are synthesized by the liver and in the embryo, the VE is capable of lipoprotein synthesis (Farese et al., 1996). However, lipoprotein synthesis cannot occur *de novo* and requires glucose to produce acetyl-coA, the backbone of many fatty acids. Lipoproteins consist of a mixture of fatty acids and cholesterol esters, where fatty acids such as linoleic acid can

only be supplied through the diet (Evans, 1960; Denisenko and Klimov, 1975; Dutta-Roy, 2000). This suggests that in addition to synthesizing lipoproteins, the VE is also responsible for the uptake of maternal cholesterol and dietary essential fatty acids. In support of this hypothesis, the VE has been shown to endocytose and efflux maternal cholesterol to the developing embryo, and studies in hamsters demonstrate that fetal cholesterol levels fluctuate depending on the amount of maternal cholesterol levels (Jollie, 1990; Woollett, 2005; Burke et al., 2009). Furthermore, disruption of a fatty acid transport protein expressed in the VE, FATP4, results in embryonic lethality by E 9.5 suggesting that the maternally provided fatty acids are required for embryo viability (Gimeno et al., 2003).

Megalin/LRP2 is an LRP family member expressed in the apical visceral endoderm

There are a number of receptors that bind lipoproteins. The most well-known receptors belong to the Low-density lipoprotein receptor-Related Proteins (LRP). Among these receptors is LRP2 which can bind to both ApoB and ApoE proteins found in lipoproteins (Moestrup and Verroust, 2001). As described in Chapter 2, LRP family members share structural similarities, notably an extracellular domain consisting of various arrangements of β-propeller/EGF domains and complement-like repeats (CLR) (Strickland et al., 2002). LRP2 contains 7 β-propeller/EGF domains, 9 additional EGF domains, and 36 CLR domains (Strickland et al., 2002). LRP2 is also known as megalin (MEG) and was originally characterized as the gp330 receptor in the kidney proximal tubule (Chatelet et al., 1986a). LRP2 in the kidney and VE is found in a complex with two other membrane receptors. One is a transmembrane receptor, Amionless (AMN),

and the other is Cubilin (CUBN) which lacks a transmembrane domain and depends on AMN and LRP2 for endocytosis (Kozyraki et al., 1999; Strope et al., 2004).

In Chapter 2, I demonstrated that the LRP5/6 β-propeller/EGF domains depend on MESD for trafficking (Lighthouse et al., submitted). Given the abundance of these domains in Megalin as well as the other LRPs, we predicted that these receptors would also require MESD for trafficking. MESD was originally shown to promote maturation of Wnt co-receptors LRP5/6. Embryos homozygous for deletions that encompass *Mesd* lack mesoderm and are unable to establish the posterior primitive streak (Holdener et al., 1994; Hsieh et al., 2003). The *Mesd* deficient polarity defects are similar to that observed in *Wnt3* or *Lrp5/6* knockouts (Liu et al., 1999; Kelly et al., 2004), suggesting that the *Mesd* interval is essential for Wnt signaling. However, embryos homozygous for deletions encompassing *Mesd* are considerably smaller, and have significantly expanded parietal endoderm compared to *Wnt3* or *Lrp5/6* mutant embryos. This phenotypic observation, combined with the *in vitro* studies presented in Chapter 2 (Lighthouse et al., submitted), suggests that the *Mesd* growth defect may result from improper maturation of related LRPs. This difference in phenotype opens the possibility that MESD function extends more broadly to trafficking multiple members of the LRP family.

In this chapter, I provide new insight into the trafficking of LRP family members and establish MESD as an important LRP-specific chaperone. To investigate the *in vivo* role of MESD for LRP function, we generated a targeted deletion of *Mesd*. Embryos homozygous for the *Mesd* knockout displayed similar polarity defects to the larger deficiency, maintain expression of pluripotency genes in the epiblast, and fail to differentiate mesoderm. In addition, loss of MESD disrupted apical membrane

localization of LRP2, but did not affect localization of AMN or CUB. Consistent with the importance of LRP2 in endocytosis, the VE in *Mesd* mutants was characterized by smaller and fewer lysosomes. These results indicate that MESD's role is not limited to maturation of LRP5/6 and WNT signaling, and demonstrate that MESD likely functions as a specific chaperone for the LRP family. For this reason, phenotypic differences between *Mesd* mutant and *Wnt3* or *Lrp5/6* mutant embryos, likely result from a global defect in MESD-mediated LRP maturation.

RESULTS

Loss of *Mesd* blocks epiblast differentiation and WNT signaling

The *Mesd* deletion phenotype was originally characterized using albino deletions that remove approximately 39 genes from a nearly 4 Mb region of chromosome 7 (Holdener et al., 1994; Hsieh et al., 2003). A *Mesd* (formerly *Mesdc2*) transgene, can restore mesoderm differentiation and gastrulation in deletion homozygotes (Hsieh et al., 2003), suggesting that these defects result from loss of a single gene from the deletion interval. To verify that other genes within the deletion do not contribute to aspects of the deletion phenotype not observed in *Wnt3* or *Lrp5/6* mutant embryos, Liqun Zhang generated a *Mesd* knockout, $Mesd^{tm1bch}$ (also referred to as *Mesd-KO*). In the *Mesd-KO* allele, most of *Mesd* exon 1 and all of exons 2 and 3 are replaced with a neomycin resistance gene (Figure 9A). Liqun Zhang used Southern blot analysis to distinguish the *Mesd-KO* allele from the parental allele; I also used a PCR strategy to distinguish between these alleles (Figure 9B and Methods).

Whole-mount analysis of embryos obtained from intercrossing animals heterozygous for the *Mesd-KO* demonstrated that the knockout and deletion phenotypes were indistinguishable (Figure 9C) (Wines et al., 2000). At embryonic day (E) 7.5, *wild-type* littermates were undergoing gastrulation. The primitive streak was fully extended, and mesoderm differentiation was well underway (Figure 9C, left). In contrast, embryos homozygous for the *Mesd-KO* were characterized by expanded parietal endoderm surrounding an underdeveloped egg cylinder lacking a primitive streak and any

mesodermal derivatives (Figure 9C, right), similar to that described for deletion homozygotes (Wines et al., 2000; Hsieh et al., 2003).

I also observed similarity between *Mesd* deletion homozygotes and the *Mesd-KO* using molecular markers. In *wild-type* embryos at E 8.5, *T* was expressed in the primitive streak as well as in the notochord (Figure 10A). As gastrulation progressed and the *wild-type* epiblast differentiated, the pluripotency markers *Oct4*, *Nanog* , and *Sox2*were characteristically down regulated (Figure 10C, E, and G) (Scholer et al., 1990; Avilion et al., 2003; Chambers et al., 2003; Hart et al., 2004). In contrast, *T* transcripts were expressed in *Mesd-KO* (n = 2) littermates in the extraembryonic ectoderm adjacent the epiblast (Figure 10B) and *Oct4* expression persisted in the epiblast (Figure 10D). These patterns are similar to that observed in deletion homozygotes and in *wild-type* embryos prior to gastrulation (Hsieh et al., 2003). Similarly, I observed continued expression of *Sox2* (n = 7) and *Nanog* (n = 3) throughout the *Mesd-KO* epiblast (Figure 10F, H) despite their down-regulation in *wild-type* littermates (Figure 10E, G). These data suggest that MESD function is essential for repression of pluripotency markers and subsequent differentiation of the epiblast.

I hypothesized that the loss of primitive streak formation and mesoderm differentiation in *Mesd* mutant embryos results from a block in WNT signaling, despite the expression of *Wnt3* in E 7.5 *Mesd* mutants (Hsieh et al., 2003). To determine if Wnt signaling was activated in *Mesd* mutants, I introduced a Wnt-reporter, BAT-gal, into the *Mesd-KO* background, and tested the ability of mutant embryos to activate the reporter (Figure 11). Embryo genotypes were confirmed by PCR (Figure 11 insets). This BAT-gal reporter encodes nuclear β-galactosidase under the control of a β-catenin-sensitive

bipartite promoter containing 7 TCF-LEF binding sites upstream of a minimal *Siamois* promoter (Maretto et al., 2003). X-gal staining in embryos heterozygous for *Mesd-KO* identified active WNT signaling in the primitive streak and nascent mesoderm at E7.5 (Figure 11A). β-gal activity was not detected in *Mesd-KO* embryos that carry the BAT-gal reporter, confirming that loss of *Mesd* blocks WNT signaling (Figure 11B).

The β-propeller/EGF domain of LRPs depends on MESD for proper folding

The *Mesd* phenotype is characterized by failure to form a primitive streak or differentiate mesoderm. The phenotype is similar to knockout of *Wnt3* or *Lrp5/6*. However, unlike *Wnt3* and *Lrp5/6*, the *Mesd* epiblast is smaller and surrounded by an expanded parietal endoderm (Figure 9C). These phenotypic differences suggest that MESD function extends beyond LRP5/6 trafficking. To begin to identify other proteins that might require MESD function, Jen-Chih Hsieh mapped LRP5/6 domains that require MESD for trafficking (Figure 12). To accomplish this, we utilized a soluble receptor secretion assay in which we assayed the ability of COS-1 cells to secrete soluble truncated LRP5/6 receptors (Figure 12A) in the presence or absence of MESD. Transfection of human IgG was used as a transfection and secretion control. In the absence of exogenous MESD, soluble receptors containing the entire extracellular domain of LRP6 (LRP6 ECD) were not secreted into the media unless *Mesd* was co-transfected, suggesting that the extracellular domain of LRP6 is highly dependent upon MESD (Figure 12B). We saw similar dependency on *Mesd* co-transfection for secretion of soluble LRP5 and LRP6 receptors containing two, three, and four β-propeller/EGF domains (LRP6 βP1-2, βP1-3, and βP1-4) as well the first LRP5 β-propeller/EGF domain

(LRP5 βP1). In contrast, the first LRP6 β-propeller/EGF domain (LRP6 βP1) is secreted independently of exogenous MESD, though LRP6 constructs containing multiple β-propeller/EGF domains that include LRP6 βP1 do require MESD for maturation. Together, these observations demonstrated that MESD facilitates trafficking of the β-propeller/EGF domains of LRP5 and 6, and are consistent with previous data suggesting a similar role for Boca (Culi et al., 2004). In addition, these data suggest that individual β-propeller/EGF domains may have distinct requirements for MESD, and that receptors containing increasing number of β-propeller/EGF domains could have greater dependency upon MESD for trafficking. This raises the possibility that MESD *in vivo* may facilitate trafficking of LRPs other than LRP5/6, and suggested that differences between the *Mesd-KO* and *Wnt3* or *LRP5/6* mutant embryos could result from defects in trafficking of these receptors. Consistent with this prediction, we determined that the LRP1 second β-propeller/EGF (LRP1 βP2) also required exogenous MESD in the soluble receptor secretion assay (Figure 12B).

LRP2 requires MESD for apical membrane localization

To determine which LRPs have the potential to contribute to the *Mesd* mutant phenotype, I characterized the expression of LRP receptors that contain β-propeller/EGF domains at E 6.5 and E7.5 using RT-PCR (Figure 13). I detected transcripts from all the LRPs with the exception of LRP1b, which is not expressed until after E 11 (Li et al., 2005). Among these receptors, *Lrp1* and *Lrp2* were strongly expressed and are two of the largest members of the LRP family, containing seven and eight β-propeller/EGF domains, respectively. Given the results from our *in vitro* secretion assays, I predicted

that the maturation of these receptors will be highly sensitive to the presence or absence of MESD.

LRP1 and 2 are strongly expressed in the VE. LRP2 was present on the apical membrane in a complex with Amnionless (AMN) and Cubilin (CUBN), similar to what is reported for other absorptive epithelia (Figure 14A, A', B, C) (Sahali et al., 1988; Kalantry et al., 2001; Kozyraki and Gofflot, 2007). I also observed LRP2 on the apical surface of the epiblast, although the distribution appeared more punctate than that observed on the VE membrane (Figure 14G'). In the absence of *Mesd*, LRP2 was detected in a diffuse intracellular pattern in the VE and epiblast (Figure 14D, D', H'). In contrast, loss of MESD did not interfere with the apical localization of AMN and CUBN (Figure 14 E, F), suggesting that MESD function is not generally required for trafficking of apically localized proteins or for localization of proteins that contain only the EGF motif (CUBN) or cysteine-rich domains (AMN) and does not generally interfere with trafficking of extra-cellular proteins (Moestrup et al., 1998; Tanner et al., 2003). Moreover, the aberrant localization of LRP2 in *Mesd* mutants provided *in vivo* evidence that MESD function was not limited to LRP5/6, but extended more broadly to the LRP family of receptors.

To determine if loss of MESD simultaneously disrupted localization and function of multiple LRP family members, I performed an endocytosis assay using receptor associated protein (RAP), which specifically binds to the complement-like repeats in the extracellular domain of LRPs (Herz et al., 1991; Bu and Schwartz, 1998). This approach was used to measure expression of membrane-localized, functional LRP1 in cortical neurons (Bu et al., 1994). Using a similar approach, I compared the uptake of

fluorescently labeled RAP (488-RAP) in *wild-type* and *Mesd* mutant embryos (Figure 15). The VE of *wild-type* embryos labeled extensively (Figure 15A, A'); whereas in the presence of 200-fold excess unlabeled RAP, labeling of the VE was greatly reduced. (Figure 15B, B'). In contrast, *Mesd* mutant VE showed a significant decrease in fluorescence, at levels comparable to that observed when *wild-type* embryos were incubated with unlabeled RAP (Figure 15C, C'). These results suggested that loss of *Mesd* disrupts general LRP function in the VE.

Loss of MESD results in smaller lysosome size in visceral endoderm

In the VE, LRP2 likely functions as a scavenger receptor similar to its role in the kidney (Willnow et al., 1996; Verroust et al., 2002). Kidney proximal tubule cells from LRP2-deficient mice fail to endocytose transferrin, lysozyme, vitamin-D binding protein, or retinol-binding protein. Instead, these proteins are improperly excreted into the urine (Leheste et al., 1999; Kozyraki et al., 2001). For this reason, I predicted that loss of a prominent scavenger receptor such as LRP2, and more likely loss of both LRP1 and LRP2, from the apical cell surface of the VE will impair endocytosis in the VE.

Ultrastructural comparison of *wild-type* and *Mesd-KO* embryos provided indirect evidence that endocytosis was impaired in the *Mesd-KO* (Figure 16A, B). In the *wild-type* embryo (Figure 16A), the visceral endoderm cells are columnar in shape with a basally located nucleus. The apical membrane of the VE is populated by numerous microvilli that maximize the surface area available for membrane receptor localization and absorption of proteins and complexes, similar to that observed in the cells in the kidney proximal convoluted tubule (PCT) (Moestrup and Verroust, 2001). In addition, the VE contains

numerous membrane-enclosed organelles in the cytoplasm, thought to be endocytic components including endosomes and lysosomes (Nagy, 2003). Although the VE cells from *Mesd-KO* embryos (Figure 16B) appeared shorter in height, they maintained apical-basal polarity and contained numerous apical microvilli and a basally-localized nucleus. In addition, I observed the fine network of ER, as well as a number of mitochondria throughout the cytoplasm indicating a basic level of normal cell function. In contrast, both the size and number of the membrane-enclosed organelles was reduced significantly in *Mesd-KO*. Given the role of LRP2 and LRP1 in endocytosis of ligands/nutrients, I hypothesized that the ultrastructural defects reflected a reduction in either endosomes or lysosomes resulting from loss of LRP-mediated endocytosis.

Lysosomes are collectively identified as membrane-enclosed organelles that contain acid hydrolases and integral lysosomal membrane proteins (Luzio et al., 2007; Saftig and Klumperman, 2009). Lysosomes can form by fusion of late endosomes and serve to breakdown material delivered through late endosomes, phagosomes, and autophagosomes (Saftig and Klumperman, 2009). I observed similar apically localized EEA1-positive early endosomes in both *wild-type* and *Mesd* mutant embryos (Figure 16C and D, magenta), suggesting that loss of *Mesd* does not generally impair endocytosis. In contrast, in *wild-type* embryos, LAMP antibodies identified large vacuole-like lysosomes throughout the apical cytoplasm (Figure 16C and C', green). These structures were concentrated basally to the early endosomes. Despite the normal distribution of early endosomes in *Mesd-KO* embryos, lysosomes were reduced both in size and number in mutant embryos (Figure 16D, D', green). I confirmed the reduction in lysosome number and size with LysoTracker Red staining (Figure 16E and F). In *wild-type* embryos,

LysoTracker Red labeled round lysosomes that averaged 2.5μm in diameter with a standard deviation of .38μm (Figure 16E) (Koike et al., 2009). In contrast, lysosomes in *Mesd-KO* embryos were less abundant, more granular, and considerably smaller in diameter, averaging 1μm in diameter with a standard deviation of .36μm (Figure 16F). Quantification of *wild-type* LysoTracker Red staining using ImageJ resulted in an average pixel intensity of 63, where quantification of Mesd LysoTracker Red staining resulted in an average pixel intensity of 27, or 43% of *wild-type* LysoTracker Red staining. These observations are consistent with the absence of large membrane-bound organelles in TEM images of mutant VE (Figure 16A, B). In LRP2-deficient kidney proximal tubule cells, the size of the lysosomes are similarly reduced, suggesting that lysosome size can be regulated by the amount of ligand uptake (Christensen et al., 2003; Nielsen et al., 2007). Taken together, these studies provide evidence that that MESD-dependent LRP localization regulates endocytosis and lysosome formation in the VE.

DISCUSSION

In this chapter, I demonstrated that MESD function *in vitro* is essential for maturation of the LRP5/6 and LRP1 β-propeller/EGF domains. Furthermore, soluble receptors that contained two or more β-propeller/EGF domains increasingly depended on exogenous MESD for maturation. Most LRPs contain at least one β-propeller/EGF domain, and LRP1 and LRP2 contain seven and eight domains, respectively (Strickland et al., 2002). For this reason, we hypothesized that MESD function extends to the LRP family of receptors, and predicted that phenotypic differences between *Mesd* deletion homozygotes and *Lrp5/6* or *Wnt3* knockouts resulted from defects in trafficking multiple LRPs. By characterizing a *Mesd* knockout, I provided *in vivo* evidence that MESD is essential for WNT signaling. Continued expression of *Oct4*, *Nanog,* and *Sox2* in *Mesd* mutants suggests that WNT signaling is essential for epiblast differentiation. Consistent with this hypothesis, *Wnt3* mutants express *Oct4* and neither *Wnt3* nor *Lrp5/6* mutants differentiate mesoderm (Liu et al., 1999; Kelly et al., 2004). The continued expression of pluripotency markers in *Mesd* and *Wnt3* mutant embryos is striking considering these mutants do not maintain expression of *Nodal,* and *Nodal* mutant epiblast lose expression of pluripotency markers and differentiate into neural precursors (Camus et al., 2006). Finally, we demonstrated that MESD is essential for apical localization of LRP2 and the endocytic function of the VE.

In the early post-implantation mouse embryo, the VE functions as an absorptive epithelium, as well as a signaling tissue (Beddington and Robertson, 1999; Bielinska et al., 1999; Baron, 2005). As an absorptive epithelium, the VE is responsible for filtering

nutrients provided by the maternal bloodstream for early embryonic development to the developing embryo (Brent et al., 1990; Jollie, 1990; Cross et al., 1994; Bielinska et al., 1999). The absence of VE abnormalities in the *Lrp2* knockout opens the possibility that structurally similar LRPs compensate for loss of LRP2 in the VE. *Lrp1* and *Lrp2* (Megalin) are structurally very similar and are both expressed in the VE (Chatelet et al., 1986b; Herz et al., 1992), suggesting that these receptors could functionally substitute for one another. However, their role in VE endocytosis was not appreciated since these defects are not present in either *Lrp1* or *Lrp2* knockouts. *Lrp1* mutants were recovered at E 13.5, with defects in neural tube patterning (Herz et al., 1992), and *Lrp2* mutants were recovered at birth, with 2% surviving to adulthood (Willnow et al., 1996; Nykjaer et al., 1999). In the rare surviving *Lrp2* mutant adults, defects in apical endocytic components of the kidney proximal convoluted tubule and proteinuria of LRP2-ligands, vitamin-D binding protein and retinol-binding protein, are consistent with our prediction that LRP2 is important for absorption in the VE (Christensen and Willnow, 1999; Leheste et al., 1999). However, VE absorption defects were not described in LRP2 knockouts, suggesting that related LRPs could compensate for lack of LRP2. LRP1 is similar in structure and is also expressed in the VE (Herz et al., 1992). Since the LRP1 β-propeller/EGFs also required exogenous MESD for trafficking in cell culture, the VE endocytosis defects observed in *Mesd* mutants likely resulted from simultaneous misfolding of LRP1 and LRP2. This hypothesis is supported by the decreased endocytosis of 488-RAP in the visceral endoderm of *Mesd* mutant embryos.

Other mouse mutations that disrupt endocytosis or trafficking in the visceral endoderm, including *Dab2, Amn, Cubn,* and *Enpp2,* share some similarity to the *Mesd*

mutant phenotype. Endocytosis of LRP2 depends on the disabled homologue-2 (Dab2) adaptor protein that binds the intracellular NPxY motif of LRP2 as well as clathrin and AP2 (Morris and Cooper, 2001; Mishra et al., 2002). *Dab2* mutants also fail to gastrulate and display a loss of apical vacuoles (Morris et al., 2002; Maurer and Cooper, 2005). However, *Dab2* mutants fail to pattern the anterior VE (AVE), suggesting that loss of *Dab2* has a wider range of effects than *Mesd.* On the apical surface in the VE, LRP2 complexes with membrane receptors Amnionless (AMN) and Cubilin (CUBN) (Strope et al., 2004). Mutations in either AMN or CUBN decrease the volume of the apical VE, suggesting that these mutations could also impair absorption (Strope et al., 2004; Smith et al., 2006). However, unlike the more severe *Mesd* or *Dab2* phenotypes, disruption of *Amn* only blocks paraxial and lateral plate mesoderm differentiation resulting in embryonic lethality before E 11.5. Disruption of *Cubn* generates an almost identical phenotype to *Amn* and mutant embryos are not recovered at E 13.5. However, *Cubn* mutants exhibit a morphological defect in the definitive endoderm not reported in the *Amn* mutant (Tomihara-Newberger et al., 1998; Smith et al., 2006). Finally, *Enpp2* mutant embryos show similar fragmentation of the characteristically large VE lysosomes (Koike et al., 2009). *Enpp2* encodes a lysophospholipase enzyme that regulates lysosome size by stimulating the Rho-ROCK-Lim pathway (Koike et al., 2009). Although mutant embryos retain the ability to differentiate mesoderm and begin neurulation, the growth of the mutant embryos is significantly impaired. Similarly, the lysosome size defect observed in the VE of *Mesd* mutants may also be due to as of yet unknown signaling pathways downstream of the LRP receptors. Combined, these mutant phenotypes suggest that growth defects in *Mesd* mutants could result from impaired endocytosis and

absorption of nutrients. However, because of the role of LRP1 and 2 in signaling (May et al., 2005; Lillis et al., 2008) we cannot exclude the possibility that defects in VE signaling also contribute to the *Mesd* mutant phenotype.

Combined, these studies provide convincing evidence that MESD facilitates trafficking of the LRP YWTD β-propeller/EGF domain and can function as a general LRP chaperone. The receptor-associated-protein (RAP) similarly facilitates trafficking LRPs through interaction with the LDL-A cysteine rich complement region (Andersen et al., 2000; Fisher et al., 2006). In contrast to *Mesd* mutants, *Rap*-/- mice are viable and fertile (Willnow et al., 1995; Birn et al., 2000). Since LRPs contain both β-propeller/EGF as well as LDL-A domains, I predict that MESD likely plays a more central role in LRP maturation and function than RAP. This is consistent with the recent proposal that the YWTD containing β-propeller repeat could facilitate release of RAP from the LRP LDL-A domain (Jensen et al., 2009). This would suggest that RAP function is dependent upon MESD mediated folding of the β-propeller/EGF domain. Given the diverse and overlapping roles of LRPs in endocytosis and cell signaling (Willnow et al., 2007), I predict conditional *Mesd* mutations will facilitate the analysis of functional redundancy among LRP members as well as the contribution of LRP misfolding to the development of diseases as diverse as atherosclerosis, Alzheimers, diabetes, osteoporosis, and kidney disease.

FIGURES

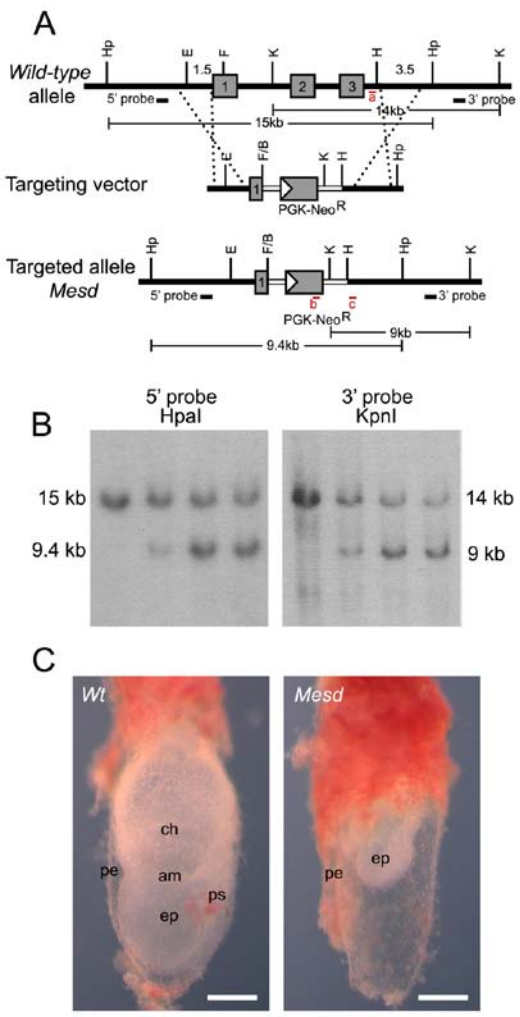

Figure 9. Generation of *Mesd*^{tm1bch} (*Mesd-KO*).

Work in (A,B) done by Liqun Zhang. **(A)** Targeted disruption of *Mesd*. The coding region of *Mesd* contains three exons (numbered gray boxes). In the targeting vector the neomycin resistance cassette partially replaces exon 1 and the entirety of exons 2 and 3. Recombination between the *Mesd* genomic locus (top) and targeting vector (middle) can occur as indicated by the dashed lines in regions of homology. Double cross over will result in the targeted allele (bottom) lacking most of exon 1, and exons 2 and 3. **(B)** Southern blot analysis of ES cell clones using a 5' probe with HpaI digested DNA and a 3' probe with KpnI digestion identified successful ES clones with a targeted disruption of *Mesd*. **(C)** The general phenotype of the *Mesd-KO* mutant compared to a *wild-type* littermate at E 7.5 was similar to the phenotype of the *Mesd* deletion phenotype previously observed (Holdener et al., 1994; Wines et al., 2000). ps, primitive streak; pe, parietal endoderm; ep, epiblast; am, amnion; ch, chorion. Scale bars in C indicate 500µm.

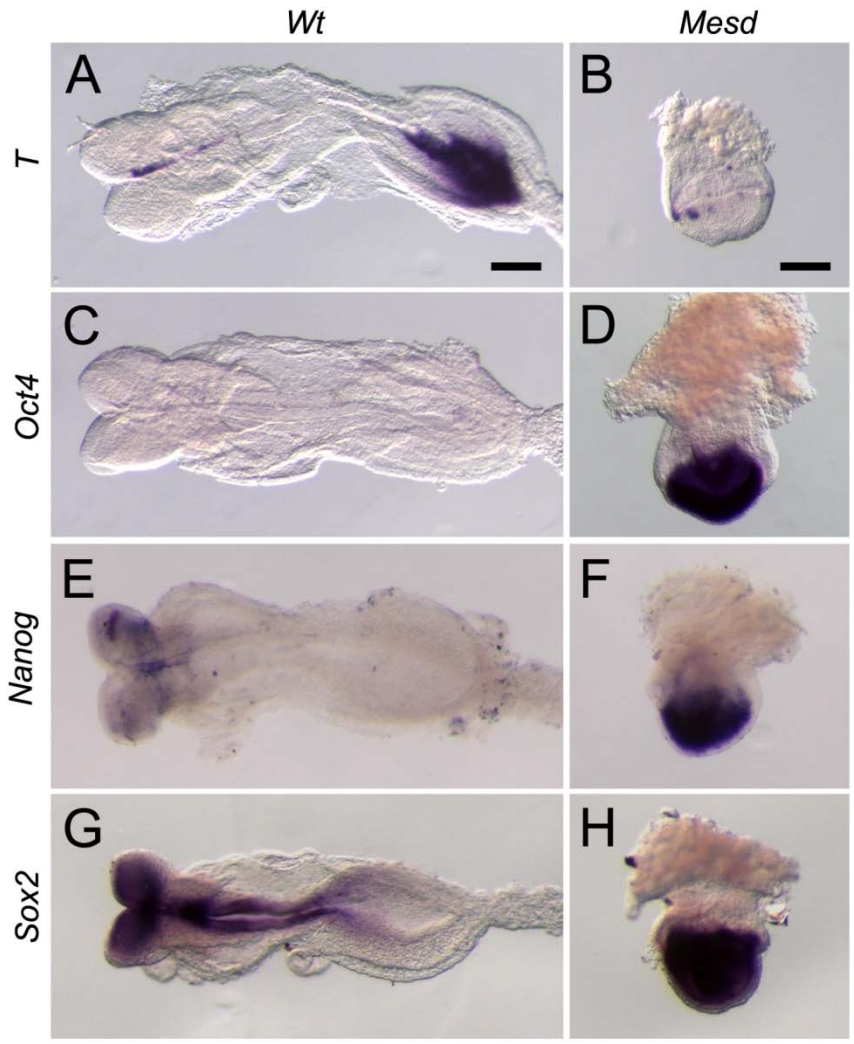

Figure 10. *Mesd-KO* embryos maintain pluripotency markers at E 8.5.

(A) *Wild-type* embryos express *T* in notochord and tail mesenchyme where **(B)** *Mesd-KO* embryos express *T* only in extraembryonic ectoderm. **(C)** *Oct4* expression was down-regulated in *wild-type*, but **(D)** maintained in the epiblast of *Mesd-KO* embryos. *Nanog* expression in **(E)** *wild-type* and **(F)** mutant embryos. *Sox2* expression in **(G)** *wild-type* and **(H)** mutant embryos. Scale bars indicate 100μm. E 8.5 mutant embryos are oriented so the anterior-posterior axis is in the z-plane.

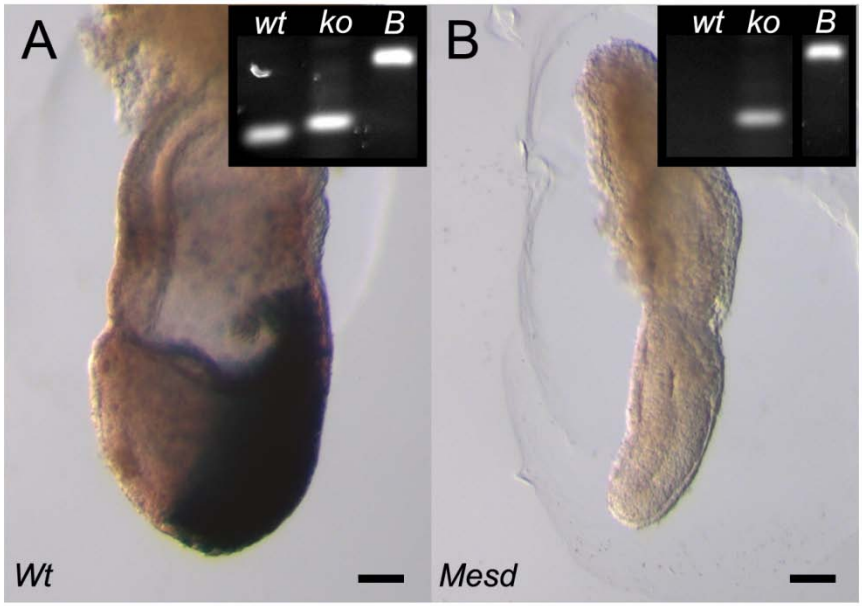

Figure 11. *Mesd-KO* embryos block WNT signaling.

(A) Embryos heterozygous for *Mesd* activated the BAT-gal reporter in the primitive streak and migrating mesoderm. **(B)** Although *Mesd* deficient embryos express *Wnt3* at E7.5 (Hsieh et al., 2003), *Mesd-KO* littermates did not form primitive streak or mesoderm and also did not activate BAT-gal reporter, indicating a defect in WNT signaling. **(Insets)** PCR genotyping confirmed embryo genotype. *wt*, *wild-type* allele; *ko*, *Mesd-KO* allele; *B*, *BAT-gal* allele. Scale bars indicate 100 µm. E 7.5 embryos are oriented with the anterior-posterior axis on the x-y plane, with the anterior on the left and posterior on the right.

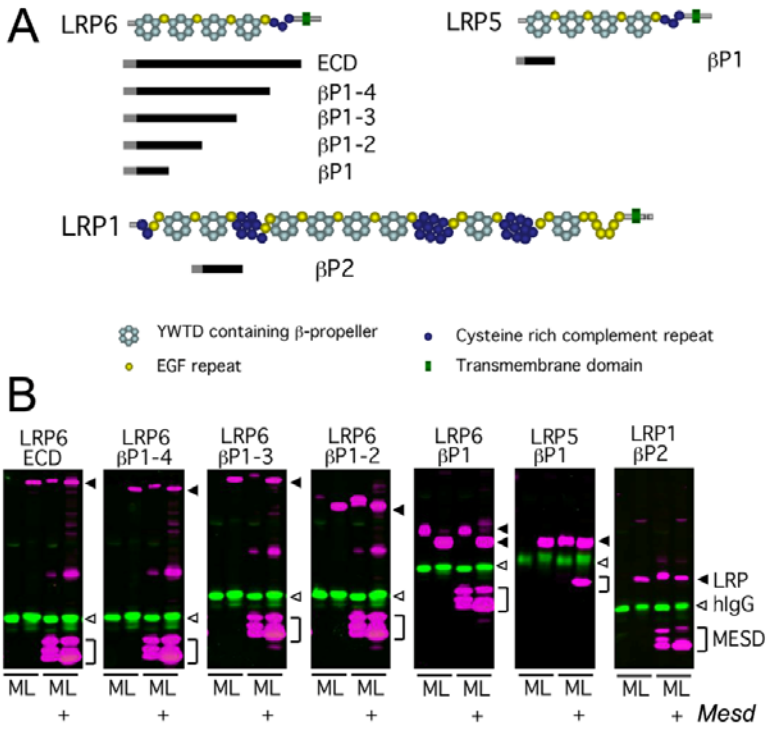

Figure 12. MESD promotes trafficking of β-propeller/EGF domains.

Experiments in this figure were performed by Jen-Chih Hsieh. We utilized a soluble receptor secretion assay to identify the minimal LRP domain that requires MESD for maturation. In this assay, soluble truncated receptors were co-transfected with or without *Mesd,* and the cell lysate (L) and media (M) collected. If the soluble receptor is dependent upon *Mesd* for maturation, we expect the receptor to accumulate in the lysate in the absence of exogenous *Mesd.* In the presence of exogenous *Mesd,* the soluble receptor transits the secretory pathway and is released into the media. **(A)** Overview of soluble receptor constructs showing a schematic representation of the predicted domain structure of the full length LRP6, LRP5, and LRP1 receptors. The extra-cellular domain (ECD) of LRPs consists of cysteine-rich complement-like repeats (CLRs, dark blue circles), Epidermal growth factor (EGF) repeats (yellow circles), and alternating YWTD containing β-propeller (light blue hexagon) and EGF domains (LRP cartoons adapted from (Strickland et al., 2002)). The black bars located below the full length LRPs indicate the portion of receptor retained in the soluble receptor constructs. The receptor construct name, indicating the β-propeller/EGF domains (βP) included in the construct, is designated to the right of the black bar. β-propeller/EGFs are numbered sequentially starting at the N-terminus. All soluble receptors lack the transmembrane domain (green triangle) present in the full length LRPs, but retain the signal peptide (grey bar) and maintain the juxtaposition of the β-propeller and C-terminal EGF motif. **(B)** Western analysis of soluble LRP5/6 or LRP1 constructs in the presence or absence of MESD. Secreted receptors are detected in the media, and immature receptors are detected in the lysate. Closed arrowhead, LRP (magenta); open arrowhead, control hIgG (green); bracket, MESD (magenta)

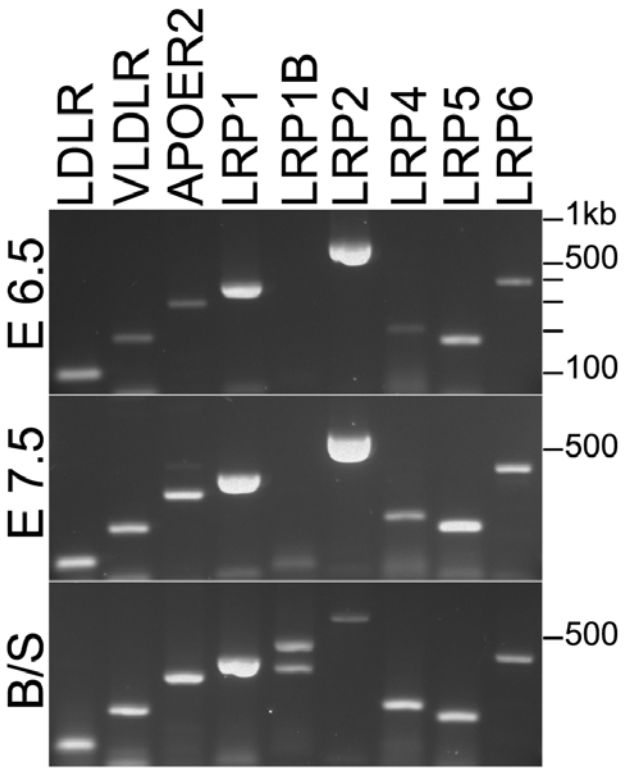

Figure 13. LRPs containing one or more β-propeller/EGF domains are expressed in *wild-type* embryos at E 6.5 and E 7.5.

Expression of LRP family members at E 6.5 (top) and E 7.5 (middle). All LRPs with the exception of LRP1B were expressed at E 6.5 and 7.5. Expression of both isoforms of LRP1B were detected in total RNA obtained from Brain and Spleen (B/S) (bottom).

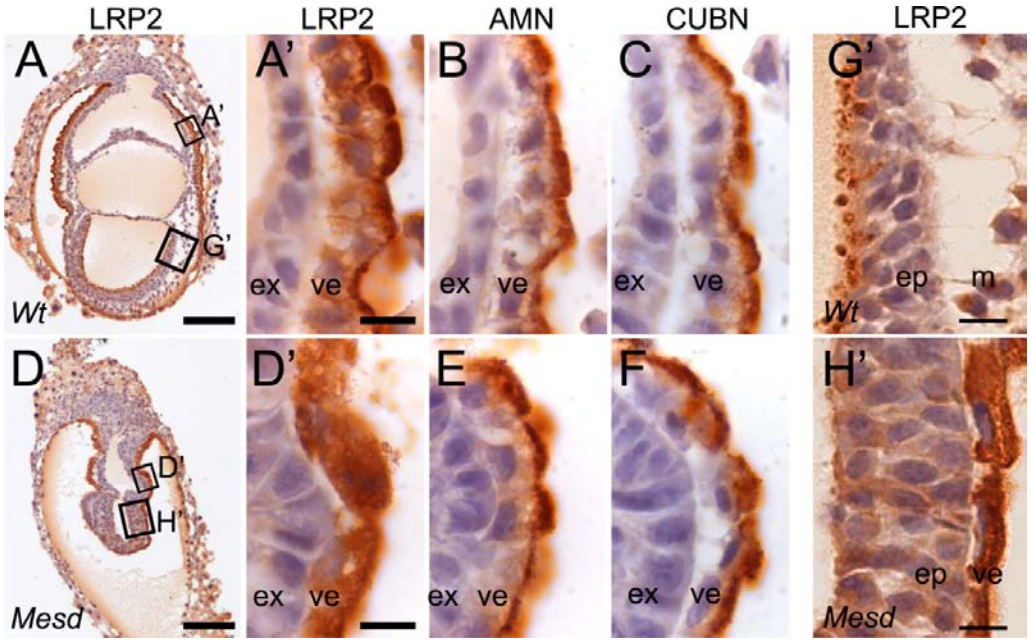

Figure 14. LRP2 requires MESD for apical membrane localization at E 7.5.

Immunohistochemistry indicated LRP2, CUBN, and AMN were apically localized in *wild-type* VE **(A, A', B, and C)**. In contrast, LRP2 was distributed diffusely throughout the *Mesd*-KO VE **(D, D')**, consistent with ER retention of improperly folded receptor (Hsieh et al.). In contrast, apical localization of CUBN and AMN was not affected by loss of MESD **(E, F)**. In addition to expression on the apical membrane of the visceral endoderm, LRP2 is also localized to the apical surface of the *wild-type* epiblast **(G')**. This localization is MESD-dependent, as epiblast expression of LRP2 appears more cytoplasmic and diffuse in *Mesd* embryos **(H')**. Black boxes in A and D indicate the region magnified in A', B, C, D', E, F, G', H'. Scale bars in A, D, G, and H indicate 100µm, and in A', D', G', and H' indicate 10µm. ep, epiblast; ve, visceral endoderm; m, mesoderm.

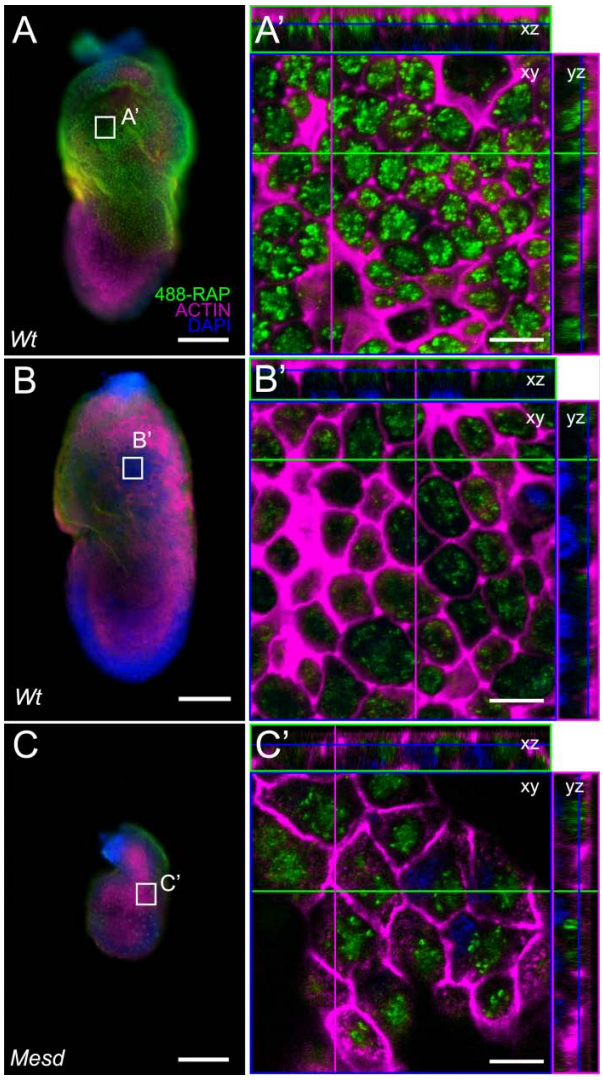

Figure 15. Endocytosis of 488-RAP is reduced in *Mesd* embryos.

E 7.5 embryos were incubated with receptor associated protein (RAP) labeled with Alexa 488 in the presence or absence of unlabeled RAP competitor. *Mesd* embryos exhibited a reduction in the amount of endocytosed 488-RAP in the absence of competitor compared to *wild-type* embryos incubated under the same conditions. This was similar to the amount endocytosed by *wild-type* embryos incubated with 488-RAP and competitor. **(A, A')** Endocytosis of 488-RAP (50nM) by *wild-type* VE at E 7.5. **(B, B')** Reduced endocytosis of 488-RAP when *wild-type* embryos are co-incubated with 50nM 488-RAP and excess 10µM unlabeled RAP. This demonstrates competition of RAP for surface-localized LRP receptors, and may also indicate LRP-independent ligand uptake mechanisms. **(C, C')** Reduced endocytosis of 488-RAP by *Mesd* VE. White boxes in A, B, and C indicate the region magnified in A', B' and C'. Scale bars in A, B, and C indicate 100µm and 10µm in A', B', and C'.

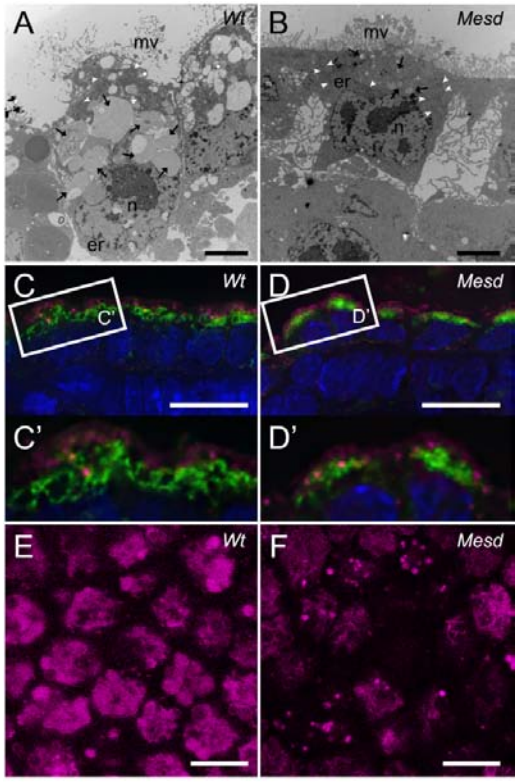

Figure 16. Lysosome size is reduced in *Mesd-KO* VE.

(A, B) TEM of sectioned embryonic VE from E 7.5 littermates. **(A)** *Wild-type* VE contained numerous small and large membrane-bound compartments (black arrows) concentrated apically relative to the nucleus (n). *Wild-type* VE cells contacted neighbors along the apical/basal boundary and thin microvilli (mv) extend from the apical surface. **(B)** VE of *Mesd-KO* embryos appeared shorter due to a decrease in vesicle size. Mutant VE had small membrane-bound compartments (black arrows), and the basal surface of the VE appeared to have lost contact with neighboring cells and the basement membrane. The apical surface had shorter and thicker microvilli (mv). TEM images at 4200x. Scale bars indicate 2 µm. er – endoplasmic reticulum, white arrowheads – mitochondria. **(C)** Identification of early endosomes (EEA1, magenta) and lysosomes (LAMP1/2, green) and nuclei (DAPI, blue) in *wild-type* VE at E 7.5. Early endosomes were more apical than the large, ring-like lysosomal structures. **(D)** We observed a reduction in the size of LAMP-positive bodies in *Mesd* VE at E 7.5, without a noticeable reduction in EEA1-positive bodies. **(C' and D')** Magnification of boxed areas in (C) and (D). **(E)** Staining of *wild-type* VE at E 7.5 with 10nM of LysoTracker Red reveals large, round lysosomes at least 2µm in diameter. **(F)** Staining of *Mesd* VE at E 7.5 showed smaller and fewer lysosomes, between 1µm and 2µm in diameter. Images were deconvolved using the Zeiss iterative deconvolution filter and nine images through 1.8µm were stacked to produce the images shown in Figure C and D. A single deconvolved Z-stack is shown in Figure C' and D'. Scale bars in (C, D, E, F) indicate 10µm.

LRP	PRIMER	REF.
LDLR	5’-CTGTCCCCCCAAGACGTG-3'	1
	5’-CCATCTAGGCAATCTCGGTCTC-3'	1
VLDLR	5'- CAGCAGTATCAGAAGTCAGTGTTC-3'	2
	5'-CAGGTCCTCTTCAGTGGTCTTC-3'	2
APOER2	5'-CAACCACTCCCAGCATTA-3'	2
	5'-CAGTGGGCGATCATAGTTG-3'	2
LRP1	5’-AGTGCTGCCCAGACACAGCTCAAGTGTG-3'	3
	5'-CACCAAGCTGGTGGATAGCAAGATCGTG-3'	2
LRP1B	5’- TTTTGAATTCTCCAGGTACATAGGGGGAGGGTCCAGTGCTTTC-3'	4
	5’- AATTGGATCCTTATGCTACTGTTTCTCTGATGCCAATTTC-3'	4
LRP2	5’- CCTTGCCAAACCCTCTGAAAAT-3'	5
	5’- CACAAGGTTTGCGGTGTCTTTA-3'	5
LRP4	5’- CAGTGAAGATGTAAAGTGG-3'	6
	5’- ATGCCTGGCTGCTGATCTCTG-3'	6
LRP5	5’- TGTACTGCAGCTTGGTCCC-3'	7
	5’- CCAGTAAATGTCGGAGTCTACAATG-3'	7
LRP6	5’- TGACTATGCTCCTAGCCGGA-3'	8
	5’- CAGCACCCACCCACTTTATAA-3'	8

Table 1. List of primers used for RT-PCR.

1 - (Mesli et al., 2004)
2 - Primer3/CLC/ IDT
3 - (Li et al., 2005)
4 - (Marschang et al., 2004)
5 - (Gerbe et al., 2008)
6 - (Yamaguchi et al., 2006)
7 - (Holmen et al., 2004)
8 - (Harwood et al., 2008)

MATERIALS AND METHODS

Mouse strains and generation of Mesd-KO. Mice heterozygous for the *Mesd* deletion (*Del(7)Tyr*$^{c\text{-}3YPSD}$*/Tyr*$^{c\text{-}ch}$) were maintained in a closed colony by crossing to (*Tyr*^{C}*/Tyr*$^{c\text{-}ch}$) (Holdener et al., 1994; Wines et al., 2000). The *Mesd*^{tm1bch} (*Mesd-KO*) was generated in 129 ES cells purchased from Cell & Molecular Technologies (Phillipsburg, NJ; currently part of Invitrogen, Inc.). Three hundred and eighty four colonies were screened by PCR and Southern blotting and three correctly targeted clones isolated. Chimeras were generated by injecting the ES-cells into C57BL/6J blastocysts. Chimeric males were tested for germline transmission of ES-cell descendants by mating to C57BL/6JxDBA/2J F1 females. ES-cell electroporation, screening, and injection into blastocysts were done with the assistance of the Stony Brook University Transgenic Facility. Heterozygous mice were backcrossed to C57BL/6J mice for over 8 generations and are currently maintained by backcross to C57BL/6J.

Southern genotyping. Tail DNA was digested with either *Hpa*I or *Kpn*I. The 5' probe was generated by PCR amplification using primers: NotI-5'-*Mesd* 5'-GCGGCCGCACCAGTTTAATTGACAGTGATATTGAAAG-3' and XhoI-5'-*Mesd* 5'-CTCGAGGAGCAACAGAAGGTCCGAGGCACACAG-3'. The amplified fragment detects a 15kb *wild-type* fragment and a 9.4kb *Mesd* targeted *Hpa* I fragment. The 3' probe was generated by PCR amplification using primers: NotI-3'A-Mesd 5'-GCGGCCGCACATGCAGGGTGTCTGTTTTGGCAGTC-3' and XhoI-3'A-*Mesd* 5'-CTCGAGCTGAAGTCTCAAACTGGCTTTGATGAG-3' or NotI-3'B-*Mesd* 5'-

GCGGCCGCACATAAGACATAGATGGAAATGACATTTC-3' and XhoI-3'B-*Mesd* 5'-CTCGAGGCCACCTGCTAAAGGTCTTCTCTTCTG-3'. The amplified fragment detects a 14kb *wild-type* fragment and a 9kb *Mesd* targeted *Kpn* I fragment.

PCR genotyping. DNA isolated from animal tail biopsies was genotyped by PCR using a common reverse primer (5'-CAAAAGGATGAGTGCCCTGT-3') located at the 3' end of the third exon, and either a Mesdc2-ko forward primer (5'-GGGAGGATTGGGAAGACAAT-3') in the neomycin resistance gene (262 bp) or a *wild-type* forward primer (5'-TCCAGTTGGTTTCCGTTCAT-3') also located 3' of the third exon (202 bp) (Figure 9A).

BAT-Gal reporter assay. Mice homozygous for the BAT-Gal reporter transgene were crossed to mice heterozygous for the *Mesd* targeted allele to generate double-heterozygous animals. Male and female mice heterozygous for the *Mesd* targeted allele and carrying at least one copy of the BAT-Gal reporter transgene were mated. Embryos were collected at E 7.5 and stained for the presence of β-galactosidase as previously described (Maretto et al., 2003). Embryos were observed and photographed (Zeiss Stereo Discovery.V8 dissecting scope, Zeiss AxioCam MRc camera), and then lysed in 20µl of lysis buffer (1xPCR buffer, 0.2mg/ml proteinase K, 10mM DTT, 1.5mM $MgCl_2$) at 50°C overnight. Lysates were boiled for 5 minutes then 2µl used for PCR genotyping using the following primers: *lacZ* forward (5'-CGGTGATGGTGCTGCGTTGGA-3'), *lacZ* reverse (5'-ACCACCGCACGATAGAGATTC-3') and *Mesd-KO* primers described above).

In situ hybridization. Embryos from a heterozygous intercross of *Mesd-KO* animals were dissected at E 7.5 (data not shown) and E 8.5. In situ hybridization was performed as previously described (Hsieh et al., 2003). DNA constructs used to generate probes were provided by Drs. Ian Chambers (*Nanog*), Hans Scholer (*Oct4*), Bernard Herrman (*T*), and *Sox2* (Du, 2010).

LRP secretion assay.

Expression constructs. Construction of FLAG-*Mesd* is previously described (Hsieh et al., 2003). Soluble LRP receptors were tagged with a C-terminal C-myc epitope (KLGGGMEQKLISEEDLNGGGLE) and cloned into pRK5. Mouse LRP5 and LRP6 soluble receptors are comprised of the following amino acid sequences: LRP6 ECD, 1-1363; LRP6 βP1-4,1-1245; LRP6 βP1-3, 1-931; LRP6 βP1-2, 1-630; LRP6 βP1, 1-328; and LRP5 βP1, 1-337. EGFP-rho (EGFP/pRK5-SK) was a gift from Jen-Chih Hsieh. Human IgG heavy chain plasmid (hIgG-pRK5) was previously described (Hsieh et al., 1999; Hsieh et al., 2003).

Transfection of COS1 Cells. COS1 cells were seeded at 50% confluency in 12-well plates and transfected 24 hours later with a total of 1 µg plasmid DNA using Fugene 6 (Roche) following manufacturer's directions. Transfections contained 0.3 µg of *mesd*, 0.4 µg of LRP6, 0.1 µg of hIgG plasmid, 0.1µg of EGFP, and pCS2+ plasmid to bring total DNA to 1 µg. The cells were detached from the plate in 1ml of 5 mM EDTA/phosphate buffered saline (PBS), collected by centrifugation in a microfuge at 3000 rpm for 3 minutes, and lysed in 55 µl cold lysis buffer (1% Triton X-100/PBS

containing final concentrations of 17mg/ml aprotinin, 10mg/ml benzamidine, 1mg/ml leupeptin, 3mg/ml antipain, 1M PMSF). 20µl of loading dye (Coligan, 1995-2002) were added to each sample and boiled for 5 minutes. The lysates (10 µl each) were used for sodium dodecyl sulfate-polyacrylamide gel electrophoresis (SDS-PAGE) in the presence of β-mercaptoethanol followed by Western blot analysis. All transfections were repeated a minimum of three times. Representative Western blots are shown.

Western blotting, antibodies, image acquisition and quantitation. After transferring the proteins from SDS-polyacrylamide gels onto nitrocellulose membrane (.45µm PROTRAN, VWR) membranes were blocked overnight in 1% casein/Tris buffered saline (TBS) at 4°C, incubated with primary antibodies for 1 hour at room temperature, followed by fluorescently-labeled secondary antibody for 1 hour at room temperature. Membranes were washed with 1xTBST (0.05% Tween-20/TBS) 3x15 minutes before and after secondary antibody incubation. All antibodies were diluted in 1% casein/TBS. Rho-tagged LRP6 was detected using mouse monoclonal anti-rhodopsin (clone 1D4) at 1:1000. Flag-tagged MESD was detected using mouse monoclonal anti-FLAG (clone M2, Sigma) at 1:5000. Secondary antibody Alexa 680-labeled anti-mouse (Invitrogen) was used at 1:4000, and human IgG heavy chain was directly detected using IRDye800-labeled anti-human IgG (Rockland) at 1:10,000. Membranes were scanned using the Odyssey-Infrared Imaging System (LI-COR Biosciences), and the intensities of the bands of interest were determined from the captured images using the Odyssey imaging software.

RT-PCR. Total RNA from embryos or brain and spleen tissue lysates were prepared. First strand cDNA was synthesized with SuperScript III First-Strand Synthesis System (Invitrogen). Primer sequences used to amplify LRP family gene products are listed in Supplementary Table 1.

Immunohistochemical analysis of embryos. Mouse embryos were dissected at E 7.5 and fixed in 4% paraformaldehyde for 1 hour at 4°C. Embryos were embedded in paraffin (Leica EG1160) and sectioned (RMC MT910) at 7µm and mounted on glass slides (Fisherbrand Colorfrost/Plus). Embryo sections were dewaxed, rehydrated, and antigen retrieved by microwaving the slides for 5 min at 40% power in 0.1M sodium citrate pH 9/1xTBST. Slides were washed in 1xTBST(0.05% Tween 20), and blocked overnight in 5% bovine serum albumin (BSA)/1xTBST at 4°C. Primary antibodies used were sheep anti-gp330, 1:1000 (Dr. Pierre Verroust); rabbit anti-amnionless, 1:4000 (Dr. Elizabeth Lacy); and goat anti-cubilin, A-16/Y-20/T-16, 1:1000 (Santa Cruz Biotechnologies). Secondary antibodies used were goat anti-rabbit 1:1000, goat anti-sheep 1:1000, rabbit anti-goat 1:1000 (Vector Labs).

Immunofluorescence of embryo sections. Mouse embryos were dissected at E7.5 and fixed in 4% paraformaldehyde for 1 hour at 4°C. Embryos were washed with 1xPBS and infused with 30% sucrose/1xPBS overnight at 4°C. Embryos were then infused with OCT embedding media and frozen solid in cryomolds. Embryos were sectioned on a Microm HM-505E at 7-9µm and stored at -20°C. Cryosections were hydrated in 1xPBS for 15 minutes at room temperature, then sequentially treated with 0.5% saponin and

0.1%saponin/0.1%sodium borohydride/PBS for 10 minutes each. Sections were washed in 0.1%saponin/PBS 3x15 minutes and blocked in 0.1%saponin/PBS/5%NGS for 3 hours at room temperature, then probed with goat anti-LAMP1 or goat anti-LAMP2 (1D4B, ABL-93, Santa Cruz Biotechnology), and rabbit anti-EEA1 (324610, Calbiochem; sc-33585, Santa Cruz Biotechnology) at 1:50 overnight at 4°C. After incubation, slides were washed and probed with Alexa 488 anti-goat or 488 anti-rabbit. After washing, slides were treated with DAPI at 50ng/ml for 10 minutes at room temperature, mounted in Gel Mount, and sealed with nail polish.

Preparation of embryos for transmission electron microscopy. Samples used for transmission electron microscopy were processed using standard techniques by Susan van Horn of the electron microscopy facility at Stony Brook University. Briefly, samples were fixed with 2% paraformaldehyde and 2.5% EM grade glutaraldehyde in 0.1M phosphate buffer saline (PBS), pH7.4, overnight. Samples were then placed in 2% osmium tetroxide in 0.1M PBS pH 7.4, dehydrated in a graded series of ethyl alcohol and embedded in Durcupan resin. Ultrathin sections of 80nm were cut with a Reichert-Jung UltracutE ultramicrotome and placed on formvar coated slot copper grids. Sections were then counterstained with uranyl acetate and lead citrate and viewed with a FEI Tecnai12 BioTwinG^2 electron microscope. Digital images were acquired with an AMT XR-60 CCD Digital Camera system and compiled using Adobe Photoshop.

LysoTracker Red staining. Embryos were dissected at E 7.5 in DMEM at 37°C and freed from the parietal endoderm and Reichert's membrane. Embryos were allowed

to recover for 15 minutes at 37°C in DMEM/10%FBS in a tissue culture incubator. Staining was performed as described (Koike et al., 2009) and visualized on a Leica DMIRE2. Lysosome pixel intensity and diameter measurements were done with ImageJ. To measure pixel intensity, ten regions of interest (ROI) corresponding to ten individual cells were measured. The mean gray value for each ROI was multiplied by the area of the ROI to obtain the "integrated density". The integrated density values were averaged, and a standard deviation was calculated. To measure lysosome diameters, eleven measurements were taken, ten corresponding to individual lysosomes, and one corresponding to the 8µm scale bar. The measurements were converted to µm using the 8µm scale bar measurement, averaged, and a standard deviation value was calculated.

488-RAP endocytosis assay. Embryos were dissected at E 7.5 in DMEM at 37°C and freed from the parietal endoderm and Reichert's membrane. Embryos were washed in 1mL of PBSc at 4°C (1xPBS/1mM $CaCl_2$/0.5mM $MgCl_2$) and incubated with either 50mM 488-RAP in 100µL PBSc at 4°C, or 50mM 488-RAP/10uM RAP in 50µL cold PBSc for 1.5 hours at 4°C. Embryos were washed on ice with 2 x 1mL PBSc, then placed in 1mL of pre-warmed 37°C PBSc and incubated for 10 minute at 37°C. After incubation, embryos were fixed for 1 hour at 4°C in 4% paraformaldehyde and permeabilized for 5 minutes in 0.5% saponin/PBS. Embryos were then stained for 20 minutes at room temperature with DAPI (200ng/mL) and rhodamine-phalloidin (1:50, Invitrogen), mounted in Gel Mount, sealed with nail polish and visualized on a Zeiss LSM 510 META NLO Two-Photon Laser Scanning Confocal Microscope.

CHAPTER 4:

Tissue-Specific Knockout of MESD

SUMMARY

In Chapter 3, I demonstrated that MESD likely serves *in vivo* as a general LRP chaperone. Although structurally similar, LRPs have a range of functions in both embryonic and adult tissues, and disruption of LRPs often leads to developmental defects and disease. Over the last decade, dysfunction of two or more functionally overlapping LRPs was linked to disruption of basic cellular processes such as migration and signaling. Additionally, our data suggests that LRPs are also required for embryonic growth and development. We hypothesize that conditional knockout of *Mesd* will allow us to dissect the role of MESD-mediated LRP maturation in both embryogenesis and disease. In this chapter, I identify defects in an *Ozgene* conditional allele, and discuss potential applications for a future conditional deletion of *Mesd* as a tool for exploring LRP-related diseases and phenotypes.

INTRODUCTION

Low-density lipoprotein Receptor-related Proteins(LRPs) are a family of structurally related receptors that have a broad role in human and mouse physiology. Despite a high degree of similarity between modules found in their extracellular domains, individual LRPs can bind to many different ligands and are important in diverse cellular processes. Previous mouse models have targeted individual LRPs to investigate the contribution of one LRP to a specific phenotype. However, several studies in mouse suggest that LRPs can functionally overlap and that loss of multiple LRPs can exacerbate the severity of diseases such as hypercholesterolemia and atherosclerosis (Tacken et al., 2000; Boucher et al., 2003). I demonstrated in Chapter 2 and Chapter 3 that MESD can promote maturation of multiple LRPs *in vivo*. I hypothesize that tissue-specific deletion of *Mesd* will allow us to study the collective requirement of LRPs in both embryonic development and adult organ function. Several tissues stand out as targets for further study as they express a number of LRPs. These include hepatocytes, neurons, smooth muscle epithelia, and embryonic epiblast and VE (May et al., 2005). In addition, conditional deletion of *Mesd* in the embryonic epiblast or VE, will distinguish the defective tissue responsible for the unique characteristics of the *Mesd*-deficient embryos.

We contracted an outside company, *Ozgene*, to generate a conditional allele of *Mesd*. They designed a targeting vector that contained a 5' homology arm, loxP1 site, loxP1 arm, neomycin-resistance selection cassette, loxP2 arm, loxP2 site, and 3' homology arm. After cloning, and ligating each of these individual components together, they sequenced across the entire targeting construct to confirm the presence of each

component, and digested the targeting construct with restriction enzymes to confirm the sequencing results. They electroporated the targeting construct into mouse embryonic stem (ES) cells and grew individual neomycin resistant ES cell colonies. They performed Southern blots to identify cell lines that incorporated both the 5' loxP site and 3' loxP sites, and verified only one integration of the selection cassette. They isolated one colony, 4A9, that was targeted at the both 5' and 3' sites, and injected this colony into blastocysts to generate chimeras for the targeted *Mesd* allele.

Ozgene determined germline transmission by mating chimeric animals to a PGK-Cre line, and identified progeny that carried the floxed *Mesd* allele and/or PGK-Cre by Southern analysis. They predicted that PGK-driven expression of Cre would result in recombination of the targeted allele of *Mesd*, and used Southern blotting and DNA digested with SphI to predict that Cre^{+} animals heterozygous for the floxed allele had recombined to generate a conditional *Mesd* knockout allele. After receiving animals either heterozygous for the *Mesd* floxed allele or heterozygous for the floxed *Mesd* allele and hemizygous for *PGK-Cre*, I began to confirm the animal genotypes by PCR genotyping and Southern blotting and verify that the floxed *Mesd* allele recombined with Cre-recombinase.

RESULTS

Conditional deletion of *Mesd* was not detected by PCR

The *phosphoglycerate kinase* (*Pgk*) promoter coupled to *Cre recombinase* drives global and maternal expression of Cre (Lallemand et al., 1998). I designed a PCR strategy to detect the *wild-type* allele ($Mesd^{wt}$), the targeted allele flanked by LoxP sites ($Mesd^{floxed}$), and the conditionally deleted allele leaving a single LoxP site ($Mesd^{loxP}$) (Figure 17A). In animals heterozygous for $Mesd^{floxed}$ and hemizygous for *Cre-recombinase,* I expected the $Mesd^{loxP}$ allele to recombine in tissues expressing *Cre-recombinase*. To test recombination, I used three separate Cre strains since *in vivo* recombination depends on the strength and regulation of the promoter driving the Cre recombinase (Nagy, 2000). Results from representative genotyping is shown in Figure 17. Primer pair "1" detects both $Mesd^{wt}$ and $Mesd^{floxed}$, primer pair "4" detects the $Mesd^{loxP}$ allele, and primer pair "Cre" detects the *Cre-recombinase* transgene. I detected both the $Mesd^{floxed}$ and $Mesd^{wt}$ alleles even when animals were also hemizygous for *Cre-recombinase* (Figure 17B, 17C).

To eliminate the possibility that inefficient recombination of $Mesd^{floxed}$ in the presence of PGK-Cre was responsible for the failure to recover a $Mesd^{loxP}$ PCR product, I crossed $Mesd^{floxed}$ to animals homozygous for *Cre* driven by the albumin promoter (*Alb-Cre*) or nestin promoter (*Nes-Cre*). Albumin is a ubiquitous liver-specific protein. By three weeks of age, *Alb-Cre* triggers recombination between *LoxP* sites in 75% of cells (Postic and Magnuson, 2000). Nestin is an intermediate filament protein mainly expressed in the brain, but is also expressed in other tissues such as the pancreas, liver,

and kidney (Lardon et al., 2002; Gleiberman et al., 2005; Wagner et al., 2006). PCR genotyping using liver DNA isolated from progeny from *Mesd*^{floxed} crossed to *Alb-Cre* confirmed that recombination did not occur (Figure 17B). Genotyping results from *Mesd*^{floxed} crossed to *Nes-Cre* were not informative, as the one individual carrying Nes-Cre did not carry the *Mesd*^{floxed} allele (Figure 17C).

Generation of *Mesd*^{loxP} was not detected by Southern blotting

Since PCR genotyping did not yield recombination products, I used Southern blotting as an additional method to confirm that the *Mesd*^{floxed} allele did not recombine in the presence of Cre-recombinase. I isolated DNA from the liver and brain of offspring from *Mesd*^{floxed} crossed to *Alb-Cre* animals. In addition, I isolated DNA from the kidney of offspring from *Mesd*^{floxed} crossed to *PGK-Cre* animals. I generated a 5' probe by amplification of DNA located upstream of the first loxP site and two 3' probes by amplification of DNA located downstream of the second loxP site. I used these probes for Southern hybridization against DNA digested with HindIII . If the *Mesd*^{floxed} allele recombined in the presence of Alb-Cre or Nes-Cre, I expected the 5' probe and either of the 3' probes to detect a 6.8 kb fragment corresponding to the *Mesd*^{wt} allele, a 9.0kb fragment corresponding to the *Mesd*^{floxed} allele, and a 3.4kb fragment corresponding to the *Mesd*^{loxP} allele (Figure 18, 19, and data not shown). To confirm these results, I also digested the DNA with XbaI and ScaI. When the DNA was digested with XbaI, probing the blot with the first 3' probe and 5' probe would detect fragments of 10.7kb, 12.9kb, and 7.3 corresponding to the *Mesd*^{wt}, *Mesd*^{floxed}, and *Mesd*^{loxP} alleles respectively (Figure 18, 19, and data not shown). When the DNA was digested with ScaI, probing the blot

with the either of the 3' probes would detect fragments of 7kb, 9.2kb, and 3.6kb also corresponding to the *Mesd*^{wt}, *Mesd*^{floxed}, and *Mesd*^{loxP} alleles respectively (Figure 18, 19, and data not shown). Although the 5' and 3' probes detected the expected *wild-type* and *Mesd*^{floxed} alleles, none of the probes detected fragments consistent with recombination (Figure 20, and data not shown).

Inverted orientation of the *Mesd*^{floxed} loxP sites prevents Cre-mediated excision

Based on genotyping results from both PCR and Southern blotting, I hypothesized that *Mesd*^{floxed} was unable to recombine in the presence of Cre-recombinase. Using three separate Cre strains, I eliminated the possibility that the Cre recombinase was at fault, but the possibility remained that one or both of the loxP sites carried mutations that would prevent Cre recombination. I isolated tail DNA from animals carrying *Mesd*^{floxed} and sequenced across both loxP sites in the forward and reverse directions. I determined that the loxP sites were oriented in opposite directions, preventing excision of the flanked *Mesd* exon 1 and exon 2 (Figure 20). The original design of the targeting vector intended to orient the loxP sites as direct repeats to allow excision of the flanked DNA sequence upon Cre expression. Cre-induced recombination of inverted loxP sites would result in inversion of the flanked DNA sequence. While inversion of the DNA from the original orientation could effectively disrupt gene function, a second exposure to Cre recombinase could theoretically re-invert the flanked sequence, resulting in reversion to the original protein-coding sequence. Ultimately, this would produce a mosaic tissue where an uncontrollableand unpredictable percentage of cells would properly express functional MESD protein, possibly enough to allow for LRP maturation. Because of the inverted

orientation of LoxP sites, I concluded that the conditional allele produced by *Ozgene* was defective, and could not be used to study novel roles of MESD-dependent LRP maturation.

DISCUSSION

We worked with Ozgene to design a conditional allele of *Mesd* that could be used to investigate the requirement for *Mesd* in adult tissues. I received the animals and began to verify that the conditional allele recapitulated the knockout phenotype. However, my molecular characterization of the *Ozgene* conditional allele demonstrated that an inversion in one of the loxP sites prevented excision of the flanked Mesd DNA. Ozgene is nearing completion of the correctly executed conditional allele. After verifying the fidelity of the newly generated conditional *Mesd* allele, we can use the new strain of $Mesd^{floxed}$ to investigate the role of multiple LRPs embryonic patterning and in adult tissue function. The *Ozgene* genotyping strategy relied on the incorporation of *Sph* I sites to verify the presence of the loxP sites, flanking the *Mesd* locus. Unfortunately, the incorporation of these sites and choice of probes also prevented them from verifying recombination. For this reason, *Ozgene* failed to detect the error in loxP site orientation in the early stages of the project. I predict that a correct design of the conditional allele introducing loxP sites in direct orientation, will produce measurable data resulting from conditional deletion of MESD and consequently loss of one or more LRPs in adult tissues.

Conditional deletion of *Mesd* from the early embryo

The conditional allele of *Mesd* was originally generated with the intention of circumventing the early embryonic lethality that results from homozygous knockout of *Mesd*. However, we can also use the conditional to investigate how cell-type specific

knockout in the early embryo affects growth. The placenta is largely derived from trophoblast cells and the VE, which at E 7.5 serves as the functional precursor for the chorioallantoic placenta that begins to develop around E 9.0 (Watson and Cross, 2005). A number of mouse mutants that affect the VE or placenta exhibit phenotypic defects in nutritional transport and embryonic growth (Watson and Cross, 2005). My data demonstrates that loss of *Mesd* prevents maturation of LRP2, and may likely extend to another scavenger receptor, LRP1. This disruption of LRP2 localization impairs endocytosis in absorptive epithelia (Christensen and Willnow, 1999; Leheste et al., 1999; Nielsen et al., 2007).

The lysosome size defect observed in the VE of *Mesd* mutants and described in Chapter 3 may also be due to as of yet unknown signaling pathways downstream of the LRP receptors. However, because of the role of LRP1 and 2 in signaling (May et al., 2005; Lillis et al., 2008) I cannot exclude the possibility that defects in VE signaling also contribute to the *Mesd* mutant phenotype. This is underscored by the observation that high contribution chimeras comprised of *Mesd* mutant extraembryonic tissue and *wild-type* epiblast remain small and do not gastrulate (Hsieh et al., 2003). For this reason, it is likely that the *Mesd* phenotype is complex, resulting from defects in epiblast cell signaling, embryo nutrition, as well as possible secondary alteration in the interactions between the VE and epiblast. Using a conditional allele of *Mesd*, we can investigate how disruption of LRP maturation in either the VE or placenta affects embryo growth. If primitive streak and mesoderm differentiation defects are solely related to MESD function in the epiblast, then I predict that epiblast-specific deletion of *Mesd* will closely resembles the *Wnt3* or *Lrp5/6* knockout phenotypes. Alternatively, I predict that loss of

Mesd in the visceral endoderm could disrupt embryo nutrition as well as VE-epiblast interactions. As a result, I predict that conditional deletion of *Mesd* in the VE will result in defects more extensive than delayed embryo growth

Dysfunction of multiple LRPs and disease

A number of human diseases that have been modeled in mice have been linked to defects in one or more LRPs. A summary of these include hypercholesterolemia (LDLR, LRP1, VLDLR), Alzheimer's (*Lrp1b*, *Apoer2*, and *SorLA/Lr11*), osteoporosis-pseudoglioma (OPPG)(LRP5), familial exudative vitreoretinopathy (FEVR) and Norrie (LRP5) (Ishibashi et al., 1993; Tacken et al., 2000; Gong et al., 2001; Veniant et al., 2001; Kato et al., 2002; Boucher et al., 2003; Toomes et al., 2004; Xu et al., 2004; Marzolo and Bu, 2009). Significantly, many of the disease-causing mutations in LDLR and LRP5 are located within β-propeller/EGF domains (Bieri et al., 1995; Fass et al., 1997; Jeon et al., 2001; Toomes et al., 2004). Other mutations have already been demonstrated to disrupt interaction with MESD, such as the LRP5 high bone mass mutation, G171V, and a mutation in LRP6 that results in osteoporosis, R866W (Zhang et al., 2004; Kubota et al., 2008). Disease-causing mutations like the FEVR mutation, and the bone metabolism mutations highlight the importance of studying MESD-regulated LRP trafficking. Additional evidence comes from functional overlap between receptors such as *Lrp5/Lrp6* which result in embryonic lethality, and *Apoer2*/*Vldlr* which cause defects in neuronal migration (Trommsdorff et al., 1999; Kelly et al., 2004).

We can similarly use a conditional allele of *Mesd* to study the requirement of MESD-mediated LRP maturation in adult tissues. Conventional targeted disruption of

Mesd results in embryonic lethality after E 10.5, but use of a conditional allele of *Mesd* allows us to circumvent this embryonic lethality. Several adult tissues, including neurons, hepatocytes, and smooth muscle epithelia, express multiple LRPs and are therefore ideal candidates for investigating functional overlap of LRPs (May et al., 2005). Neurons and smooth muscle epithelia require expression of LRPs such as ApoER2, VLDLR, and LRP1 to regulate cell migration (Trommsdorff et al., 1999; Boucher et al., 2003). This suggests that MESD may play a role in diseases in neuronal and epithelial migration. Migration of smooth muscle cells in vascular epithelia to sites of injury caused by oxidized excess lipoproteins is one of the initial steps in developing atherosclerosis (Swertfeger and Hui, 2001; Young and McEneny, 2001; Boucher et al., 2003). Hepatocytes express a number of LRPs such as LDLR and LRP1 and are responsible for regulating plasma lipoprotein levels (Kang and Davis, 2000; May et al., 2005).

This suggests that MESD may also be important in other diseases that are sensitive to increases in lipoprotein levels such as atherosclerosis and hypercholesterolemia.

FIGURES

Primer name	Primer Sequence (5'-3')	Expected product size
Cre left	CGAGTGATGAGGTTCGCAAG	*Wild-type*: n/a *Mesd*^{floxed}: n/a *Mesd*^{floxed} + Cre: 870 bp
Cre right	CACCAGCTTGCATGATCT	
Primer 1-left	ATTGTGCCTTACGCTGGGCAGTC	*Wild-type*: 211 bp *Mesd*^{floxed}: 271 bp *Mesd*^{floxed} + Cre: n/a
Primer 1-right	CATCGTTGTAATCGCGGATGTCCT	
Primer 2-left	TCCAGTTGGTTTCCGTTCAT	*Wild-type*: 202 bp *Mesd*^{floxed}: 202 bp *Mesd*^{floxed} + Cre: 202
Primer 2-right	CAAAAGGATGAGTGCCCTGT	
Primer 3-left	ATTGTGCCTTACGCTGGGCAGTC	*Wild-type*: 4242 bp *Mesd*^{floxed}: 6425 bp *Mesd*^{floxed} + Cre: 843 bp
Primer 3-right	AAGAAAGCAATGGCATGGGTCTGG	
Primer 4-left	ATTGTGCCTTACGCTGGGCAGTC	*Wild-type*: 3560 bp *Mesd*^{floxed}: 5746 bp *Mesd*^{floxed} + Cre: 164 bp
Primer 4-right	TTCATAGACAGGAAAGGCCCAAGGTC	
Primer 5-left	AGATGGCCTCACTCCTCACACTTA	*Wild-type*: 918 bp *Mesd*^{floxed}: 918 bp *Mesd*^{floxed} + Cre: n/a
Primer 5-right	AAGAAAGCAATGGCATGGGTCTGG	
Primer 6-left	AGATGGCCTCACTCCTCACACTTA	*Wild-type*: 239 bp *Mesd*^{floxed}: 239 bp *Mesd*^{floxed} + Cre: n/a
Primer 6-right	TTCATAGACAGGAAAGGCCCAAGGTC	

Table 2. PCR primers used to distinguish *Mesd* alleles: *Mesd*^{floxed}, *Mesd*^{wt}, and *Mesd*^{loxP}.

This table lists sequences of primers used for genotyping the *Ozgene* conditional allele and assessing recombination in the presence of Cre-recombinase. The locations and use of these primers are shown in Figure 17. n/a – no amplification.

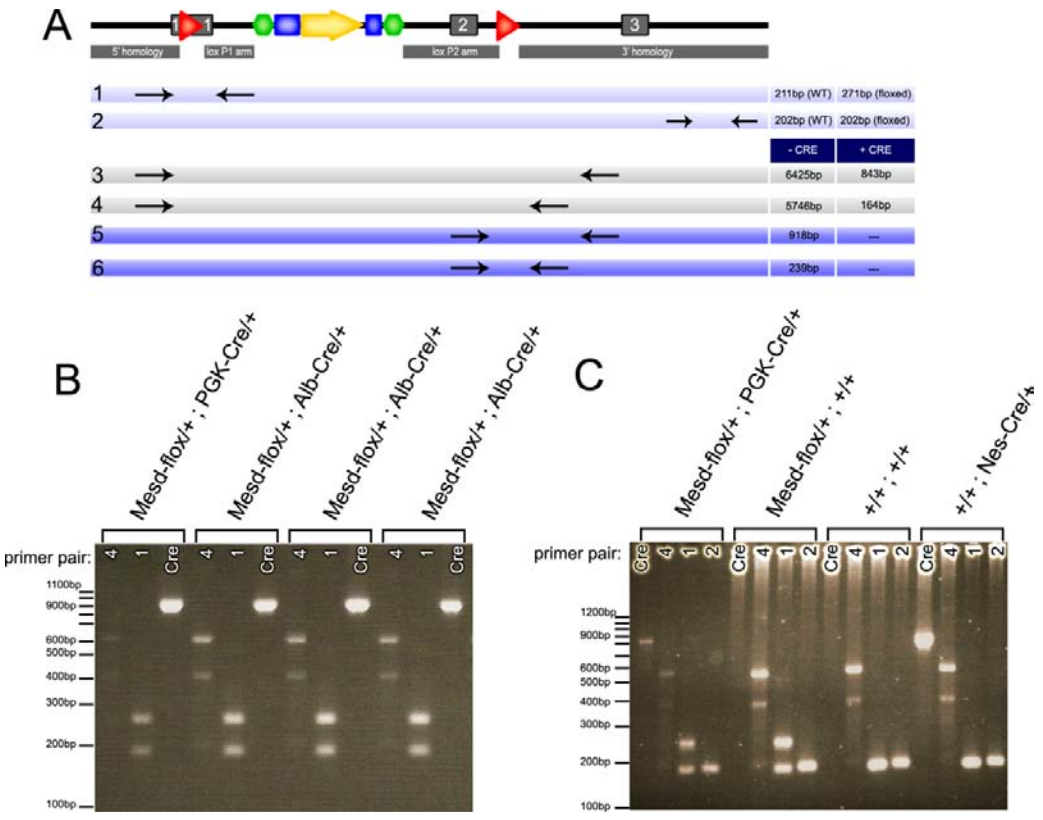
A
1
2
3
5' homology
lox P1 arm
lox P2 arm
3' homology
211bp (WT)
271bp (floxed)
202bp (WT)
202bp (floxed)
- CRE
+ CRE
6425bp
843bp
5746bp
164bp
918bp
239bp
B
Mesd-flox/+ ; PGK-Cre/+
Mesd-flox/+ ; Alb-Cre/+
Mesd-flox/+ ; Alb-Cre/+
Mesd-flox/+ ; Alb-Cre/+
primer pair:
4
1
Cre
1100bp
900bp
600bp
500bp
400bp
300bp
200bp
100bp
C
Mesd-flox/+ ; PGK-Cre/+
Mesd-flox/+ ; +/+
+/+ ; +/+
+/+ ; Nes-Cre/+
primer pair:
Cre
4
1
2
1200bp
900bp
600bp
500bp
400bp
300bp
200bp
100bp

Figure 17. PCR genotyping for *Mesd^{wt}*, *Mesd^{floxed}*, *Mesd^{loxP}*.

A carefully constructed PCR genotyping strategy can distinguish between the *Mesd^{wt}*, *Mesd^{floxed}*, and *Mesd^{loxP}* alleles **(A)**. **(A, top)** The diagram of the targeted *Mesd* locus is shown above. The *Mesd* gene is oriented 5' to 3'. Grey rectangles denote the three exons. LoxP sites (red triangles) are located within exon 1 and downstream of exon 2. Recombination between LoxP sites will result in deletion of the majority of the gene, leaving a small 5' portion of exon 1, a single LoxP site, and exon 3. FRT sites (green hexagons) are indicated in green and allow removal of the neomycin resistance gene (yellow arrow) by FLP-recombinase. The PGK promoter (left blue box) drives expression of the PGK gene, and the polyadenylation signal (right blue box) signals the end of the neomycin resistance transcription. **(A, bottom)** Six pairs of primers were used to distinguish the three *Mesd* alleles. Primer pair 1 amplifies *wild-type* and *Mesd^{floxed}* alleles. The PCR product of primer pair 1 is larger in the *Mesd^{floxed}* allele (271 bp) compared to the *Mesd^{wt}* (211 bp) due to the insertion of the LoxP site. Primer pair 2 serves as a PCR control and amplifies a 202 bp product in *Mesd^{wt}*, *Mesd^{floxed}*, and *Mesd^{loxP}* alleles. Primer pairs 3 and 4 flank the LoxP sites and were designed to detect *Mesd^{loxP}*, the recombined allele, in the presence of Cre. Therefore, combined use of primer pairs 1, 3, or 4 can be used to distinguish *Mesd^{wt}* from *Mesd^{floxed}* (primer pair 1) and *Mesd^{floxed}* from *Mesd^{loxP}* (primer pairs 3 and 4). Primer pairs 1, 5, and 6 were used to determine the sequence of the LoxP2 sites. Predicted sizes of the amplified product in the presence and absence of Cre is listed on the right. Representative electrophoresis results are shown from DNA isolated from *Mesd^{floxed}/PGK-Cre, Mesd^{floxed}/Alb-Cre,* and *Mesd^{floxed}/Nes-Cre* progeny and genotyped using primer pairs 1, 4, and Cre. Genotypes of animals are summarized above the PCR genotyping electrophoresis results **(B, C)**. Primer pair 1 amplifies both the *Mesd^{wt}* (211 bp) and *Mesd^{floxed}* (271 bp) alleles. The amplification product from the *Mesd^{floxed}* allele is larger because of the insertion of the loxP1 site. The *Cre-recombinase* transgene, detected by PCR amplification using the Cre primers (870 bp), was present in the *Ozgene* founder mouse (*Mesd$^{floxed/+}$/PGK-Cre*) and three progeny from the *Alb-Cre* crosses (*Mesd$^{floxed/+}$/PGK-Cre*) that also carried the floxed allele. Despite the presence of *Cre-recombinase,* the recombined *Mesd^{loxP}* allele was not detected using primer pair 4 (164 bp), suggesting that the *Mesd^{floxed}* allele was defective in recombination. The 400bp and 600bp bands using primer pair 4 are background **(B)**. Although the *Cre-recombinase* transgene was present in one individual from the *Nes-Cre* cross, this individual did not carry the *Mesd^{floxed}* allele. For this reason, these progeny were not informative for recombination **(C)**. Note: Kidney DNA was isolated from 6 month old offspring from of *Mesd^{floxed}/Mesd^{wt}* x *PGK-Cre* intercrosses. Liver DNA was isolated from 2 day-old littermates from *Mesd^{floxed}/Mesd^{wt}* x *Alb-Cre/Alb-Cre* parents. Brain DNA was isolated from 4 week-old littermates from *Mesd^{floxed}Mesd^{wt}* x *Nes-Cre/+* parents.

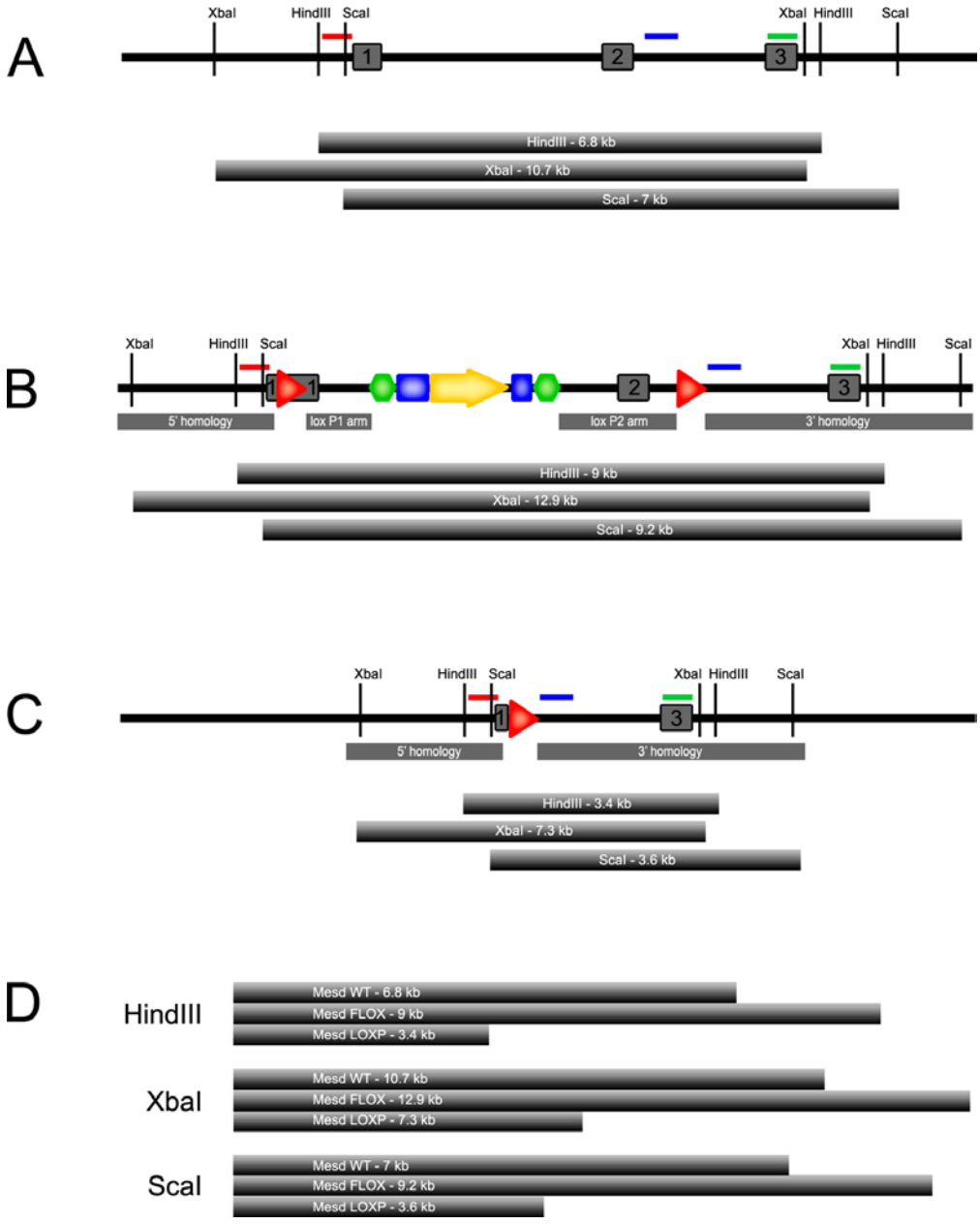
A
XbaI
HindIII
ScaI
XbaI
HindIII
ScaI
1
2
3
HindIII - 6.8 kb
XbaI - 10.7 kb
ScaI - 7 kb
B
XbaI
HindIII
ScaI
XbaI
HindIII
ScaI
1
1
2
3
5' homology
lox P1 arm
lox P2 arm
3' homology
HindIII - 9 kb
XbaI - 12.9 kb
ScaI - 9.2 kb
C
XbaI
HindIII
ScaI
XbaI
HindIII
ScaI
1
3
5' homology
3' homology
HindIII - 3.4 kb
XbaI - 7.3 kb
ScaI - 3.6 kb
D
HindIII
Mesd WT - 6.8 kb
Mesd FLOX - 9 kb
Mesd LOXP - 3.4 kb
XbaI
Mesd WT - 10.7 kb
Mesd FLOX - 12.9 kb
Mesd LOXP - 7.3 kb
ScaI
Mesd WT - 7 kb
Mesd FLOX - 9.2 kb
Mesd LOXP - 3.6 kb

Figure 18. Prediction of restriction fragment sizes in the *Mesd* locus.

The *Hind* III, *Xba* I, and *Sca* I restriction maps of three possible *Mesd* alleles are depicted. Locations of 5' (red bar) and 3' (blue and green bars) probes used for Southern hybridization and expected hybridization patterns are diagrammed. Note that *Sca* I fragments cannot be detected by the 5' probe. Two 3' probes were generated because repetitive sequences were detected downstream of exon 2 using RepeatMasker (http://www.repeatmasker.org). The 3' probes are expected to hybridize to: **(A)** 6.8-kb *Hind* III, 10.7-kb *Xba* I, and 7-kb *Sca* I fragments generated by digestion of the $Mesd^{wt}$ allele; **(B)** 9-kb *Hind* III, 12.9-kb *Xba* I, and 9.2-kb *Sca* I fragments generated by digestion of the $Mesd^{floxed}$ allele; and **(C)** 3.4-kb *Hind* III, 7.3-kb *Xba* I, and 3.6-kb *Sca* I fragments generated by digestion of the $Mesd^{loxP}$ allele. **(D)** Summary and comparison of predicted DNA fragments from Southern analysis of $Mesd^{wt}$, $Mesd^{floxed}$, $Mesd^{loxP}$ alleles. Red triangles, LoxP sites; green hexagons, FRT sites; yellow arrow, neomycin resistance gene; blue boxes, PGK promoter and polyadenylation signal from left to right respectively. Exons 1, 2 and 3 of *Mesd* are indicated in dark gray boxes outlined in black.

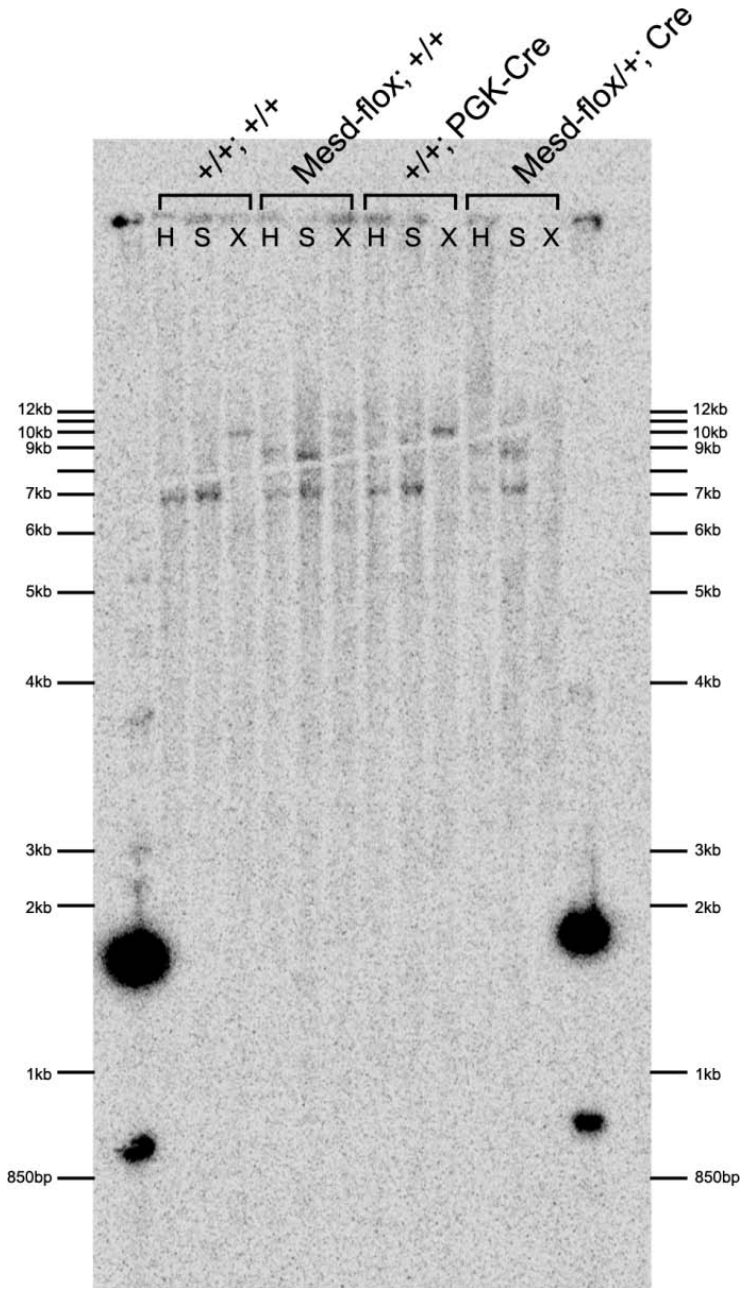
+/+; +/+
Mesd-flox; +/+
+/+; PGK-Cre
Mesd-flox/+; Cre
H S X H S X H S X H S X
12kb
10kb
9kb
7kb
6kb
5kb
4kb
3kb
2kb
1kb
850bp

Figure 19. Southern blot of genomic DNA isolated from kidney of *Mesd*^{floxed}/*PGK-Cre* animals.

Kidney DNA isolated was isolated from *Mesd*$^{floxed/+}$/*PGK-Cre* animals at 6 months of age. To genotype animals, DNA was digested with *Hind* III, *Sca* I, or *Xba* I, separated overnight by gel electrophoresis, transferred to nylon membrane, probed with a random-primed radioactive 3' probe A (blue line in Figure 19), and exposed to phosphor screen overnight. Presence of *Cre-recombinase* was determined by PCR genotyping (described in Figure 18). Although the fourth animal is heterozygous for the *Mesd*$^{floxed/+}$ allele and is positive for *PGK-Cre* (not shown), we only detected bands consistent with the *Mesd*^{floxed} (9-kb *Hind* III, 12.9-kb *Xba* I, and 9.2-kb *Sca* I fragments) and *Mesd*^{wt} (6.8-kb *Hind* III, 10.7-kb *Xba* I, and 7-kb *Sca* I fragments) alleles. Bands consistent with the *Mesd*^{LoxP} allele (3.4-kb *Hind* III, 7.3-kb *Xba* I, and 3.6-kb *Sca* I fragments) were undetectable. These results confirm that *Mesd*^{floxed} fails to recombine in the presence of PGK-Cre (*Mesd-flox/+;PGK-Cre*). Sizes of 1kb^{+} ladder from *Invitrogen* are indicated on either side of the blot. Lanes are grouped by animal genotype, and DNA from each animal was digested with *Hind* III (H), *Sca* I (S), or *Xba* I (X) to triple-confirm the lack of recombination.

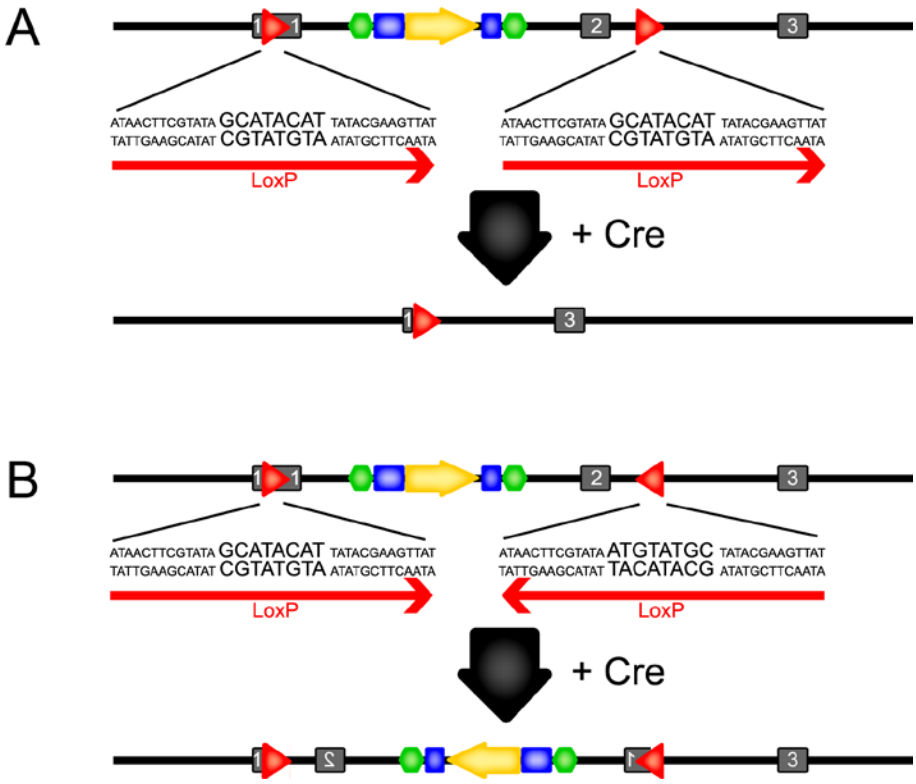

Figure 20. Diagram of possible loxP orientations and outcomes.

Diagram comparing the recombination outcome when the LoxP sites are present in direct (A) or inverted (B) orientation in the presence of Cre-recombinase. **(A)** In the presence of Cre-recombinase, recombination between LoxP sites integrated as direct repeats (in same orientation) results in the excision of the intervening DNA. **(B)** In contrast, recombination between LoxP sites integrated as inverted repeats (opposite orientation) results in the inversion of the intervening DNA in the presence of Cre. The inversion can revert to the original protein-coding orientation upon continuous exposure to Cre. Red triangles, LoxP sites; green hexagons, FRT sites; yellow arrow, neomycin resistance gene; blue boxes, PGK promoter and polyadenylation signal from left to right respectively. Exons 1, 2 and 3 of *Mesd* are indicated in dark gray boxes lined in black.

MATERIALS AND METHODS

Generation of animal strains. Construction of the targeting vector and generation of the ES cells and mice were done by Ozgene (431 Menhir project). Lines were maintained by backcrossing to C57BL/6J after quarantine.

PCR genotyping of *Mesd*^{wt}, *Mesd*^{floxed}, and *Mesd*^{loxP}. Sequences of primers used are located in Table 1, and a diagram in Figure 18.

Genomic DNA digestion for Southern blotting. 10µg of DNA isolated from brain, liver, or kidney of *Mesd*^{floxed}/Cre mice was digested overnight at 37°C with 50U HindIII, ScaI, or XbaI (5U enzyme/µg DNA) and checked for complete digestion on a 0.5% agarose gel. Digested DNA was purified by ethanol precipitation, resuspended to a concentration of 0.5µg/µl, and electrophoresed on an extra-long (10+ inches) 0.7% agarose gel for 14+ hours at 30 volts.

Transfer of DNA from agarose gel to membrane. Agarose gel was stained for 30 minutes in ethidium bromide, imaged, then denatured in two 30-minute washes of 0.5M NaOH/1.5M NaCl with gentle rocking in a shallow glass dish. Hybond-N+ nylon membranes (Amersham Biosciences/GE Healthcare) were cut to a size slightly larger than the agarose gel and hydrated for 15 minutes in sterile water, then 2xSSC. DNA was transferred from agarose gel to nylon membrane overnight at room temperature (Ausubel, 1993).

Probe generation for Southern blotting. Southern probes were amplified from 171m12 DNA. Probe sequences used in Southern blotting are located in Appendix D. Amplified probe DNA was diluted to 25ng in 9µl total volume, boiled for 10 minutes to denature DNA, and labeled using a Random Primed DNA Labeling Kit (Roche). Labeled probe was purified with a G-50 Sephadex column in a clinical centrifuge and radioactive incorporation was measured in a scintillation counter (Beckman-Coulter LS6500).

Probe hybridization to membrane. Nylon membrane was pre-hybridized in ExpressHyb (ClonTech) then 100µl of the radioactive probe labeling mix was added directly to the ExpressHyb without contacting the membrane. Membrane was incubated in a roller tube at 65°C overnight, then washed three times with 50mL wash 1 (2xSSC/0.05% SDS) at room temperature, then twice with 200mL wash 2 (0.1xSSC/0.1%SDS). Membrane was wrapped in plastic wrap, exposed to phosphor screen (Kodak X-Omatic) overnight at room temperature, and imaged on a Storm 860 PhosphoImager (Molecular Dynamics).

CHAPTER 5:

General Conclusions and Future Directions

In my studies, I have determined that MESD functions to promote maturation of LRP5/6, two members of the Low-density lipoprotein Receptor-related Protein (LRP) superfamily. I demonstrate that the basis for this interaction is a MESD-dependent domain found in multiple LRP family members, and consists of a β-propeller with a C-terminal EGF domain. When isolated from full-length LRP family members such as LRP5, LRP6, or LRP1, this β-propeller/EGF domain requires MESD for maturation in cell culture, and this requirement increases as the number of β-propeller/EGF domains increases. I also demonstrate that MESD promotes *in vivo* membrane localization of LRP2 in the embryonic visceral endoderm, and more likely promotes general LRP localization in this tissue. Loss of MESD results in a decrease in lysosome size, suggesting decreased uptake of LRP ligands in the visceral endoderm. My studies raise several important questions that I will discuss below: 1) How does MESD interact with LRP β-propeller/EGFs? 2) How does loss of MESD and mislocalization of LRP2 affect lysosome biogenesis? 3) Does MESD function extend to other LRP family members beyond LRP5/6 and LRP2?

A structural prediction on the MESD-LRP interaction

The β-propeller/EGF domain found in LRPs is similar to domains found in *Drosophila* nidogen and sevenless, though neither nidogen nor sevenless require boca (*Drosophila* homologue of MESD) for maturation (Culi et al., 2004). Nidogen contains a

single β-propeller domain with a C-terminal EGF. However, the nidogen β-propeller domain contains two disulfide bonds and hydrophilic residues instead of hydrophobic residues in the β-propeller/EGF interface. Sevenless contains three β-propeller domains, but contains fibronectin type III repeats instead of EGF-like repeats (Culi et al., 2004). These results suggest that a C-terminal EGF with the β-propeller domain in LRPs is for a fundamental requirement for interaction with MESD/boca. Only pro-EGF, the precursor to the epidermal growth factor, contains the same type of β-propeller and C-terminal EGF found in LRPs, and requires boca for maturation. It is possible that MESD may influence signaling by regulating maturation of EGF. However, unlike *Egfr*-deficient animals, *Egf*-deficient animals do not appear to have a phenotype, suggesting that other EGF-family ligands, such as TGFα or amphiregulin, may compensate for the lack of EGF (Hansen et al., 1997; Luetteke et al., 1999; Dreux et al., 2006). The possibility that MESD may regulate EGF signaling has not yet been investigated and could be explored in the future. Together, these data strongly support the hypothesis that MESD promotes maturation of the β-propeller/EGF domain that is found almost exclusively in the LRP family.

To determine how MESD physically interacts with the LRP β-propeller, we collaborated with Christian Koehler and Hartmut Oshkinat to combine an *in vitro* mutagenesis assay with a prediction of full-length MESD. Based on our results, we predicted that the unfolded LRP β-propeller/EGF interacts with an N-terminal extension as well as the MESD core. Within the MESD core, we predicted a transiently exposed hydrophobic domain. This hydrophobic domain may function to position the EGF in close proximity to the β-propeller blades. We also predicted that basic residues in the LRP β-propeller ring interact with acidic domain on the MESD N-terminal helix (Koehler

et al., submitted). My *in vitro* functional analysis of the effects of MESD mutations on LRP6 maturation underscores the importance of these domains. However, another group recently proposed an alternate MESD structure also based on NMR-spectral characterization (Chen et al., 2010). The alternative model, proposed by Chen et al, suggests that the exposed hydrophobic residues in the Koehler model are instead integral, buried components of the MESD core. Resolution of this discrepancy between the Koehler and Chen models may require the co-crystallization or co-prediction of MESD directly interacting with a β-propeller/EGF. This will likely be a formidable task, given the potentially transient nature of the MESD/β-propeller/EGF, the possibility for multiple conformations of the MESD/β-propeller/EGF complex, and the potential pH sensitivity of the complex.

Regulation of lysosome biogenesis by receptor-mediated endocytosis

Little is known about the *in vivo* requirement for MESD-dependent trafficking of LRPs. Targeted knockout of *Mesd* suggests that MESD functions in the WNT signaling pathway, but the size of the developing embryo is much smaller than that of mutants in other components of the WNT pathway such as *Lrp5/6* or *Wnt3* {Liu, 1999 #337}{Kelly, 2004 #275}. This suggests that WNT signaling is not the only pathway disrupted in *Mesd* mutant embryos, and that loss of MESD may result in the mislocalization and dysfunction of other LRPs, contributing to the more severe phenotype of *Mesd* mutants. Currently, the only *in vivo* data demonstrating that MESD is required for maturation of LRP family members is in *Drosophila*, where a mutation in the MESD homologue, boca, results in improper localization of Arrow (LRP5/6 homologue) and Yolkless to the cell

membrane (Culi and Mann, 2003). Based on *in vitro* observations and the phenotype of the *Mesd* mutant embryo, I predict that mouse MESD is similarly required for *in vivo* maturation of LRPs other than LRP5/6. In chapter 3, I provide the first evidence that MESD is required for *in vivo* maturation of LRP2 in the mouse visceral endoderm.

LRP2 is a scavenger receptor in the LRP superfamily, and binds to over 35 different ligands (Strickland et al., 2002). It is highly expressed in absorptive epithelia such as the mouse visceral endoderm, intestinal gut epithelia, kidney proximal tubule cells, and developing embryonic neuroepithelium (Muller et al., 2003; May et al., 2007). In the kidney and embryonic visceral endoderm, LRP2 is expressed in a complex with Cubilin (CUBN) and Amnionless (AMN). Endocytosis of LRP2-bound ligands depends on a cytoplasmic adaptor protein, DAB2. Defects in protein expression of CUBN, AMN, DAB2, LRP2, or MESD all result in a visible decrease in the apical endocytic vesicles of the kidney proximal tubule cells or visceral endoderm (Christensen and Willnow, 1999; Leheste et al., 1999; Strope et al., 2004; Maurer and Cooper, 2005; Smith et al., 2006). I demonstrated that loss of MESD resulted in a decrease in lysosome size. This raises the possibility that defects in receptor-mediated endocytosis may regulate lysosome size and impair tissue function.

Despite their discovery over 50 years ago, the details of lysosome biogenesis and size regulation remain unclear (de Duve, 2005). Lysosomes consist of over 200 membrane-bound and soluble hydrolases that provide structural support and functional activity (Bagshaw et al., 2005a; Bagshaw et al., 2005b). These hydrolases are modified in the trans-Golgi network with a phosphomannosyl tag to allow for recognition by the mannose-6-phosphate receptor and packaged for delivery to the lysosome (Kornfeld,

1986). Once in the lysosome, they act to degrade cargo delivered to the lysosomes by SNARE-mediated fusion of late endosomes and phagosomes (Luzio et al., 2009; Saftig and Klumperman, 2009). Occasionally, lysosomal proteins are incorrectly sorted into the secretory pathway at the trans-Golgi network and are secreted out of the cell. A small fraction of these secreted lysosomal enzymes can be recognized and recaptured by mannose-6-phosphate receptors (Kornfeld, 1986). However, alternate mechanisms must exist, since lysosomal enzyme levels are relatively normal in the liver, kidney, brain, and spleen in the absence of the phosphomannosyl tag (Dittmer et al., 1999).

Recently, Nielsen et al demonstrated that LRP2-mediated endocytosis in the kidney proximal tubule cells serves as an alternative pathway to recapture these secreted lysosomal enzymes (Nielsen et al., 2007). Animals deficient for *Lrp2* excrete excessive amounts of lysosomal protein, cathepsin B, and pro-cathepsin B compared to *wild-type* animals, suggesting that kidney proximal tubule function is compromised in the absence of LRP2. Although they did not report a decrease in expression of LAMP1, another integral lysosomal protein, previous reports demonstrate a visible decrease in the size of apical membrane bound organelles in LRP2-deficient animals (Willnow et al., 1996; Christensen and Willnow, 1999; Leheste et al., 1999). Based on the results in Chapter 3, I hypothesized that the affected organelles are lysosomes.

A number of human diseases associated with lysosome storage disorders, including: Chediak-Higashi syndrome (formation of giant lysosomes), I-cell disease (excessive secretion of lysosomal proteins), and type C Niemann-Pick disease (lysosomal accumulation of unesterified cholesterol) (Perou et al., 1997) (Blanchette-Mackie et al., 1988; Dittmer et al., 1999; Castaneda et al., 2008) which result in the enlargement of

lysosomes due to enzyme deficiency and protein accumulation. In contrast, mutations that prevent formation of large lysosomes can result in embryonic lethality. Loss of *Enpp2* results in defects in the actin cytoskeleton and fragmentation of the large lysosomes of the visceral endoderm (Koike et al., 2009). *Enpp2*-deficient embryos are also smaller than *wild-type* littermates, similar to *Mesd*-deficient embryos. This provides further evidence that integrity of visceral endoderm function is crucial for embryo survival. Together, these phenotypes also demonstrate that lysosome size can be regulated in multiple ways. Based on the observations that loss of MESD results in decreased lysosome size and that the size of the lysosome is likely reduced in the surviving *Lrp2* knockout, we proposed that receptor-mediated endocytosis may also contribute to lysosome size and function in tissues specialized for absorption.

Mislocalization of multiple LRPs in the visceral endoderm may contribute to the small embryo phenotype of *Mesd*

The visceral endoderm (VE) is an embryonic epithelium that has both absorptive and signaling capacities. Receptors expressed on the apical surface of the VE help endocytose maternal nutrients that can either be broken down to basic materials such as amino acids and fatty acids, or act as ligands that have important roles in signaling and patterning the underlying epiblast. The VE is also responsible for the synthesis of important serum proteins such as transthyretin and very low-density lipoproteins (VLDL). LRP2, or Megalin, is normally expressed on the apical membrane of the VE where it functions as a scavenger receptor, similar to its role in the kidney proximal tubule, another absorptive epithelium. In the absence of MESD, LRP2 is mislocalized

and is detected diffusely through the cell. This distribution likely reflects ER or proteosomal localization of the mis-folded receptor. Mislocalization of LRP2 may contribute to the small embryo phenotype observed in *Mesd* mutants. We observe that the lysosomes of *Mesd*-deficient embryos are smaller and fewer in number, which is consistent with the appearance of the kidney proximal tubule cells of *Lrp2*-deficient mice (Christensen and Willnow, 1999). The lysosomes normally function to breakdown proteins for reuse in cellular processes, and a decrease in size and number of VE lysosomes may impair the ability of the VE to synthesize serum proteins that can be used by the developing embryo.

My RT-PCR data demonstrates that a total of eight mammalian LRPs are expressed in the gastrulation-stage embryo. For this reason, the possibility exists that the small embryo size observed in *Mesd-KO* embryos results from the combined loss of multiple receptors in several tissues of the embryo. Conditional deletion of *Mesd* will help to verify whether the small embryo phenotype indeed results from disruption of LRP trafficking in the visceral endoderm. If the small embryo phenotype results from MESD in the visceral endoderm, and is not related to the role of LRP5/6, LRP2, or other LRPs in the epiblast, then deletion of *Mesd* in the epiblast, using a *Sox2-Cre* (Hayashi and McMahon, 2002) should restore embryo size and recapitulate the *Wnt3* and *Lrp5/6* knockout phenotypes (Liu et al., 1999; Kelly et al.). Conversely, deletion of *Mesd* in the visceral endoderm using *Ttr-Cre* (Kwon and Hadjantonakis, 2009) or trophoblast using *Cyp19-Cre* (Wenzel and Leone, 2007) will facilitate the analysis of LRP function in nutrient absorption by these tissues. I expect that deletion of *Mesd* in the visceral endoderm will likely result in endocytosis defects and potentially impaired embryo

growth while deletion of *Mesd* in the trophoblast will likely result in defects in trophoblast invasion and/or placenta formation similar to that observed in *Lrp1-/-* embryos (Herz et al., 1992; Herz et al., 1993).

Conditional knockout of *Mesd* will extend our understanding of LRP-related diseases

Conditional knockout of *Mesd* will be a valuable tool for as assessing whether all LRPs require MESD for *in vivo* trafficking as well as dissecting LRP function in embryonic and adult tissues. Many organs and tissues in the embryo and adult express multiple LRPs and some of these LRPs functionally overlap. However, because of functional redundancy of proteins, the role of individual LRPs in a tissue is often ambiguous or overlooked. One specific example of functional redundancy is the role of ApoER2 and VLDLR in the brain. Although loss of either gene does not result in a brain phenotype, simultaneous disruption of these receptors phenocopies the *Reeler* phenotype, resulting in defects in neuronal migration and cortical disorganization (Trommsdorff et al., 1999).

I predict that tissue specific knockout of *Mesd* would simultaneously disrupt multiple LRPs, For this reason, conditional knockout of *Mesd* in the brain will allow us to address one of two questions: (1) does MESD promote trafficking of ApoER2 and VLDLR in the cortex, and (2) are other LRPs important for neuronal organization in the adult brain? LRP1 is also expressed in the adult brain, but animals lacking LRP1 in differentiated neurons do not display the same motor defects as *Apoer2/Vldlr* deficient and *Reeler* animals, and also do not have defects in cortical organization (Trommsdorff et

al., 1999; May et al., 2004). If MESD is essential for promoting ApoER2 and VLDLR maturation, then we predict that brain-specific deletion of *Mesd* will recapitulate the *Reeler* phenotype. Moreover, selective deletion of *Mesd* in neurons, surrounding glial cells, or at different times during neuronal migration could help to define the temporal and cellular requirements for Reelin signaling. If deletion of *Mesd* in the brain disrupts processes other than neuronal migration and cortical organization, these data will argue for involvement of LRPs other than ApoER2 and VLDLR in brain development.

In Chapter 3, I demonstrated that MESD is required for localization of LRP2, which contains 7 β-propeller/EGFs. However, results from Jen-Chih Hsieh's *in vitro* receptor secretion assay suggest that individual β-propeller/EGFs do not always require MESD to promote their maturation. This raises the question of whether MESD is required for trafficking of LRPs containing a single β-propeller/EGF. Since ApoER2 and VLDLR are two examples of LRP receptors that contain only one β-propeller/EGF, comparison of the *Reeler* and brain specific deletion of *Mesd* phenotypes will also help to clarify whether LRPs with only a single β-propeller/EGF require MESD *in vivo* for trafficking.

LDLR also only contains one β-propeller/EGF and it is highly expressed in the liver and vascular endothelia, along with LRP1 (May et al., 2005). *Ldlr*-deficient mice maintained on a diet containing 1.25% cholesterol exhibited a ten-fold increase in plasma cholesterol and development of atherosclerosis by 7 months of age compared to chow-fed controls (Ishibashi et al., 1994). This phenotype is exacerbated by deletion of *Lrp1* in the vascular smooth muscle cells, and results in acceleration of fatty plaque formation in the arteries with virtually no increase in plasma triglyceride levels (Boucher et al., 2003). I

predict that conditional deletion of *Mesd* in the vascular smooth muscle will result in a phenotype that is less severe than the conditional deletion of *Lrp1* in an *Ldlr*-deficient background. I further hypothesize that the phenotype would instead bear a greater resemblance to the conditional deletion of *Lrp1* in a *wild-type* background, which has a lower susceptibility to developing atherosclerotic plaques (Boucher et al., 2003). This hypothesis is based on the observation that conditional knockout of LRP1 in the liver in an *Ldlr*-deficient background results in a significant increase in plasma lipoprotein levels over *Ldlr*-deficient animals alone (Rohlmann et al., 1998). This suggests that the high hepatic expression of LRP1 which would remain functional to to reduce the amount of plasma cholesterol by clearing chylomicron remnants and LDL particles from the plasma. However, if *Mesd* were conditionally removed from the vascular smooth muscle in an *Ldlr-/-* background, I predict that we would observe a significant increase in the formation of atherosclerotic plaques, accompanied by an increase in plasma LDL particles. I expect that this phenotype would be much more severe than deletion of a single *Lrp* in an *Ldlr-/-* background due to disruption of multiple lipoprotein clearance receptors in a sensitized background.

Similarly, conditional deletion of *Mesd* in hepatocytes can address the question of whether MESD is required for trafficking LRPs with a single β-propeller/EGF, such as LDLR. *Ldlr-/-* animals have historically been used as a model for hypercholesterolemia, however, a floxed allele of *Ldlr* has not yet been generated to study the conditional removal of *Ldlr* from hepatocytes. Based on the increase of plasma LDL in Lrp^{flox}/*Ldlr-/-* animals lacking *Lrp1* in the liver compared to *Ldlr-/-* animals (Rohlmann et al., 1998), I predict that conditional deletion of *Mesd* in hepatocytes will result in a clear increase in

plasma lipoprotein levels. This would suggest that MESD plays an important role in regulating hepatic lipoprotein clearance and progression of hypercholesterolemia and atherosclerosis. It would also suggest that MESD is required for trafficking of LRP receptors containing a single β-propeller/EGF, which would likely complement conditional knockout studies of MESD-dependent trafficking of ApoER2 and VLDLR in the brain. In the absence of a phenotype, this would suggest that expression of extra-hepatic LRP and MESD have a greater contribution in regulating lipoprotein metabolism than previously anticipated (Kroon and Powell, 1992).

As reviewed in the Introduction, dysfunction of many LRPs can contribute to human diseases. A greater understanding of how MESD functions to regulate such a large family of receptors will provide valuable data that will extend our knowledge of MESD-mediated folding defects, and LRP-related diseases.

BIBLIOGRAPHY

Abrami L, Kunz B, Iacovache I, van der Goot FG. 2008. Palmitoylation and ubiquitination regulate exit of the Wnt signaling protein LRP6 from the endoplasmic reticulum. Proc Natl Acad Sci U S A 105:5384-5389.

Adamska M, MacDonald BT, Meisler MH. 2003. Doubleridge, a mouse mutant with defective compaction of the apical ectodermal ridge and normal dorsal-ventral patterning of the limb. Dev Biol 255:350-362.

Adamska M, MacDonald BT, Sarmast ZH, Oliver ER, Meisler MH. 2004. En1 and Wnt7a interact with Dkk1 during limb development in the mouse. Dev Biol 272:134-144.

Andersen OM, Christensen LL, Christensen PA, Sorensen ES, Jacobsen C, Moestrup SK, Etzerodt M, Thogersen HC. 2000. Identification of the minimal functional unit in the low density lipoprotein receptor-related protein for binding the receptor-associated protein (RAP). A conserved acidic residue in the complement-type repeats is important for recognition of RAP. J Biol Chem 275:21017-21024.

Ausubel F, M.; Brent, Roger; Kingston, Robert, E.; Moore, David, D.; Seidman, J. G.; Smith, John, A.; Struhl, Kevin, editor. 1993. Current Protocols in Molecular Biology. Boston, MA: Wiley. 2.9.1-2.9.11 pp.

Avilion AA, Nicolis SK, Pevny LH, Perez L, Vivian N, Lovell-Badge R. 2003. Multipotent cell lineages in early mouse development depend on SOX2 function. Genes Dev 17:126-140.

Bagshaw RD, Mahuran DJ, Callahan JW. 2005a. Lysosomal membrane proteomics and biogenesis of lysosomes. Mol Neurobiol 32:27-41.

Bagshaw RD, Mahuran DJ, Callahan JW. 2005b. A proteomic analysis of lysosomal integral membrane proteins reveals the diverse composition of the organelle. Mol Cell Proteomics 4:133-143.

Baron MH. 2005. Early patterning of the mouse embryo: implications for hematopoietic commitment and differentiation. Exp Hematol 33:1015-1020.

Beddington RS, Robertson EJ. 1999. Axis development and early asymmetry in mammals. Cell 96:195-209.

Bejsovec A. 2005. Wnt pathway activation: new relations and locations. Cell 120:11-14.

Bielinska M, Narita N, Wilson DB. 1999. Distinct roles for visceral endoderm during embryonic mouse development. Int J Dev Biol 43:183-205.

Bieri S, Djordjevic JT, Daly NL, Smith R, Kroon PA. 1995. Disulfide bridges of a cysteine-rich repeat of the LDL receptor ligand-binding domain. Biochemistry 34:13059-13065.

Birn H, Vorum H, Verroust PJ, Moestrup SK, Christensen EI. 2000. Receptor-associated protein is important for normal processing of megalin in kidney proximal tubules. J Am Soc Nephrol 11:191-202.

Blanchette-Mackie EJ, Dwyer NK, Amende LM, Kruth HS, Butler JD, Sokol J, Comly ME, Vanier MT, August JT, Brady RO, et al. 1988. Type-C Niemann-Pick disease: low density lipoprotein uptake is associated with premature cholesterol accumulation in the Golgi complex and excessive cholesterol storage in lysosomes. Proc Natl Acad Sci U S A 85:8022-8026.

Bock HH, Herz J. 2003. Reelin activates SRC family tyrosine kinases in neurons. Curr Biol 13:18-26.

Bosshard HR, Marti DN, Jelesarov I. 2004. Protein stabilization by salt bridges: concepts, experimental approaches and clarification of some misunderstandings. J Mol Recognit 17:1-16.

Boucher P, Gotthardt M, Li WP, Anderson RG, Herz J. 2003. LRP: role in vascular wall integrity and protection from atherosclerosis. Science 300:329-332.

Brent RL, Beckman DA, Jensen M, Koszalka TR. 1990. Experimental yolk sac dysfunction as a model for studying nutritional disturbances in the embryo during early organogenesis. Teratology 41:405-413.

Brown MS, Goldstein JL. 1986. A receptor-mediated pathway for cholesterol homeostasis. Science 232:34-47.

Brown SD, Twells RC, Hey PJ, Cox RD, Levy ER, Soderman AR, Metzker ML, Caskey CT, Todd JA, Hess JF. 1998. Isolation and characterization of LRP6, a novel member of the low density lipoprotein receptor gene family. Biochem Biophys Res Commun 248:879-888.

Bu G, Maksymovitch EA, Nerbonne JM, Schwartz AL. 1994. Expression and function of the low density lipoprotein receptor-related protein (LRP) in mammalian central neurons. J Biol Chem 269:18521-18528.

Bu G, Schwartz AL. 1998. RAP, a novel type of ER chaperone. Trends Cell Biol 8:272-276.

Burke KT, Colvin PL, Myatt L, Graf GA, Schroeder F, Woollett LA. 2009. Transport of maternal cholesterol to the fetus is affected by maternal plasma cholesterol concentrations in the golden Syrian hamster. J Lipid Res 50:1146-1155.

Cadigan KM, Liu YI. 2006. Wnt signaling: complexity at the surface. J Cell Sci 119:395-402.

Camus A, Perea-Gomez A, Moreau A, Collignon J. 2006. Absence of Nodal signaling promotes precocious neural differentiation in the mouse embryo. Dev Biol 295:743-755.

Castaneda JA, Lim MJ, Cooper JD, Pearce DA. 2008. Immune system irregularities in lysosomal storage disorders. Acta Neuropathol 115:159-174.

Chambers I, Colby D, Robertson M, Nichols J, Lee S, Tweedie S, Smith A. 2003. Functional expression cloning of Nanog, a pluripotency sustaining factor in embryonic stem cells. Cell 113:643-655.

Chatelet F, Brianti E, Ronco P, Roland J, Verroust P. 1986a. Ultrastructural localization by monoclonal antibodies of brush border antigens expressed by glomeruli. I. Renal distribution. Am J Pathol 122:500-511.

Chatelet F, Brianti E, Ronco P, Roland J, Verroust P. 1986b. Ultrastructural localization by monoclonal antibodies of brush border antigens expressed by glomeruli. II. Extrarenal distribution. Am J Pathol 122:512-519.

Chen J, Li Q, Liu CC, Zhou B, Bu G, Wang J. 2010. NMR structure note: solution structure of the core domain of MESD that is essential for proper folding of LRP5/6. J Biomol NMR 47:283-288.

Christensen EI, Devuyst O, Dom G, Nielsen R, Van der Smissen P, Verroust P, Leruth M, Guggino WB, Courtoy PJ. 2003. Loss of chloride channel ClC-5 impairs endocytosis by defective trafficking of megalin and cubilin in kidney proximal tubules. Proc Natl Acad Sci U S A 100:8472-8477.

Christensen EI, Willnow TE. 1999. Essential role of megalin in renal proximal tubule for vitamin homeostasis. J Am Soc Nephrol 10:2224-2236.

Clevers H. 2006. Wnt/beta-catenin signaling in development and disease. Cell 127:469-480.

Coligan J, E.; Dunn, Ben, M.; Speicher, David, W.; Wingfield, Paul, T., editor. 1995-2002. Current Protocols in Protein Science. John Wiley and Sons, Inc.

**Constam DB.
http://www.isrec.ch/research/groups/research_groups_detail_eid_801_lid_2.htm.**

Cox B, Kotlyar M, Evangelou AI, Ignatchenko V, Ignatchenko A, Whiteley K, Jurisica I, Adamson SL, Rossant J, Kislinger T. 2009. Comparative systems biology of human and mouse as a tool to guide the modeling of human placental pathology. Mol Syst Biol 5:279.

Cross JC, Werb Z, Fisher SJ. 1994. Implantation and the placenta: key pieces of the development puzzle. Science 266:1508-1518.

Culi J, Mann RS. 2003. Boca, an endoplasmic reticulum protein required for wingless signaling and trafficking of LDL receptor family members in Drosophila. Cell 112:343-354.

Culi J, Springer TA, Mann RS. 2004. Boca-dependent maturation of beta-propeller/EGF modules in low-density lipoprotein receptor proteins. EMBO J 23:1372-1380.

Daniels DL, Weis WI. 2005. Beta-catenin directly displaces Groucho/TLE repressors from Tcf/Lef in Wnt-mediated transcription activation. Nat Struct Mol Biol 12:364-371.

de Duve C. 2005. The lysosome turns fifty. Nat Cell Biol 7:847-849.

Denisenko AD, Klimov AN. 1975. [Comparative characteristics of the fatty acid composition of lipoproteins in human blood plasma and aortic wall]. Biull Eksp Biol Med 79:44-47.

Dittmer F, Ulbrich EJ, Hafner A, Schmahl W, Meister T, Pohlmann R, von Figura K. 1999. Alternative mechanisms for trafficking of lysosomal enzymes in mannose 6-phosphate receptor-deficient mice are cell type-specific. J Cell Sci 112 (Pt 10):1591-1597.

Doran AC, Meller N, McNamara CA. 2008. Role of smooth muscle cells in the initiation and early progression of atherosclerosis. Arterioscler Thromb Vasc Biol 28:812-819.

Dreux AC, Lamb DJ, Modjtahedi H, Ferns GA. 2006. The epidermal growth factor receptors and their family of ligands: their putative role in atherogenesis. Atherosclerosis 186:38-53.

Du JT, Hideyuki; Leonhard-Melief, Christina; Shroyer, Kenneth R.; Dlugosz, Malgosia; Haltiwanger, Robert S.; Holdener, Bernadette C. 2010. O-Fucosylation of Thrombospondin Type 1 Repeats Restricts Epithelia to Mesenchymal Transition (EMT) and Maintains Epiblast Pluripotency During Mouse Gastrulation. Developmental Biology In Press.

Dutta-Roy AK. 2000. Transport mechanisms for long-chain polyunsaturated fatty acids in the human placenta. Am J Clin Nutr 71:315S-322S.

Evans LP, S.; McCarthy, R. D. 1960. Fatty Acid Composition of the Lipid Fractions from Bovine Serum Lipoproteins. Journal Series of the Pennsylvania Agricultural Experiment Station:8.

Farese RV, Jr., Cases S, Ruland SL, Kayden HJ, Wong JS, Young SG, Hamilton RL. 1996. A novel function for apolipoprotein B: lipoprotein synthesis in the yolk sac is critical for maternal-fetal lipid transport in mice. J Lipid Res 37:347-360.

Fass D, Blacklow S, Kim PS, Berger JM. 1997. Molecular basis of familial hypercholesterolaemia from structure of LDL receptor module. Nature 388:691-693.

Ferrari SL, Deutsch S, Antonarakis SE. 2005. Pathogenic mutations and polymorphisms in the lipoprotein receptor-related protein 5 reveal a new biological pathway for the control of bone mass. Curr Opin Lipidol 16:207-214.

Fisher C, Beglova N, Blacklow SC. 2006. Structure of an LDLR-RAP complex reveals a general mode for ligand recognition by lipoprotein receptors. Mol Cell 22:277-283.

Frykman PK, Brown MS, Yamamoto T, Goldstein JL, Herz J. 1995. Normal plasma lipoproteins and fertility in gene-targeted mice homozygous for a disruption in the gene encoding very low density lipoprotein receptor. Proc Natl Acad Sci U S A 92:8453-8457.

Gardai SJ, Xiao YQ, Dickinson M, Nick JA, Voelker DR, Greene KE, Henson PM. 2003. By binding SIRPalpha or calreticulin/CD91, lung collectins act as dual function surveillance molecules to suppress or enhance inflammation. Cell 115:13-23.

Gerbe F, Cox B, Rossant J, Chazaud C. 2008. Dynamic expression of Lrp2 pathway members reveals progressive epithelial differentiation of primitive endoderm in mouse blastocyst. Dev Biol 313:594-602.

Gerthoffer WT. 2007. Mechanisms of vascular smooth muscle cell migration. Circ Res 100:607-621.

Gimeno RE, Hirsch DJ, Punreddy S, Sun Y, Ortegon AM, Wu H, Daniels T, Stricker-Krongrad A, Lodish HF, Stahl A. 2003. Targeted deletion of fatty acid transport protein-4 results in early embryonic lethality. J Biol Chem 278:49512-49516.

Gleiberman AS, Encinas JM, Mignone JL, Michurina T, Rosenfeld MG, Enikolopov G. 2005. Expression of nestin-green fluorescent protein transgene marks oval cells in the adult liver. Dev Dyn 234:413-421.

Goldstein JL, Brown MS. 1974. Binding and degradation of low density lipoproteins by cultured human fibroblasts. Comparison of cells from a normal subject and from a patient with homozygous familial hypercholesterolemia. J Biol Chem 249:5153-5162.

Goldstein JL, Brown MS. 2001. Molecular medicine. The cholesterol quartet. Science 292:1310-1312.

Gomez-Puertas P, Martin-Benito J, Carrascosa JL, Willison KR, Valpuesta JM. 2004. The substrate recognition mechanisms in chaperonins. J Mol Recognit 17:85-94.

Gong Y, Slee RB, Fukai N, Rawadi G, Roman-Roman S, Reginato AM, Wang H, Cundy T, Glorieux FH, Lev D, Zacharin M, Oexle K, Marcelino J, Suwairi W, Heeger S, Sabatakos G, Apte S, Adkins WN, Allgrove J, Arslan-Kirchner M, Batch JA, Beighton P, Black GC, Boles RG, Boon LM, Borrone C, Brunner HG, Carle GF, Dallapiccola B, De Paepe A, Floege B, Halfhide ML, Hall B, Hennekam RC, Hirose T, Jans A, Juppner H, Kim CA, Keppler-Noreuil K, Kohlschuetter A, LaCombe D, Lambert M, Lemyre E, Letteboer T, Peltonen L, Ramesar RS, Romanengo M, Somer H, Steichen-Gersdorf E, Steinmann B, Sullivan B, Superti-Furga A, Swoboda W, van den Boogaard MJ, Van Hul W, Vikkula M, Votruba M, Zabel B, Garcia T, Baron R, Olsen BR, Warman ML. 2001. LDL receptor-related protein 5 (LRP5) affects bone accrual and eye development. Cell 107:513-523.

Goudriaan JR, Tacken PJ, Dahlmans VE, Gijbels MJ, van Dijk KW, Havekes LM, Jong MC. 2001. Protection from obesity in mice lacking the VLDL receptor. Arterioscler Thromb Vasc Biol 21:1488-1493.

Guo Y, Yu X, Rihani K, Wang QY, Rong L. 2004. The role of a conserved acidic residue in calcium-dependent protein folding for a low density lipoprotein (LDL)-A module: implications in structure and function for the LDL receptor superfamily. J Biol Chem 279:16629-16637.

Hammad SM, Barth JL, Knaak C, Argraves WS. 2000. Megalin acts in concert with cubilin to mediate endocytosis of high density lipoproteins. J Biol Chem 275:12003-12008.

Hansen LA, Alexander N, Hogan ME, Sundberg JP, Dlugosz A, Threadgill DW, Magnuson T, Yuspa SH. 1997. Genetically null mice reveal a central role for epidermal growth factor receptor in the differentiation of the hair follicle and normal hair development. Am J Pathol 150:1959-1975.

Hart AH, Hartley L, Ibrahim M, Robb L. 2004. Identification, cloning and expression analysis of the pluripotency promoting Nanog genes in mouse and human. Dev Dyn 230:187-198.

Harwood BN, Cross SK, Radford EE, Haac BE, De Vries WN. 2008. Members of the WNT signaling pathways are widely expressed in mouse ovaries, oocytes, and cleavage stage embryos. Dev Dyn 237:1099-1111.

Hayashi S, McMahon AP. 2002. Efficient recombination in diverse tissues by a tamoxifen-inducible form of Cre: a tool for temporally regulated gene activation/inactivation in the mouse. Dev Biol 244:305-318.

Herman GE. 2003. Disorders of cholesterol biosynthesis: prototypic metabolic malformation syndromes. Hum Mol Genet 12 Spec No 1:R75-88.

Herz J, Clouthier DE, Hammer RE. 1992. LDL receptor-related protein internalizes and degrades uPA-PAI-1 complexes and is essential for embryo implantation. Cell 71:411-421.

Herz J, Couthier DE, Hammer RE. 1993. Correction: LDL receptor-related protein internalizes and degrades uPA-PAI-1 complexes and is essential for embryo implantation. Cell 73:428.

Herz J, Goldstein JL, Strickland DK, Ho YK, Brown MS. 1991. 39-kDa protein modulates binding of ligands to low density lipoprotein receptor-related protein/alpha 2-macroglobulin receptor. J Biol Chem 266:21232-21238.

Hogan BL. 1994. Developmental signalling. Sorting out the signals. Curr Biol 4:1122-1124.

Holdener BC, Faust C, Rosenthal NS, Magnuson T. 1994. msd is required for mesoderm induction in mice. Development 120:1335-1346.

Holmen SL, Giambernardi TA, Zylstra CR, Buckner-Berghuis BD, Resau JH, Hess JF, Glatt V, Bouxsein ML, Ai M, Warman ML, Williams BO. 2004. Decreased BMD and limb deformities in mice carrying mutations in both Lrp5 and Lrp6. J Bone Miner Res 19:2033-2040.

Hsieh JC, Kodjabachian L, Rebbert ML, Rattner A, Smallwood PM, Samos CH, Nusse R, Dawid IB, Nathans J. 1999. A new secreted protein that binds to Wnt proteins and inhibits their activities. Nature 398:431-436.

Hsieh JC, Lee L, Zhang L, Wefer S, Brown K, DeRossi C, Wines ME, Rosenquist T, Holdener BC. 2003. Mesd encodes an LRP5/6 chaperone essential for specification of mouse embryonic polarity. Cell 112:355-367.

Ishibashi S, Brown MS, Goldstein JL, Gerard RD, Hammer RE, Herz J. 1993. Hypercholesterolemia in low density lipoprotein receptor knockout mice and its reversal by adenovirus-mediated gene delivery. J Clin Invest 92:883-893.

Ishibashi S, Goldstein JL, Brown MS, Herz J, Burns DK. 1994. Massive xanthomatosis and atherosclerosis in cholesterol-fed low density lipoprotein receptor-negative mice. J Clin Invest 93:1885-1893.

Jensen JK, Dolmer K, Schar C, Gettins PG. 2009. Receptor-associated protein (RAP) has two high-affinity binding sites for the low-density lipoprotein receptor-related protein (LRP): consequences for the chaperone functions of RAP. Biochem J 421:273-282.

Jeon H, Meng W, Takagi J, Eck MJ, Springer TA, Blacklow SC. 2001. Implications for familial hypercholesterolemia from the structure of the LDL receptor YWTD-EGF domain pair. Nat Struct Biol 8:499-504.

Johnson EB, Hammer RE, Herz J. 2005. Abnormal development of the apical ectodermal ridge and polysyndactyly in Megf7-deficient mice. Hum Mol Genet 14:3523-3538.

Jollie WP. 1990. Effects of sustained dietary ethanol on the ultrastructure of the visceral yolk-sac placenta of the rat. Teratology 42:541-552.

Kalantry S, Manning S, Haub O, Tomihara-Newberger C, Lee HG, Fangman J, Disteche CM, Manova K, Lacy E. 2001. The amnionless gene, essential for mouse gastrulation, encodes a visceral-endoderm-specific protein with an extracellular cysteine-rich domain. Nat Genet 27:412-416.

Kang DE, Pietrzik CU, Baum L, Chevallier N, Merriam DE, Kounnas MZ, Wagner SL, Troncoso JC, Kawas CH, Katzman R, Koo EH. 2000. Modulation of amyloid beta-protein clearance and Alzheimer's disease susceptibility by the LDL receptor-related protein pathway. J Clin Invest 106:1159-1166.

Kang S, Davis RA. 2000. Cholesterol and hepatic lipoprotein assembly and secretion. Biochim Biophys Acta 1529:223-230.

Kato M, Patel MS, Levasseur R, Lobov I, Chang BH, Glass DA, 2nd, Hartmann C, Li L, Hwang TH, Brayton CF, Lang RA, Karsenty G, Chan L. 2002. Cbfa1-independent decrease in osteoblast proliferation, osteopenia, and persistent embryonic eye vascularization in mice deficient in Lrp5, a Wnt coreceptor. J Cell Biol 157:303-314.

Kelly OG, Pinson KI, Skarnes WC. 2004. The Wnt co-receptors Lrp5 and Lrp6 are essential for gastrulation in mice. Development 131:2803-2815.

Khan Z, Vijayakumar S, de la Torre TV, Rotolo S, Bafico A. 2007. Analysis of endogenous LRP6 function reveals a novel feedback mechanism by which Wnt negatively regulates its receptor. Mol Cell Biol 27:7291-7301.

Koduri V, Blacklow SC. 2007. Requirement for natively unstructured regions of mesoderm development candidate 2 in promoting low-density lipoprotein receptor-related protein 6 maturation. Biochemistry 46:6570-6577.

Koehler C, Andersen OM, Diehl A, Krause G, Schmieder P, Oschkinat H. 2006. The solution structure of the core of mesoderm development (MESD), a chaperone for members of the LDLR-family. J Struct Funct Genomics 7:131-138.

Koehler C, Lighthouse JK, Werther T, Andersen OM, Diehl A, Schmieder P, Du J, Holdener BC, Oschkinat H. submitted. The structure of MESD 45-184 sheds light into the mechanism of LRP folding.

Koike S, Keino-Masu K, Ohto T, Sugiyama F, Takahashi S, Masu M. 2009. Autotaxin/lysophospholipase D-mediated lysophosphatidic acid signaling is required to form distinctive large lysosomes in the visceral endoderm cells of the mouse yolk sac. J Biol Chem 284:33561-33570.

Kokubu C, Heinzmann U, Kokubu T, Sakai N, Kubota T, Kawai M, Wahl MB, Galceran J, Grosschedl R, Ozono K, Imai K. 2004. Skeletal defects in ringelschwanz mutant mice reveal that Lrp6 is required for proper somitogenesis and osteogenesis. Development 131:5469-5480.

Kornfeld S. 1986. Trafficking of lysosomal enzymes in normal and disease states. J Clin Invest 77:1-6.

Kozyraki R, Fyfe J, Kristiansen M, Gerdes C, Jacobsen C, Cui S, Christensen EI, Aminoff M, de la Chapelle A, Krahe R, Verroust PJ, Moestrup SK. 1999. The intrinsic factor-vitamin B12 receptor, cubilin, is a high-affinity apolipoprotein A-I receptor facilitating endocytosis of high-density lipoprotein. Nat Med 5:656-661.

Kozyraki R, Fyfe J, Verroust PJ, Jacobsen C, Dautry-Varsat A, Gburek J, Willnow TE, Christensen EI, Moestrup SK. 2001. Megalin-dependent cubilin-mediated endocytosis is a major pathway for the apical uptake of transferrin in polarized epithelia. Proc Natl Acad Sci U S A 98:12491-12496.

Kozyraki R, Gofflot F. 2007. Multiligand endocytosis and congenital defects: roles of cubilin, megalin and amnionless. Curr Pharm Des 13:3038-3046.

Kroon PA, Powell EE. 1992. Liver, lipoproteins and disease: I. Biochemistry of lipoprotein metabolism. J Gastroenterol Hepatol 7:214-224.

Kubota H. 2009. Quality control against misfolded proteins in the cytosol: a network for cell survival. J Biochem 146:609-616.

Kubota T, Michigami T, Sakaguchi N, Kokubu C, Suzuki A, Namba N, Sakai N, Nakajima S, Imai K, Ozono K. 2008. Lrp6 hypomorphic mutation affects bone mass through bone resorption in mice and impairs interaction with Mesd. J Bone Miner Res 23:1661-1671.

Kumar S, Nussinov R. 1999. Salt bridge stability in monomeric proteins. J Mol Biol 293:1241-1255.

Kumar S, Nussinov R. 2001. Fluctuations in ion pairs and their stabilities in proteins. Proteins 43:433-454.

Kwon GS, Hadjantonakis AK. 2009. Transthyretin mouse transgenes direct RFP expression or Cre-mediated recombination throughout the visceral endoderm. Genesis 47:447-455.

Lai SL, Chien AJ, Moon RT. 2009. Wnt/Fz signaling and the cytoskeleton: potential roles in tumorigenesis. Cell Res 19:532-545.

Lallemand Y, Luria V, Haffner-Krausz R, Lonai P. 1998. Maternally expressed PGK-Cre transgene as a tool for early and uniform activation of the Cre site-specific recombinase. Transgenic Res 7:105-112.

Lardon J, Rooman I, Bouwens L. 2002. Nestin expression in pancreatic stellate cells and angiogenic endothelial cells. Histochem Cell Biol 117:535-540.

Lee D, Walsh JD, Mikhailenko I, Yu P, Migliorini M, Wu Y, Krueger S, Curtis JE, Harris B, Lockett S, Blacklow SC, Strickland DK, Wang YX. 2006. RAP uses a histidine switch to regulate its interaction with LRP in the ER and Golgi. Mol Cell 22:423-430.

Leheste JR, Rolinski B, Vorum H, Hilpert J, Nykjaer A, Jacobsen C, Aucouturier P, Moskaug JO, Otto A, Christensen EI, Willnow TE. 1999. Megalin knockout mice as an animal model of low molecular weight proteinuria. Am J Pathol 155:1361-1370.

Li Y, Lu W, Bu G. 2005. Striking differences of LDL receptor-related protein 1B expression in mouse and human. Biochem Biophys Res Commun 333:868-873.

Li Y, Lu W, Schwartz AL, Bu G. 2002. Receptor-associated protein facilitates proper folding and maturation of the low-density lipoprotein receptor and its class 2 mutants. Biochemistry 41:4921-4928.

Lighthouse JK, Zhang L, Hsieh J-C, Rosenquist T, Holdener BC. submitted. MESD is Essential for Apical Localization of Megalin/LRP2 in the Visceral Endoderm. Developmental Dynamics.

Lillis AP, Van Duyn LB, Murphy-Ullrich JE, Strickland DK. 2008. LDL receptor-related protein 1: unique tissue-specific functions revealed by selective gene knockout studies. Physiol Rev 88:887-918.

Little RD, Carulli JP, Del Mastro RG, Dupuis J, Osborne M, Folz C, Manning SP, Swain PM, Zhao SC, Eustace B, Lappe MM, Spitzer L, Zweier S, Braunschweiger K, Benchekroun Y, Hu X, Adair R, Chee L, FitzGerald MG, Tulig C, Caruso A, Tzellas N, Bawa A, Franklin B, McGuire S, Nogues X, Gong G, Allen KM, Anisowicz A, Morales AJ, Lomedico PT, Recker SM, Van Eerdewegh P, Recker RR, Johnson ML. 2002. A mutation in the LDL receptor-related protein 5 gene results in the autosomal dominant high-bone-mass trait. Am J Hum Genet 70:11-19.

Liu P, Wakamiya M, Shea MJ, Albrecht U, Behringer RR, Bradley A. 1999. Requirement for Wnt3 in vertebrate axis formation. Nat Genet 22:361-365.

Loukinova E, Ranganathan S, Kuznetsov S, Gorlatova N, Migliorini MM, Loukinov D, Ulery PG, Mikhailenko I, Lawrence DA, Strickland DK. 2002. Platelet-derived growth factor (PDGF)-induced tyrosine phosphorylation of the low density lipoprotein receptor-related protein (LRP). Evidence for integrated co-receptor function betwenn LRP and the PDGF. J Biol Chem 277:15499-15506.

Luetteke NC, Qiu TH, Fenton SE, Troyer KL, Riedel RF, Chang A, Lee DC. 1999. Targeted inactivation of the EGF and amphiregulin genes reveals distinct roles for EGF receptor ligands in mouse mammary gland development. Development 126:2739-2750.

Luzio JP, Parkinson MD, Gray SR, Bright NA. 2009. The delivery of endocytosed cargo to lysosomes. Biochem Soc Trans 37:1019-1021.

Luzio JP, Pryor PR, Bright NA. 2007. Lysosomes: fusion and function. Nat Rev Mol Cell Biol 8:622-632.

Maretto S, Cordenonsi M, Dupont S, Braghetta P, Broccoli V, Hassan AB, Volpin D, Bressan GM, Piccolo S. 2003. Mapping Wnt/beta-catenin signaling during mouse development and in colorectal tumors. Proc Natl Acad Sci U S A 100:3299-3304.

Marschang P, Brich J, Weeber EJ, Sweatt JD, Shelton JM, Richardson JA, Hammer RE, Herz J. 2004. Normal development and fertility of knockout mice lacking the tumor suppressor gene LRP1b suggest functional compensation by LRP1. Mol Cell Biol 24:3782-3793.

Marzolo MP, Bu G. 2009. Lipoprotein receptors and cholesterol in APP trafficking and proteolytic processing, implications for Alzheimer's disease. Semin Cell Dev Biol 20:191-200.

Maurer ME, Cooper JA. 2005. Endocytosis of megalin by visceral endoderm cells requires the Dab2 adaptor protein. J Cell Sci 118:5345-5355.

May P, Herz J, Bock HH. 2005. Molecular mechanisms of lipoprotein receptor signalling. Cell Mol Life Sci 62:2325-2338.

May P, Rohlmann A, Bock HH, Zurhove K, Marth JD, Schomburg ED, Noebels JL, Beffert U, Sweatt JD, Weeber EJ, Herz J. 2004. Neuronal LRP1 functionally associates with postsynaptic proteins and is required for normal motor function in mice. Mol Cell Biol 24:8872-8883.

May P, Woldt E, Matz RL, Boucher P. 2007. The LDL receptor-related protein (LRP) family: an old family of proteins with new physiological functions. Ann Med 39:219-228.

Mesli S, Javorschi S, Berard AM, Landry M, Priddle H, Kivlichan D, Smith AJ, Yen FT, Bihain BE, Darmon M. 2004. Distribution of the lipolysis stimulated receptor in adult and

embryonic murine tissues and lethality of LSR-/- embryos at 12.5 to 14.5 days of gestation. Eur J Biochem 271:3103-3114.

Mishra SK, Keyel PA, Hawryluk MJ, Agostinelli NR, Watkins SC, Traub LM. 2002. Disabled-2 exhibits the properties of a cargo-selective endocytic clathrin adaptor. EMBO J 21:4915-4926.

Moestrup SK, Kozyraki R, Kristiansen M, Kaysen JH, Rasmussen HH, Brault D, Pontillon F, Goda FO, Christensen EI, Hammond TG, Verroust PJ. 1998. The intrinsic factor-vitamin B12 receptor and target of teratogenic antibodies is a megalin-binding peripheral membrane protein with homology to developmental proteins. J Biol Chem 273:5235-5242.

Moestrup SK, Verroust PJ. 2001. Megalin- and cubilin-mediated endocytosis of protein-bound vitamins, lipids, and hormones in polarized epithelia. Annu Rev Nutr 21:407-428.

Morris SM, Cooper JA. 2001. Disabled-2 colocalizes with the LDLR in clathrin-coated pits and interacts with AP-2. Traffic 2:111-123.

Morris SM, Tallquist MD, Rock CO, Cooper JA. 2002. Dual roles for the Dab2 adaptor protein in embryonic development and kidney transport. EMBO J 21:1555-1564.

Muller D, Nykjaer A, Willnow TE. 2003. From holoprosencephaly to osteopathology: role of multifunctional endocytic receptors in absorptive epithelia. Ann Med 35:290-299.

Nagy A. 2000. Cre recombinase: the universal reagent for genome tailoring. Genesis 26:99-109.

Nagy AG, Marina; Vintersten, Kristina; Behringer, Richard. 2003. Manipulating the Mouse Embryo. A Laboratory Manual. Cold Spring Harbor, NY: Cold Spring Harbor Laboratory Press. 764 p.

Nielsen R, Courtoy PJ, Jacobsen C, Dom G, Lima WR, Jadot M, Willnow TE, Devuyst O, Christensen EI. 2007. Endocytosis provides a major alternative pathway for lysosomal biogenesis in kidney proximal tubular cells. Proc Natl Acad Sci U S A 104:5407-5412.

Nykjaer A, Dragun D, Walther D, Vorum H, Jacobsen C, Herz J, Melsen F, Christensen EI, Willnow TE. 1999. An endocytic pathway essential for renal uptake and activation of the steroid 25-(OH) vitamin D3. Cell 96:507-515.

Patel M, Morrow J, Maxfield FR, Strickland DK, Greenberg S, Tabas I. 2003. The cytoplasmic domain of the low density lipoprotein (LDL) receptor-related protein, but not that of the LDL receptor, triggers phagocytosis. J Biol Chem 278:44799-44807.

Perou CM, Leslie JD, Green W, Li L, Ward DM, Kaplan J. 1997. The Beige/Chediak-Higashi syndrome gene encodes a widely expressed cytosolic protein. J Biol Chem 272:29790-29794.

Pinson KI, Brennan J, Monkley S, Avery BJ, Skarnes WC. 2000. An LDL-receptor-related protein mediates Wnt signalling in mice. Nature 407:535-538.

Postic C, Magnuson MA. 2000. DNA excision in liver by an albumin-Cre transgene occurs progressively with age. Genesis 26:149-150.

Qiu Z, Strickland DK, Hyman BT, Rebeck GW. 2002. alpha 2-Macroglobulin exposure reduces calcium responses to N-methyl-D-aspartate via low density lipoprotein receptor-related protein in cultured hippocampal neurons. J Biol Chem 277:14458-14466.

Ralston A, Rossant J. 2005. Genetic regulation of stem cell origins in the mouse embryo. Clin Genet 68:106-112.

Rivera-Perez JA. 2007. Axial specification in mice: ten years of advances and controversies. J Cell Physiol 213:654-660.

Rohlmann A, Gotthardt M, Hammer RE, Herz J. 1998. Inducible inactivation of hepatic LRP gene by cre-mediated recombination confirms role of LRP in clearance of chylomicron remnants. J Clin Invest 101:689-695.

Russell ES. 1949. A Quantitative Histological Study of the Pigment Found in the Coat-Color Mutants of the House Mouse. III. Interdependence among the Variable Granule Attributes. Genetics 34:133-145.

Saftig P, Klumperman J. 2009. Lysosome biogenesis and lysosomal membrane proteins: trafficking meets function. Nat Rev Mol Cell Biol 10:623-635.

Sahali D, Mulliez N, Chatelet F, Dupuis R, Ronco P, Verroust P. 1988. Characterization of a 280-kD protein restricted to the coated pits of the renal brush border and the epithelial cells of the yolk sac. Teratogenic effect of the specific monoclonal antibodies. J Exp Med 167:213-218.

Scholer HR, Dressler GR, Balling R, Rohdewohld H, Gruss P. 1990. Oct-4: a germline-specific transcription factor mapping to the mouse t-complex. EMBO J 9:2185-2195.

Shen MM. 2007. Nodal signaling: developmental roles and regulation. Development 134:1023-1034.

Sibmooh N, Yamanont P, Krudsood S, Leowattana W, Brittenham G, Looareesuwan S, Udomsangpetch R. 2004. Increased fluidity and oxidation of malarial lipoproteins: relation with severity and induction of endothelial expression of adhesion molecules. Lipids Health Dis 3:15.

Simon-Chazottes D, Tutois S, Kuehn M, Evans M, Bourgade F, Cook S, Davisson MT, Guenet JL. 2006. Mutations in the gene encoding the low-density lipoprotein receptor LRP4 cause abnormal limb development in the mouse. Genomics 87:673-677.

Smith BT, Mussell JC, Fleming PA, Barth JL, Spyropoulos DD, Cooley MA, Drake CJ, Argraves WS. 2006. Targeted disruption of cubilin reveals essential developmental roles in the structure and function of endoderm and in somite formation. BMC Dev Biol 6:30.

Spoelgen R, Hammes A, Anzenberger U, Zechner D, Andersen OM, Jerchow B, Willnow TE. 2005. LRP2/megalin is required for patterning of the ventral telencephalon. Development 132:405-414.

Strickland DK, Gonias SL, Argraves WS. 2002. Diverse roles for the LDL receptor family. Trends Endocrinol Metab 13:66-74.

Strickland DK, Ranganathan S. 2003. Diverse role of LDL receptor-related protein in the clearance of proteases and in signaling. J Thromb Haemost 1:1663-1670.

Strope S, Rivi R, Metzger T, Manova K, Lacy E. 2004. Mouse amnionless, which is required for primitive streak assembly, mediates cell-surface localization and endocytic function of cubilin on visceral endoderm and kidney proximal tubules. Development 131:4787-4795.

Swertfeger DK, Hui DY. 2001. Apolipoprotein E: a cholesterol transport protein with lipid transport-independent cell signaling properties. Front Biosci 6:D526-535.

Tacken PJ, Teusink B, Jong MC, Harats D, Havekes LM, van Dijk KW, Hofker MH. 2000. LDL receptor deficiency unmasks altered VLDL triglyceride metabolism in VLDL receptor transgenic and knockout mice. J Lipid Res 41:2055-2062.

Takaoka K, Yamamoto M, Shiratori H, Meno C, Rossant J, Saijoh Y, Hamada H. 2006. The mouse embryo autonomously acquires anterior-posterior polarity at implantation. Dev Cell 10:451-459.

Tam PP, Loebel DA. 2007. Gene function in mouse embryogenesis: get set for gastrulation. Nat Rev Genet 8:368-381.

Tam PP, Loebel DA, Tanaka SS. 2006. Building the mouse gastrula: signals, asymmetry and lineages. Curr Opin Genet Dev 16:419-425.

Tanner SM, Aminoff M, Wright FA, Liyanarachchi S, Kuronen M, Saarinen A, Massika O, Mandel H, Broch H, de la Chapelle A. 2003. Amnionless, essential for mouse gastrulation, is mutated in recessive hereditary megaloblastic anemia. Nat Genet 33:426-429.

Tomihara-Newberger C, Haub O, Lee HG, Soares V, Manova K, Lacy E. 1998. The amn gene product is required in extraembryonic tissues for the generation of middle primitive streak derivatives. Dev Biol 204:34-54.

Toomes C, Bottomley HM, Jackson RM, Towns KV, Scott S, Mackey DA, Craig JE, Jiang L, Yang Z, Trembath R, Woodruff G, Gregory-Evans CY, Gregory-Evans K, Parker MJ, Black GC, Downey LM, Zhang K, Inglehearn CF. 2004. Mutations in LRP5 or FZD4 underlie the common familial exudative vitreoretinopathy locus on chromosome 11q. Am J Hum Genet 74:721-730.

Trommsdorff M, Gotthardt M, Hiesberger T, Shelton J, Stockinger W, Nimpf J, Hammer RE, Richardson JA, Herz J. 1999. Reeler/Disabled-like disruption of neuronal migration in knockout mice lacking the VLDL receptor and ApoE receptor 2. Cell 97:689-701.

Veniant MM, Withycombe S, Young SG. 2001. Lipoprotein size and atherosclerosis susceptibility in Apoe(-/-) and Ldlr(-/-) mice. Arterioscler Thromb Vasc Biol 21:1567-1570.

Verroust PJ, Birn H, Nielsen R, Kozyraki R, Christensen EI. 2002. The tandem endocytic receptors megalin and cubilin are important proteins in renal pathology. Kidney Int 62:745-756.

Wagner N, Wagner KD, Scholz H, Kirschner KM, Schedl A. 2006. Intermediate filament protein nestin is expressed in developing kidney and heart and might be regulated by the Wilms' tumor suppressor Wt1. Am J Physiol Regul Integr Comp Physiol 291:R779-787.

Waldron E, Heilig C, Schweitzer A, Nadella N, Jaeger S, Martin AM, Weggen S, Brix K, Pietrzik CU. 2008. LRP1 modulates APP trafficking along early compartments of the secretory pathway. Neurobiol Dis 31:188-197.

Watson ED, Cross JC. 2005. Development of structures and transport functions in the mouse placenta. Physiology (Bethesda) 20:180-193.

Weatherbee SD, Anderson KV, Niswander LA. 2006. LDL-receptor-related protein 4 is crucial for formation of the neuromuscular junction. Development 133:4993-5000.

Wenzel PL, Leone G. 2007. Expression of Cre recombinase in early diploid trophoblast cells of the mouse placenta. Genesis 45:129-134.

Willnow TE, Armstrong SA, Hammer RE, Herz J. 1995. Functional expression of low density lipoprotein receptor-related protein is controlled by receptor-associated protein in vivo. Proc Natl Acad Sci U S A 92:4537-4541.

Willnow TE, Hammes A, Eaton S. 2007. Lipoproteins and their receptors in embryonic development: more than cholesterol clearance. Development 134:3239-3249.

Willnow TE, Hilpert J, Armstrong SA, Rohlmann A, Hammer RE, Burns DK, Herz J. 1996. Defective forebrain development in mice lacking gp330/megalin. Proc Natl Acad Sci U S A 93:8460-8464.

Wines ME, Lee L, Katari MS, Zhang L, DeRossi C, Shi Y, Perkins S, Feldman M, McCombie WR, Holdener BC. 2001. Identification of mesoderm development (mesd) candidate genes by comparative mapping and genome sequence analysis. Genomics 72:88-98.

Wines ME, Shi Y, Lindor M, Holdener BC. 2000. Physical localization of the mesoderm development (mesd) functional region. Genomics 68:322-329.

Wines ME, Tiffany AM, Holdener BC. 1998. Physical localization of the mouse aryl hydrocarbon receptor nuclear translocator-2 (Arnt2) gene within the c112K deletion. Genomics 51:223-232.

Woollett LA. 2005. Maternal cholesterol in fetal development: transport of cholesterol from the maternal to the fetal circulation. Am J Clin Nutr 82:1155-1161.

Xu Q, Wang Y, Dabdoub A, Smallwood PM, Williams J, Woods C, Kelley MW, Jiang L, Tasman W, Zhang K, Nathans J. 2004. Vascular development in the retina and inner ear: control by Norrin and Frizzled-4, a high-affinity ligand-receptor pair. Cell 116:883-895.

Yamaguchi YL, Tanaka SS, Kasa M, Yasuda K, Tam PP, Matsui Y. 2006. Expression of low density lipoprotein receptor-related protein 4 (Lrp4) gene in the mouse germ cells. Gene Expr Patterns 6:607-612.

Ye X, Wang Y, Cahill H, Yu M, Badea TC, Smallwood PM, Peachey NS, Nathans J. 2009. Norrin, frizzled-4, and Lrp5 signaling in endothelial cells controls a genetic program for retinal vascularization. Cell 139:285-298.

Yepes M, Sandkvist M, Moore EG, Bugge TH, Strickland DK, Lawrence DA. 2003. Tissue-type plasminogen activator induces opening of the blood-brain barrier via the LDL receptor-related protein. J Clin Invest 112:1533-1540.

Young IS, McEneny J. 2001. Lipoprotein oxidation and atherosclerosis. Biochem Soc Trans 29:358-362.

Zhang Y, Wang Y, Li X, Zhang J, Mao J, Li Z, Zheng J, Li L, Harris S, Wu D. 2004. The LRP5 high-bone-mass G171V mutation disrupts LRP5 interaction with Mesd. Mol Cell Biol 24:4677-4684.

APPENDIX

Appendix A: *Mesd* mutant clone screen with isolated follow-up single mutations.

Colony #	Mutations	NC Mut.	Stop Mut.	Clone activity % of WT	Std Dev	Follow-up Single Mut.	Activity % of WT	Std Dev
1	C15stop, L22F, E35G, D45G, D53V, E68G, R77stop	-	2	-	-			
2	D53V	1	-	65%	5%	**D53V**	34%	3%
3	D45V, D51V	2	-	64%	4%	-	-	-
5	Q60H, D214N	2	-	110%	14%	-	-	-
11	D48G, Y49H, N114I	3	-	44%	3%	-	-	-
12	E62K, E190G	2	-	69%	4%	**E62K**	71%	5%
14	W61R, Y136N, E190K	3	-	22%	1%	**W61R**	24%	9%
16	P39R, K43E	2	-	7%[1] 65%[2]	0%[1] 46%[2]	-	-	-
17	N50K, K76E, S79T, T124A	3	-	62%	0%	**N50K**	92%	1%
18	S17L, D48Y, N50D, S94R, M98T	4	-	39%	8%	-		
19	W61R, Y136N, E190K	3	-	31%	7%	**W61R**	24%	9%
26	-	-	-	-	-	-	-	-
27	K42E, D45V, K91stop, A199P	1	1	10%[1] 43%[2]	3%[1] 17%[2]	-	-	-
29	W6C, R8P, D53V, E74stop	3	1	-	-			
31	L57P, N133Y	2	-	27%	9%	**L57P, N133Y**	20%, 43%	5%, 9%
33	Q168stop	-	1	16%[1] 110%[2]	1%[1] 8%[2]	-	-	-
34	A29G, K63N, E69D, P78H, P81S, S167R	5	-	-	-	-	-	-
35	K43R, D53E, K97V, S125R, G129S, D137A, A172T	5	-	52%[1] 79%[2]	8%[1] 5%[2]	**K97V**	106%	1%
37	C15stop	-	1	-	-	-	-	-

Colony #	Mutations	NC Mut.	Stop Mut.	Clone activity % of WT	Std Dev	Follow-up Single Mut.	Activity % of WT	Std Dev
39	P39R, K43E	2	-	90%[1] 96%[2] 101%[3]	3%[1] 4%[2] 5%[3]	-	-	-
41	K44R, C171Y, K201R, K212E	2	-	3%[1] 14%[2]	1%[1] 3%[2]	**C171Y**	91%	0%
42	W6S, P40S, M54T	2	-	41%[1] 56%[2] 76%[3]	1%[1] 14%[2] 2%[3]	**P40S, M54T**	80%, 75%	8%, 9%
43	W6S, P40S, M54T	2	-	92%	7%	**P40S, M54T**	80%, 75%	8%, 9%
44	Q168stop	-	1	-	-	-	-	-
46	N133Y, F150C	2	-	74%[1] 94%[2]	8%[1] 9%[2]	**N133Y**	43%	9%
49	-	-	-	-	-	-	-	-
51	-	-	-	-	-	-	-	-
56	-	-	-	-	-	-	-	-
57	-	-	-	-	-	-	-	-
58	L20Q	1	-	-	-	-	-	-
59	-	-	-	-	-	-	-	-
62	I142T, G144E	2	-	94%[1] 107%[2]	6%[1] 10%[2]	-	-	-
63	L58M, Q128L	2	-	99%	7%	-	-	-
64	L58M, Q128L	2	-	73%	25%	-	-	-
66	-	-	-	-	-	-	-	-
67	E117K, L176Q, E190G, T194M	2	-	-	-	-	-	-
68	W61-, M98T, I149V, F164S	1	-	10%[1] 19%[2]	9%[1] 2%[2]	-	-	-
69	N50S, K103E, W127R, E160K, P182H	4	-	14%[1] 18%[2]	4%[1] 1%[2]	**K103E, W127R, E160K**	63%, 5%, 95%	2%, 2%, 1%
70	K212R	-	-	17%[1] 101%[2]	3%[1] 2%[2]	-	-	-
71	S167T	-	-	-	-	-	-	-
74	A29G, E35D, K63N, E69D, P78H, P81S, S167R	5	-	4%[1] 17%[2]	1%[1] 1%[2]	-	-	-
75	F164Y, Q168L	1	-	97%	2%	-	-	-
76	R56L, K189E	2	-	106%	3%	-	-	-
77	Q168stop	-	1	107%	2%	-	-	-
79	K42R, E197D	-	-	89%	6%	**K42R**	91%	0%
85	K212R	-	-	105%	1%	-	-	-
88	S4P	1	-	-	-	-	-	-
89	P92R	1	-	-	-	-	-	-

Colony #	Mutations	NC Mut.	Stop Mut.	Clone activity % of WT	Std Dev	Follow-up Single Mut.	Activity % of WT	Std Dev
90	L20M	1	-	109%	9%	-	-	-
91	-	-	-	-	-	-	-	-
93	D18V, T37S, D53V	2	-	51%	9%	**D53V**	34%	3%
95	D51N, E69D, K100N, G102E, F164L, T175S	4	-	-	-	-	-	-
98	K42R, E197D	-	-	40%[1] 96%[2]	2%[1] 5%[2]	**K42R**	91%	0%
100	F164Y, Q168L	1	-	94%	9%	-	-	-
104	N26Y, D66E, K91stop, F108L, V111A, L165M, K193I	1	1	-	-	-	-	-
105	A36T, P39S, L105Q, G129D	4	-	81%	8%	-	-	-
106	L20M	1	-	101%	10%	-	-	-
111	G183D, G204E	2	-	98%[1] 113%[2]	9%[1] 0%[2]	-	-	-
114	E74D, K101N, Q128L	2	-	34%	2%	-	-	-
115	S94R, I95F, E190G	3	-	104%	7%	-	-	-
119	E35D, G183C	1	-	96%	13%	-	-	-
125	D64V, Q128H, F141S	3	-	-	-	-	-	-
134	A27T, P33Q, T37A, K76stop, T175I	3	1	-	-	-	-	-
137	-	-	-	-	-	-	-	-
141	E122D, G144stop, F150I, K202N K212N,	-	1	-	-	-	-	-
143	G183D, G204E	2	-	-	-	-	-	-
145	E93K	1	-	89%[1] 92%[2]	21% [1] 4%[2]	-	-	-
156	-	-	-	-	-	-	-	-
159	G34D, P73S, S156N	3	-	-	-	-	-	-
162	-	-	-	-	-	-	-	-
165	S130N, F141V	1	-	-	-	-	-	-
167	G34D, M180K	2	-	102%	11%	-	-	-

Colony #	Mutations	NC Mut.	Stop Mut.	Clone activity % of WT	Std Dev	Follow-up Single Mut.	Activity % of WT	Std Dev
170	-	-	-	-	-	-	-	-
171	M107K, E119stop, D154E, W159R, R216Q	1	1	-	-	**W159R**	61%	2%
173	R41P, K100stop	1	1	-	-	-	-	-
174	-	-	-	-	-	-	-	-
175	K43R, K44stop	-	1	-	-	-	-	-
179	V109D, E190D, P208S	2	-	19%[1] 78%[2]	6%[1] 10%[2]	-	-	-
180	I123F, A134T, V166G, N192I	4	-	38%	4%	**I123F, A134T**	84%, 78%	9%, 11%
183	E69stop	-	1	-	-	-	-	-
184	D66E, L96stop, V143E, K195E	-	1	-	-	-	-	-
189	T104I, F164L	2	-	71%	6%	**T104I**	99%	2%
190	W6R, H75Q, K193R	2	-	13%[1] 15%[2]	0%[1] 2%[2]	-	-	-
193	L126Q, K202N	2	-	88%[1] 104%[2]	16%[1] 3%[2]	-	-	-
194	-	-	-	-	-	-	-	-
197	D51V, M98V, M151L, K212stop	3	1	-	-	-	-	-
199	Q168stop	-	1	-	-	-	-	-
	TOTAL	**115***	**18**					

[1/2/3] Indicates trial number of triplicate screen performed on *Mesd* mutant clone.
* unique point mutations
NC – nonconservative
Mut – mutation
Std dev – standard deviation

Key for determining conservative or non-conservative mutation

Residue	Functional property
V,A,I,L	hydrophobic aliphatic
F,W,Y	hydrophobic aromatic
C,M,N,Q,S,T	polar neutral
H,R,K	basic
D,E	acidic
G	glycine
P	proline

Appendix B: Quantification of MESD, normalized to IgG. Raw data for Figure 4.

	T1	T2	T3	AVG	STD DEV
no				**0.04**	0.15
wt				**130.04**	76.61
VSR	10	13	9	**10.67**	2.08
DVSR	1	0	0	**0.33**	0.58
D64-66A	58	58.5	54.2	**56.90**	2.35
L57P	320	319.5	344.5	**328.00**	14.29
D53V	121.5	83.33	89.33	**98.06**	20.52
N133Y	163	227.5	199	**196.50**	32.32
M54T	359	227.67	383.50	**323.39**	83.80
P40S	131.75	161.67	143.67	**145.69**	15.06
I123F	61.33	90.5	109.5	**87.11**	24.26
E62K	289	512	457	**419.33**	116.17
K103E	128	156	114	**132.67**	21.39
I149R	166.5	158.5	116.5	**147.17**	26.86
F108R	35	82	129	**82.00**	47.00
F141R	48.33	49.00	40.67	**46.00**	4.63
V143R	33	64	66	**54.33**	18.50
M151R	140.25	124	136.75	**133.67**	8.55
F141R/F108R	29	30	27	**28.67**	1.53
F141R/M151R	105	107	84	**98.67**	12.74
W127R	127.83	130.8	114.25	**124.29**	8.82
W61R				**119.35**	88.72
W159R	147.5	134	119	**133.50**	14.26
A134T	111	100	105	**105.33**	5.51
C171Y	231	250.75	251.33	**244.36**	11.57
N50K	264.5	246	233.2	**247.90**	15.74
T104I	92	86.33	94.67	**91.00**	4.26
K97V	118.6	132	123.75	**124.78**	6.76
E122K	537.5	1000	713	**750.17**	233.48
D169K	540	632	609	**593.67**	47.88
E160K	599	569	415	**527.67**	98.72
E122K/ E160K	145.8	130.5	167.25	**147.85**	18.46
D169K/ E160K	143.13	151.5	151	**148.54**	4.70
D169K/ E122K	163.5	152	119.2	**144.90**	22.99
K97E	136	105	128	**123.00**	16.09
K76E	87	105.2	95.67	**95.96**	9.10
K42R	219.6	267.33	285	**257.31**	33.83

Appendix C: Quantitation of mature LRP6. Raw data for Figure 4.

	Mature/ER LRP6							1-way ANOVA	
	T1	**T2**	**T3**	**(T4)**	**AVG**	**STD DEV**	**% of WT**	**q-value**	**Summary**
no					**4%**	3%	**6%**	68.04	***
wt					**64%**	8%	**100%**	-	-
VSR	0.64	0.62	0.59	0.68	**63%**	4%	**99%**	0.2352	ns
DVSR	0.06		0.03	0.06	**5%**	2%	**8%**	22.4	***
D64-66A	0.34	0.34	0.40	0.32	**35%**	3%	**55%**	12.45	***
L57P	0.09	0.11	0.11	0.19	**13%**	5%	**20%**	22.21	***
D53V	0.19	0.21	0.21	0.25	**22%**	3%	**34%**	18.4	***
N133Y	0.22	0.21	0.26	0.41	**28%**	9%	**43%**	15.74	***
M54T	0.44	0.42	0.45	0.61	**48%**	9%	**75%**	6.949	***
P40S	0.47	0.48	0.46	0.63	**51%**	8%	**80%**	5.651	*
I123F	0.47	0.50	0.50	0.66	**53%**	9%	**84%**	4.532	ns
E62K	0.44	0.41	0.45	0.53	**46%**	5%	**71%**	7.954	***
K103E	0.42	0.41	0.4	0.37	**40%**	2%	**63%**	10.38	***
I149R	0.12	0.09	0.13	0.08	**10%**	2%	**16%**	23.2	***
F108R	0.45	0.39	0.39	0.37	**40%**	3%	**62%**	10.43	***
F141R	0.50	0.52	0.49	0.53	**51%**	2%	**80%**	5.593	*
V143R	0.64	0.66	0.66	0.66	**65%**	1%	**102%**	0.5967	ns
M151R	0.79	0.75	0.72	0.73	**75%**	3%	**117%**	4.722	ns
F141R/F108R	0.14	0.11	0	0.20	**11%**	8%	**17%**	22.95	***
F141R/M151R	0.42	0.47	0.54	0.44	**46%**	5%	**73%**	7.542	***
W127R	0.02	0.02	0.06	0.02	**3%**	2%	**5%**	26.39	***
W61R					**16%**	9%	**24%**	43.62	***
W159R	0.41	0.39	0.36	0.40	**39%**	2%	**61%**	10.78	***
A134T	0.56	0.56	0.38		**50%**	11%	**78%**	6.285	**
C171Y	0.58	0.58	0.58		**58%**	0%	**91%**	2.486	ns
N50K	0.60	0.58	0.59		**59%**	1%	**92%**	2.211	ns
T104I	0.65	0.63	0.61		**63%**	2%	**99%**	0.2541	ns
K97V	0.67	0.68	0.67		**68%**	1%	**106%**	1.665	ns
E122K	0.57	0.58	0.58		**58%**	1%	**90%**	2.697	ns
D169K	0.59	0.58	0.57		**58%**	1%	**91%**	2.533	ns
E160K	0.59	0.62	0.61		**61%**	2%	**95%**	1.457	ns
E122K/ E160K	0.59	0.62	0.61		**61%**	2%	**95%**	1.399	ns
D169K/ E160K	0.59	0.62	0.64		**62%**	3%	**97%**	0.9575	ns
D169K/ E122K	0.64	0.63	0.60		**62%**	2%	**98%**	0.6605	ns
K97E	0.63	0.56	0.69		**62%**	7%	**98%**	0.6177	ns
K76E	0.63	0.66	0.63		**64%**	2%	**100%**	0.0296	ns
K42R	0.59	0.58	0.58		**58%**	0%	**91%**	-	-

q – False Discover Rate (FDR) adjusted p-value for 1-way ANOVA

Appendix D: Probe sequences used in Southern blotting.

5’ probe (red bar, Figure 18)

5’-GCGGCCGCACCAGTTTAATTGACAGTGATATTGAAAGAATGGTGGG
TCGAAAATCATCCGTGGAGCAGAATAACAATAGACCCTATAATTACAGTCTT
CGAGAAAAGTTGCCCTAGCTGTCCTTAGCTTTTCAGCAGGCGGTTTGTTCTTG
CTAGAAATTACTAGGGAGCGTAGTTGAATGTCAACACCCTGAAAAGGGCCTC
AGGGTCAAGGTAGTTTGCATATCTTCCAACTCATTCATTTCATAGGCTTCGAG
GACTCTGTCACTGAAACCCTGAGGGAACTTTCAGACCCTGGCTAGAGAATGA
GAGACAAAAGGGCTGACTTCTAACAAAACCCCCAAATAGTGGAGAAAGCAC
AGTTGGGCAGGACCCAGCTAGAGTAGATTGTTTGGCCAGGCCAAGGGGCGGA
GCTCGCGGGGCGGAGCCTGGCAAGGGGAGGAACCAGGAGGAAGAACCCTTG
GTCCCCAGCCAGGTGAGCTCCCAGAGCTATGGGGCGGAGTCTGGTGAGGAGG
CGGTACCCTAGGGGCGGAGTCAGGAGACCGTGGCTGAGGGGTGGAGTCAAG
TGGTGAAAGGCTCGATGACGGGGAGGAGCCTGAGGTTGGGAGCCCCAAGGG
AATGCAGTTGTGGGCGGAGCCAAGGGGGTCGGAGCTACCGGATGAGGTCCG
GACAGGAGGAACCAGAACGAGGCGGGGTGCGGTAGGCTACGGACTCCTCGG
AGGCGGAGCCATTGGGACTTGAGTCCGCGAGGGTGGGACGGGGTCAAGTACT
GGGTTTAGTTCTGCGCAGAACACGCTTAGGGACTGGATTGGAAGGCCGGGGG
CGGGGTGGGGGCGAGGCCCCGGCGTCCGGACTCCGCACGCTGTCTGCGCAGG
CTCATTGTGCCTTACGCTGGGCAGTCCGTTACGCTAGGCTGCTAACATGGCTG
CCTCCAGGTGGCTGCGCGCGGTTCTACTGTTTCTGTGTGCCTCGGACCTTCTG
TTGCTCCTCGAG-3’

Residues marked in red indicate NotI restriction site (5’) and XhoI restriction site (3’).

3’ probe A (blue bar, Figure 18)

5’-GCGGCCGCACATGCAGGGTGTCTGTTTTGGCAGTCTTTCCAAGGAC
CTTGGGCCTTTCCTGTCTATGAATCCTTTTATTTAATTTTTTTTTCTTGAAACAT
TGGTTTACTTGTTTGTTTATTGGCCAAAATTAGTATGTTTGTTT
TAATATCTTGTCTTGGAAATTTGGCTTGTCTTTTATCTCTTTAACCTTTGCTTC
ATCAGAATAAAAATGGCATTGCTTAGTCTCTTTGAAGAATGAATGAGTTCCA
GTTCCATGGTTCATGGTGTAGCTGTGCTGACACATGTGGT
TGTAACACGTGGTTAATAAAACGAATGTGAACAAGTCTGTGTTCAAA
GGCCATATGATCTTAAAGTTTGAAATCTCAAAATATGAAAGGTTCTACTTTAT
ATATTTTATACAGTATATTTTTTATCATATTCACCATCCTCTACC
CCCTTCTAAATCTGTCCTTCCCACCCTCACCTCCCTACCCATCCAACTGAGTTT
TGGTTTTTCGGGGTTTTTTTTTATAGCCTATTTTTTCTGTTTAACAATAGTTCCA
AAAACCCAAGTCTTTAGTATCTTAATTGAGGAAGTAAGAAAGTGATAAGAAA
GAACGGAAGGAGTTGCTAAGAATGCTCTCTGTAACTCCCATCAGATATCTTG
GTGGTGACTGTTCTCTGATGGTCTGCTGCTTAGGAGCACAGCATCATGCCTTG
TGGGCACGCTTTTATGTGTCACCCAGACCCATGCCATTGCTTTCTTCTTCCTGG
GCACTAATGTATGGGGATACACTGAGTGCTTGTTGCTGACCTTGGAGGTTAG
GATTTCTGTCTGCTTCCCTTGGATCTTTGTGGGCCCTTGAGGAGGAGTCTTGT
AGGACCTGTTCCATGCAGTGGCTTTTAGCCTTCTCATCAAAGCCAGTTTGAGA
CTTCAGCTCGAG-3’

Residues marked in red indicate NotI restriction site (5') and XhoI restriction site (3').

3' probe B (green bar, Figure 18)

5'-
GCGGCCGCACATAAGACATAGATGGAAATGACATTTCATGTTAAAGATAAAA
ATGGGAATTTCTCACCTCTGCAGCACACCTGTGTCCCTTGCAGCTCCCTAAGG
AGTTTGTCATTTATAATCTCTTCACAGCGTCATTTATGTATGCTTCAGGACCAT
CAAGCATCTGCTTCTGTCTTGATCTTAGCAGGATGCTTGTTTAGAGCTCAGTG
AACATTAAAGTCAGCAGCCACTTGGCCCAAGGCAGAACAGTTCAGCATTTGG
GTGGAATTGAAATGTAGGCCTCCCAGCCTTCTCTGACCCCAGGCACCTCACTT
ACATTGCTAACTGCTGGCTTCTCTGGCTAGGTTCATCGTGGGATCCGACCGCG
CCATCTTCATGCTCCGGGATGGGAGCTATGCCTGGGAGATCAAGGACTTTTTG
GTCAGTCAAGACCGGTGTGCTGAAGTCACTCTAGAGGGACAGATGTATCCTG
GCAAAGGAGGAGGAAGCAAGGAGAAAAATAAAACAAAGCCAGAGAAGGCT
AAAAAGAAGGAGGGAGATCCCAAACCACGTGCTTCCAAGGAAGACAATCGA
GCTGGGAGCAGAAGAGAAGACCTTTAGCAGGTGGCCTCGAG-3'

Residues marked in red indicate NotI restriction site (5') and XhoI restriction site (3').